UNIVERSITI TEKNOLOGI MARA

THERMAL COMFORT AND AIRFLOW EVALUATION OF AN AUTOMATED RAPID TRANSIT (ART) USING PREDICTED MEAN VOTE (PMV) AND PREDICTED PERCENTAGE OF DISSATISFIED (PPD)

AINA BALQIS BINTI AZRIN

MSc

March 2026

UNIVERSITI TEKNOLOGI MARA

THERMAL COMFORT AND AIRFLOW EVALUATION OF AN AUTOMATED RAPID TRANSIT (ART) USING PREDICTED MEAN VOTE (PMV) AND PREDICTED PERCENTAGE OF DISSATISFIED (PPD)

AINA BALQIS BINTI AZRIN

Thesis submitted in fulfilment
of the requirements for the degree of
Master of Science in
(Mechanical Engineering)

Faculty of Mechanical Engineering

March 2026

CONFIRMATION BY PANEL OF EXAMINERS

I certify that a Panel of Examiners has met on 16 October 2025 to conduct the final examination of Aina Balqis Binti Azrin on her Masters of Science thesis entitled "Thermal Comfort and Airflow Evaluation of an Automated Rapid Transit (ART) Using Predicted Mean Vote (PMV) and Predicted Percentage of Dissatisfied (PPD)" in accordance with Universiti Teknologi MARA Act 1976 (Akta 173). The Panel of Examiner recommends that the student be awarded the relevant degree. The Panel of Examiners was as follows:

Noor Azlina Mohd Salleh, PhD
Associate Professor
Faculty of Mechanical Engineering
Universiti Teknologi MARA
(Chairman)

Muhammad Fairuz Remeli, PhD
Associate Professor
Faculty of Mechanical Engineering
Universiti Teknologi MARA
(Internal Examiner)

Haslinda Mohamed Kamar, PhD
Professor
Faculty of Mechanical Engineering
Universiti Teknologi Malaysia
(External Examiner)

PROFESSOR DR HJH ZURAEDA BINTI IBRAHIM
Dean
Institute of Postgraduates Studies
Universiti Teknologi MARA

Date: 4 March 2026

AUTHOR'S DECLARATION

I declare that the work in this thesis was carried out in accordance with the regulations of Universiti Teknologi MARA. It is original and is the results of my own work, unless otherwise indicated or acknowledged as referenced work. This thesis has not been submitted to any other academic institution or non-academic institution for any degree or qualification.

I, hereby, acknowledge that I have been supplied with the Academic Rules and Regulations for Post Graduate, Universiti Teknologi MARA, regulating the conduct of my study and research.

Name of Student	:	Aina Balqis Binti Azrin
Student ID. No.	:	2020647998
Programme	:	Master of Science in Mechanical Engineering – EM750
Faculty	:	Mechanical Engineering
Thesis Title	:	Thermal Comfort and Airflow Evaluation of an Automated Rapid Transit (ART) Using Predicted Mean Vote (PMV) and Predicted Percentage of Dissatisfied (PPD)
Signature of Student	:	……..
Date	:	4 March 2026

ABSTRACT

The optimization of airflow and thermal comfort in public transportation is essential for improving passenger satisfaction and energy efficiency, particularly in hot and humid climates such as Malaysia. This study investigates airflow distribution and passenger thermal comfort within an Automated Rapid Transit (ART) middle carriage using Computational Fluid Dynamics (CFD) integrated with Fanger's Predicted Mean Vote (PMV) and Predicted Percentage of Dissatisfied (PPD) indices. The ART carriage was modelled in SolidWorks to replicate the actual geometry, and field measurements were conducted to validate the CFD model, resulting in an average error of 7.01%, which confirms the reliability of the numerical approach. Airflow and temperature distributions were analyzed under three passenger-loading conditions: AW1 (16 seated passengers), AW2 (16 seated and 58 standing passengers), and AW3 (16 seated and 74 standing passengers). Simulations were performed at inlet air velocities of 1.6, 2.9, and 3.2 m/s and inlet air temperatures of 14.7°C and 8.7°C. The results indicate that increasing passenger density leads to higher cabin temperatures and reduced airflow uniformity. Breathing-zone air velocities increased from approximately 0.23 m/s at 1.6 m/s to about 0.60 m/s at 3.2 m/s, raising the risk of draft discomfort. In high-density conditions, central cabin regions were up to 5.7°C warmer than side areas due to metabolic heat accumulation. Thermal comfort evaluation using PMV and PPD indices, supported by selected passenger analysis via the CBE Thermal Comfort Tool, identified AW2 at an inlet velocity of 2.9 m/s and temperature of 8.7°C as the optimal operating condition. Under this condition, most passengers experienced near-neutral thermal sensation (PMV = −0.67 to +0.47) with low dissatisfaction levels (PPD = 6–14%). In contrast, AW3 exhibited severe thermal non-uniformity, with PMV values ranging from −3.6 to +4.3 and PPD reaching 96–100%. These findings provide validated numerical insights for optimizing ART HVAC design and enhancing passenger-oriented thermal comfort in tropical public transport systems.

ACKNOWLEDGEMENT

First and foremost, I express my heartfelt gratitude to my supervisor, Assoc Prof Ts. Dr. Wan Mazlina Wan Mohamed, Ir. Hazran Husain as my Co Supervisor and Dr. Shafiq Suhaimi, for their invaluable guidance, constructive feedback, and unwavering support throughout the course of this research. Their expertise and encouragement have been pivotal in shaping the direction and outcomes of this work.

I would like to extend my sincere thanks to Faculty of Mechanical Engineering, Universiti Teknologi MARA (UiTM) Shah Alam and Malaysia Institute of Transport (MITRANS) Universiti Teknologi MARA (UiTM) for providing the resources and facilities needed for this study, and to my colleagues and peers for their insightful discussions and collaboration, which greatly enriched my research experience.

To my beloved husband, Ainul Mustaqim, and my dear son, Aryan Malique, thank you for your unconditional love, patience, and understanding throughout this journey. Your unwavering belief in me has been my greatest source of strength and motivation. To my parents, your endless support, encouragement, and sacrifices have made this accomplishment possible.

A special thanks to my friends for always being there to listen, provide advice, and lift my spirits when I needed it most. Your support and encouragement have been a source of comfort and joy throughout this process.

Finally, I am deeply grateful to all participants and contributors involved in this study. Your cooperation and input have been invaluable in the successful completion of this work. To everyone who has played a role, whether directly or indirectly, in supporting and encouraging me throughout this journey, I extend my deepest gratitude.

TABLE OF CONTENTS

		Page
CONFIRMATION BY PANEL OF EXAMINERS		**ii**
AUTHOR'S DECLARATION		**iii**
ABSTRACT		**iv**
ACKNOWLEDGEMENT		**v**
TABLE OF CONTENTS		**vi**
LIST OF TABLES		**ix**
LIST OF FIGURES		**x**
LIST OF SYMBOLS		**xi**
LIST OF ABBREVIATIONS		**xii**
LIST OF NOMENCLATURE		**xiii**
CHAPTER 1 INTRODUCTION		**1**
1.1	Research Background	1
1.2	Problem Statement	3
1.3	Objectives	4
1.4	Significance of Study	4
1.5	Scope and Limitations	5
CHAPTER 2 LITERATURE REVIEW		**6**
2.1.	Introduction	6
2.2	Analysis of Air flow in a Long Vehicle	8
	2.2.1 Method of Measuring Air Flow	10
2.3	Thermal Comfort	12
	2.3.1 Thermal Comfort Factors	14
2.4	Thermal comfort Evaluation by Using Fanger's Predicted Mean Vote (PMV) and Predicted Percentage Dissatisfied (PPD)	19
2.5	Previous Research using Predicted Mean Vote (PMV) and Predicted Percentage Dissatisfied (PPD) Indices to Evaluate Thermal Comfort	21
2.6	Simulation of Air Flow and Thermal Comfort Employing Computer Fluid Dynamic (CFD)	23

CHAPTER 3 RESEARCH METHODOLOGY **27**
3.1 Introduction 27
3.2 Selected Space and Characteristics 28
3.3 Field Measurements 30
3.4 Numerical Modelling Physical Modelling 31
3.4.1 Measurement of ART 31
3.4.1.1 Geometry Development and Passenger Modelling 33
3.4.1.2 Modelling Assumptions 35
3.4.1.3 Boundary Conditions for CFD Simulation 35
3.4.2 Modelling Consideration of Human 35
3.4.3 Airflow System 37
3.5 Inlet and Outlet Mechanism 42
3.6 Thermal Parameters 43
3.7 Meshing and CFD Framework 45
3.8 Model Validation 46
3.9 Evaluation of PMV and PPD 48
3.9.1 Theory 48

CHAPTER 4 RESULTS AND DISCUSSION **53**
4.1 Introduction 53
4.2 Air Velocity Distribution 55
4.3 Temperature Distribution 62
4.4 Predicted Mean Vote (PMV) and Predicted Percentage Dissatisfied (PPD) Data 67
4.4.1 Predicted Mean Vote (PMV) 67
4.4.2 Percentage Dissatisfied (PPD) 71
4.4.3 PMV and PPD Value based on CBE Thermal Comfort Tool (AW2) 76
4.4.4 PMV and PPD Value based on CBE Thermal Comfort Tool (AW3) 84

CHAPTER 5 CONCLUSION **92**
5.1 Recommendations 93

REFERENCES **95**

APPENDICES **101**

AUTHOR'S PROFILE **108**

LIST OF TABLES

Tables	Title	Page
Table 1	PMV–PPD Thermal Comfort Scale	12
Table 2:	Recommended Indoor Temperature and RH Values	17
Table 3	Estimation of Metabolic Rate for Basic Activities	18
Table 4	Clothing Levels and Thermal Insulation	19
Table 5	Thermal Sensation Scale of PMV	19
Table 6	Researches on Air Flow and Thermal Comfort with The Application of CFD Simulation	23
Table 7	Transport Capacity	29
Table 8	Measurement of Seated and Standing Passengers	36
Table 9	Boundary Conditions	44
Table 10	Mesh Independence Test	46
Table 11	Measured Surrounding Temperature Inside ART	53
Table 12	Air Velocity Distributions for Category AW1	56
Table 13	Air Velocity Distributions for Category AW2	58
Table 14	Air Velocity Distributions for Category AW3	60
Table 15	Air Temperature Distributions for Category AW1	63
Table 16	Air Temperature Distributions for Category AW2	65
Table 17	Air Temperature Distributions for Category AW3	66
Table 18	PMV Value for Category AW1	68
Table 19	PMV Value for Category AW2	69
Table 20	PMV Value for Category AW3	70
Table 21	PPD for Category AW1	72
Table 22	PPD for Category AW2	73
Table 23	PPD for Category AW3	74
Table 24	Summary Table for AW2 Category at 14.7 °C	78
Table 25	PMV Thermal Comfort Scale	79
Table 26	Summary Table for AW2 Category at 8.7 °C	82
Table 27	Summary Table for AW3 Category at 14. 7 °C	86
Table 28	Summary Table for AW3 Category at 8.7°C	89

LIST OF FIGURES

Figures	Title	Page
Figure 1	Automated Rapid Transit (ART)	1
Figure 2	Automated Rapid Transit (ART) in Malaysia	6
Figure 3	The Relationship Between PMV and PPD	20
Figure 4	General Drawing of ART	29
Figure 5	Measurement of ART Middle Carriage	31
Figure 6	(i) ART Model Isometric View (AW1) and (ii) Top View (AW1)	33
Figure 7	(i) ART Model Isometric View (AW2) and (ii) Top View (AW2)	33
Figure 8	(i) ART Model Isometric View (AW3) and (ii) Top View (AW3)	34
Figure 9	Location of Air Diffuser and Air Return Grill	42
Figure 10	ART Meshed Model	45
Figure 11	Zoomed-in Mesh Near Diffusers	45
Figure 12	Simulated ART Under AW0 Condition	53
Figure 13	Selected Passengers for CBE Thermal Comfort Tool Analysis (AW2)	76
Figure 14	PMV Value of Selected Passengers at 14.7°C	76
Figure 15	PPD Value of Selected Passengers at 14.7°C	77
Figure 16	PMV Value of Selected Passengers at 8.7°C	81
Figure 17	PPD Value of Selected Passengers at 8.7°C	81
Figure 18	Selected Passengers for CBE Thermal Comfort Tool Analysis (AW3)	84
Figure 19	PMV Value of Selected Passengers at 14.7° C	84
Figure 20	PPD Value of Selected Passengers at 14.7 °C	85
Figure 21	PMV Value of Selected Passengers at 8.7°C	88
Figure 22	PPD Value of Selected Passengers at 8.7 °C	88

LIST OF SYMBOLS

Symbols

ε	Turbulent dissipation rate
k	Turbulent kinetic energy
μ	Dynamic viscosity
ν	Kinematic viscosity
P	Pressure
q	Heat flux
R	Gas constant
T	Air temperature
U	Air velocity
u, v, w	Velocity in three axes
ρ	Air density
ρg	Shear stress

LIST OF ABBREVIATIONS

Abbreviations

ART	Automated Rapid Transit
ASHRAE	American Society of Heating, Refrigerating, and Air-Conditioning Engineers
CBE	Centre for the Built Environment
CFD	Computational Fluid Dynamics
ISO	International Organization for Standardization
PMV	Predicted Mean Vote
PPD	Predicted Percentage Dissatisfied
RH	Relative Humidity

LIST OF NOMENCLATURE

Nomenclatures

clo	Clothing insulation
m/s	Metre per Second
met	Metabolic rate
W/m^2	Watt per Metre Square

CHAPTER 1
INTRODUCTION

1.1 Research Background

In recent years, the development of an efficient public transportation system has become one of the most crucial components contributing positively to national, societal, and individual well-being. Such systems offer significant social, economic, and environmental sustainability benefits [1]. The introduction of automated public transport modes, including automated buses and taxis, is expected to generate various advantages such as improved traffic safety, enhanced productivity within the transit sector, reduced congestion and fuel consumption, as well as more efficient use of parking spaces. Figure 1 below illustrates the Automated Rapid Transit (ART) vehicle during its pilot testing phase in Malaysia.

Figure 1: Automated Rapid Transit (ART)

For public buses in particular, the integration of air-conditioning systems has long been regarded as a key element in enhancing passenger comfort during travel, whether for commuting to work, attending university, or reaching other destinations [2]. Automated buses are no exception; maintaining passenger comfort remains a critical factor that depends largely on optimizing airflow distribution and ensuring satisfactory thermal comfort. A well-designed ventilation system within the passenger compartment is essential to deliver adequate fresh air while maintaining consistent airflow velocity and uniform temperature distribution [3].

Over the years, numerous studies have investigated the airflow characteristics and thermal comfort levels in public transportation vehicles, particularly buses.

Continuous research and system improvements are vital to enhance passenger comfort, as this aspect significantly influences the overall attractiveness of public transport systems [4]. Previous research has focused on the uniformity of airflow velocity, temperature distribution, and thermal comfort inside bus compartments. Findings from these studies indicate that thermal comfort strongly affects the perceived level of service and the passengers' decision to utilize public transport[5].

Indoor air circulation and thermal comfort are particularly critical in confined spaces with high passenger density, such as buses, where temperature tends to rise quickly and may lead to discomfort [3]. A study conducted in Catania emphasized that passenger comfort in public transport has become an increasingly important issue, highlighting that thermal comfort and indoor air quality remain key concerns in the transportation sector [6]. For long vehicles such as buses, air-conditioning plays a pivotal role in ensuring that public transport serves as a viable and comfortable alternative to private vehicles.

Previous investigations have analysed airflow and thermal comfort performance in large, air-conditioned buses approximately 14.6 meters in length, accommodating up to 167 passengers [7]. Recognizing the importance of these factors underscores the need to conduct further studies on emerging modes of public transport such as the Automated Rapid Transit (ART) system. Such research is essential to ensure that optimal airflow and thermal comfort levels are maintained within the passenger compartment under both nominal and maximum passenger load conditions.

Thermal comfort evaluation in indoor and transportation environments is commonly guided by international standards such as ISO 7730 [8] and ASHRAE 55 [9]. These standards provide essential guidelines for designing optimal ventilation systems and maintaining thermal comfort for occupants. They identify two primary categories of factors influencing thermal comfort—individual factors (such as metabolic rate and clothing insulation) and environmental factors (including air temperature, air velocity, humidity, and mean radiant temperature). Together, these parameters determine human thermal balance and enable researchers to assess and achieve appropriate thermal comfort levels according to standardized methods. The application of these international standards is crucial, as they establish clear comfort

criteria and support the creation of thermally comfortable indoor environments.

Ultimately, achieving thermal comfort in mass transportation vehicles can be realized by defining optimal temperature ranges and acceptable comfort zones perceived by passengers, or by evaluating passengers' thermal sensations under specific conditions in accordance with established standards and regulations.

1.2 Problem Statement

An ideal public transportation system should ensure efficient air circulation and maintain optimal thermal comfort for passengers under all operating conditions. Comfortable cabin environments rely on consistent airflow, uniform temperature distribution, and effective ventilation systems that balance energy efficiency with passenger satisfaction.

In reality, maintaining thermal comfort in public transport remains a major challenge, particularly in hot and humid climates like Malaysia. Overcrowding during peak hours, combined with heat generated by motors, lighting, and human bodies, often causes cabin temperatures to rise rapidly and reduces air circulation. These conditions create stuffy and uncomfortable environments, leading to passenger dissatisfaction, discomfort, and loss of confidence in public transportation if not properly managed.

Such issues not only affect service quality but also threaten the long-term success and sustainability of public transport systems. As Malaysia introduces the Automated Rapid Transit (ART) system to enhance urban mobility, addressing passenger thermal comfort is essential for ensuring its acceptance, reliability, and long-term viability.

This research aims to evaluate airflow and thermal comfort conditions within the ART cabin operating under hot and humid environments. The objectives are to (1) analyse airflow and temperature distribution under different air velocities and passenger loads, (2) assess the corresponding thermal comfort levels using validated models, and (3) identify the optimum airflow conditions that ensure comfort while maintaining energy efficiency.

Computational Fluid Dynamics (CFD) simulations, validated with real ART operating data, are used to model air distribution and temperature patterns, while Fanger's Predicted Mean Vote (PMV) and Predicted Percentage of Dissatisfied (PPD) models quantify passenger comfort. The findings provide new insights into thermal comfort performance in tropical ART systems and offer practical recommendations for designing energy-efficient, climate-responsive, and passenger-oriented public transport solutions.

1.3 Objectives

The aim of this research is to determine the air flow and thermal comfort of Automated Rapid Transit's Passengers in Malaysia. There are THREE (3) main objectives for this research, listed as follow:

a) To measure the current air temperature and airflow velocity in the Automated Rapid Transit (ART) carriages throughout the pilot testing period.
b) To investigate the effects of airflow and temperature distribution within Automated Rapid Transit (ART) carriages under varying passenger loads and air-conditioning speeds using Computational Fluid Dynamics (CFD) simulation.
c) To analyse airflow and passenger thermal comfort across different operating conditions using the PMV–PPD model.

1.4 Significance of Study

The study of airflow and thermal comfort in public vehicles, particularly in the Automated Rapid Transit (ART) system, is essential due to its capacity to transport a large number of passengers within a confined space. Optimizing airflow and thermal conditions is crucial for preventing discomfort and ensuring passenger satisfaction. This research will assess the ART's ability to maintain optimal indoor air circulation and thermal comfort, thereby enhancing the overall passenger experience. By conducting a detailed analysis, including targeted assessments of thermal comfort for selected passengers using the CBE Thermal Comfort Tools, the study provides valuable insights

into how public transport can be designed for maximum comfort. The findings from this study have the potential to inform the design and operation of ART systems, contributing to more sustainable and user-friendly public transport solutions. Ensuring a comfortable environment for future passengers will not only improve ridership satisfaction but also encourage wider adoption of the ART, helping to reduce urban traffic congestion and lower transportation-related carbon emissions. This research is a significant step towards advancing public transportation systems that are both efficient and environmentally responsible.

1.5 Scope and Limitations

The study focuses specifically on the middle carriage of the ART, where both thermal comfort and airflow dynamics were closely examined. The ART model was developed in SolidWorks using actual measurements of 8.78 m (L) × 2.65 m (W) × 3.32 m (H), based on the general design specifications of the ART (Appendix 1). The interior of the middle carriage, including passenger seats and human models, was incorporated into the simulation. Passengers were assumed to be stationary, fixed in place, and to act as heat sources. The number of passengers was varied at 16, 74, and 90, corresponding to conditions AW1, AW2, and AW3, respectively. Field measurements of actual air temperature and air velocity were conducted and integrated into the simulation to ensure realistic boundary conditions. Additional factors influencing thermal comfort, such as metabolic rate and clothing insulation, were also included in the analysis. The simulations were performed under steady-state conditions to represent stable airflow and temperature distributions within the ART cabin. Furthermore, an in-depth thermal comfort assessment was conducted for five selected passengers under AW2 and AW3 conditions using the CBE Thermal Comfort Tools

CHAPTER 2
LITERATURE REVIEW

2.1. Introduction

Figure 2: Automated Rapid Transit (ART) in Malaysia

Automated Vehicles usually equipped with both hardware and software that assures driving capability with or without remote monitoring of the vehicle, without the need for human interference in the vehicle's control mechanisms [10]. Automated Rapid Transit or ART as shown in Figure 2 is known as transit system with a medium capacity that functioned to transport urban passenger using advanced technology and allowing greater passenger capacity to be deployed at a much lower cost compared to conventional light-rail systems, besides it runs on a clean energy sources which is either electricity or hydrogen [11]. Multi-carriages are fitted with sensors that read virtual tracks on the lane, allowing them to navigate their own route automatically, drive up to 70 km per hour and hold more than 300 passengers on three carriages.

The capacity of an ART vehicle with five carriages can be expanded to approximately 500 passengers. At present, in different cities throughout China, ART is being rapidly embraced, with the latest being in Yibin, Sichuan. The T1 Line, the first of the city's seven routes, was officially launched following a trial period in December 2019. In 2017, China's CRRC Zhuzhou Electric Locomotive Institute developed and introduced the ART system [12]. The electricity-powered multi-carriage unit is equipped with sensors which can read the dimensions of a lane, allowing it to plan its

own route automatically rather than following traditional rail tracks. The ART system is characterized by its low cost, high flexibility, and strong adaptability. Unlike traditional rail systems, ART does not require the installation of physical tracks, allowing it to utilize existing road infrastructure, thereby reducing construction costs and enabling completion of route development within approximately one year [13]. On 20 January, Malaysia's first automated rapid transit system arrived in the southern state of Johor, where a pilot test program already started in the first quarter of 2021 in Iskandar, Malaysia [14]. The implementation of the ART pilot project reported to be a huge step towards helping Iskandar Malaysia boost public transport and supporting the rapid growth of the region's economy and society [15]. Additionally, in February 2024, Putrajaya initiated a pilot trial of the Autonomous Rapid Transit (ART) trackless tram system as part of its ongoing efforts to evaluate innovative, sustainable, and cost-effective public transportation solutions [16].

The ART system, developed by CRRC Zhuzhou Electric Locomotive Institute in 2017, has been implemented in several Chinese cities, including Zhuzhou and Yibin, where the T1 Line commenced operation in December 2019. These deployments demonstrate the feasibility of ART as an electric, sensor-guided, multi-carriage vehicle capable of autonomous lane tracking and efficient passenger transport [17] Although China’s experience provides valuable insights into ART’s operational and technological performance, its climatic conditions differ markedly from Malaysia’s hot and humid tropical environment. In temperate regions such as Zhuzhou and Yibin, research primarily addresses automation and safety, whereas Malaysia’s consistently high temperatures and humidity make airflow distribution, ventilation efficiency, and cooling effectiveness critical for passenger comfort.

Evaluating ART’s thermal performance under tropical conditions is therefore essential, as excessive heat and humidity may lead to discomfort if air distribution is not properly managed. Passenger comfort—particularly airflow and thermal conditions in tropical climates—remains underexplored in current literature. This research addresses this gap by examining airflow characteristics and thermal comfort (PMV–PPD) within a Malaysian ART environment.

2.2 Analysis of Air flow in a Long Vehicle

Airflow is defined as the movement of air driven by pressure differences, where air behaves as a fluid that naturally moves from regions of higher pressure to regions of lower pressure. It is governed by the fundamental principles of fluid dynamics and plays a critical role in determining ventilation effectiveness and thermal comfort within enclosed or open environments [9] [18] In engineering, airflow is defined as the volumetric measure of air passing through a given system per unit time, and is commonly investigated either experimentally (e.g., via wind-tunnel tests) or numerically using Computational Fluid Dynamics (CFD) modelling. These methods are extensively employed to study airflow patterns around vehicles, marine vessels, aircraft and building envelopes, and their application has increasingly extended to public-transport interiors and bus cabins [17][19]. The use of Computational Fluid Dynamics (CFD) in public transport studies has increased in recent years, particularly for analysing airflow distribution, ventilation efficiency, and passenger thermal comfort within vehicle cabins. CFD has become the preferred approach due to its flexibility, lower cost, and ability to simulate complex air movements and temperature variations under real operating conditions. Recent studies in [5] and [20] highlight the growing application of CFD in bus environments, demonstrating its effectiveness in evaluating air distribution and thermal comfort in modern transit systems.

Computational Fluid Dynamics (CFD) provides a powerful tool for evaluating airflow and thermal comfort in Automated Rapid Transit (ART) systems due to their complex internal environments. Unlike conventional buses, ART vehicles accommodate a larger passenger capacity within a multi-carriage, enclosed space, where airflow behaviour is influenced by numerous heat sources, passenger density, and ventilation design. These conditions create non-uniform temperature and velocity distributions, making experimental measurements challenging and often impractical. CFD allows for detailed simulation of air distribution, temperature gradients, and local comfort indices under varying inlet and outlet configurations, providing insights into how design and operational parameters influence passenger comfort. Studies on bus and rail environments [5][21] have demonstrated CFD's reliability in capturing complex air movement patterns and identifying thermal discomfort zones—an approach equally applicable to ART systems.

Given ART's fully enclosed design, dependence on HVAC systems, and high passenger occupancy, CFD becomes essential for optimizing ventilation performance and ensuring thermal comfort under realistic tropical conditions. It enables performance evaluation without the high cost or disruption associated with full-scale experiments, making it an effective and sustainable method for thermal comfort analysis in ART environments.

Passenger thermal comfort depends on the internal atmosphere and the way air is transported, Inefficient or uneven airflow distribution can lead to stagnant zones or excessive air resistance, resulting in localized regions of high or low temperature. Such irregularities not only increase energy consumption but also negatively impact passenger thermal comfort. [22]. The air flow profile is very important and it has a major effect on the distribution of temperature and comfort level of passengers [23]. According to Kale et al. previous study was done on a non-airconditioned bus to simulate the air flow through a bus with open windows, and the results is quite complex since the flow is highly three dimensional and unsteady [24]. In the paper, both numerical and experimental investigations were performed where the visualization experiments in a water channel with a model in order to facilitate the comparison with the simulations. In a moving bus on a straight stretch, flow visualization with smoke and tuft was performed. The bus had seats but no passengers, and the doors and windows had been altered to create virtually symmetrical spaces on both sides. The tests were carried out in the absence of wind, all flows are turbulent and three-dimensional. As a result, passengers at the back near the windows will get fresh air from outside, while those in the front will get air flowing outwards from within, which has repercussions for the general public.

There is also a study regarding air flow and thermal comfort of a bus passenger conducted on an air-conditioned bus, several cases or conditions were considered in the study such as ventilation system is working on maximum capacity, implementing air deflectors to improve air distributions and also by opening the rear window of the bus [25]. The simulation of airflow was carried out only to the passenger space, where the temperature and velocity of the air distribution were observed including the PMV and PPD values. The results obtained were used to determines the practicality of the bus's

design. In [3] A computational study using CFD approach was implied to investigate the impact of air supply diffuser placement on air flow velocity and temperature distributions within a university shuttle bus's passenger compartment. A standard k-epsilon flow model was used to analyse turbulent flow inside the bus compartment model. Hence, the contour representation of the air temperature and velocity distribution were analysed and observed for each type of ventilation setup; mixing ventilation and displacement ventilation setups. All of the previous studies applied a CFD simulations method in order to analyses the fluid flow inside the bus. The applications of CFD simulations have a very significant contribution in terms of obtaining a precise result for the air flow temperature at every certain point besides determine the velocities' directions. CFD analysis also helps in improving thermal comfort levels for peoples [26]. Previous studies have primarily focused on airflow and thermal comfort in conventional buses and other public transport vehicles. However, limited research has specifically examined these parameters within the context of Autonomous Rapid Transit (ART) systems. Given the larger passenger capacity, enclosed cabin design, and varying inlet–outlet configurations of ART vehicles, understanding internal airflow behaviour is crucial for optimizing ventilation performance and passenger comfort. Therefore, this study employs Computational Fluid Dynamics (CFD) to evaluate airflow distribution and thermal comfort in an ART operating under Malaysia's tropical climate conditions.

2.2.1 Method of Measuring Air Flow

Previous research has highlighted the need for accurate measurement of airflow and temperature when evaluating thermal comfort in public transport environments. For example, Rorres in [27] conducted an investigation on airflow characteristics in intercity, transit, and articulated buses using a Mannix 8906 digital flow meter. The Mannix 8906 was selected in their study due to its ability to directly measure volumetric airflow in Cubic Feet per Minute (CFM), allowing airflow rates to be obtained without further conversion. This was advantageous in minimizing calculation errors and improving the reliability of volumetric airflow estimation. Similarly, an experimental study on bus air-conditioning performance reported in [28] employed a vane anemometer to measure air velocity and temperature at each evaporator outlet. In that case, volumetric airflow was derived by multiplying the measured velocity in Feet per

Minute (FPM) with the corresponding duct cross-sectional area in square feet (ft^2). Furthermore, research in [3] utilized a V816B digital anemometer with an accuracy of ±2°C for temperature and ±3% for velocity to obtain airflow and thermal distribution profiles at diffuser level, passenger seating, and floor level inside a university shuttle bus.

In the present study, the UNI-T Mini LCD Anemometer UT363 is selected to measure air temperature and airflow velocity within the Automated Rapid Transit (ART) carriage. The selection is based on practicality, portability, and cost-efficiency. Compared to instruments like the Mannix 8906, which is more specialized and relatively expensive, the UT363 provides a more accessible and convenient option for repeated measurements in multiple locations inside the vehicle cabin. Its compact size and ease of handling make it particularly suitable for confined or crowded spaces such as passenger seating areas, overhead diffusers, and aisle zones. While the UT363 does not offer the same advanced capabilities as some higher-end measurement instruments, it provides sufficient accuracy for evaluating general airflow patterns and temperature distribution relevant to the thermal comfort assessment in this study. Thus, the selection reflects a balanced consideration between measurement accuracy, operational convenience, and resource constraints.

The field measurements obtained from the UT363 will form the basis of the boundary conditions required for the subsequent computational analysis. SolidWorks Flow Simulation will be used to model airflow and temperature distribution within the ART carriage using the collected data. Integrating empirical measurements with computational simulation enables a more comprehensive assessment of thermal comfort conditions, particularly through comfort indices such as Predicted Mean Vote (PMV) and Predicted Percentage of Dissatisfied (PPD). This approach ensures that the airflow distribution and thermal environment inside the ART are evaluated systematically to determine whether the system meets the required comfort standards for passengers under varying operational scenarios.

2.3 Thermal Comfort

Thermal comfort refers to the state in which an individual expresses satisfaction with the surrounding thermal environment. It is influenced by both environmental and personal factors. Exposure to elevated air temperature and humidity can lead to discomfort and heat stress, which reduces the body's capacity to regulate its temperature effectively [29]. In the context of vehicles, thermal comfort is perceived when the human body attains heat balance under specific environmental parameters such as air temperature, humidity, radiant temperature, air velocity, metabolic activity level, and clothing insulation [30].

Comfort studies in public transport vehicles often encompass thermal, acoustic, luminous, vibration, air quality, and ergonomic comfort dimensions, as these factors collectively affect passenger perception of service quality and influence their choice to use public transportation systems [31]. Among these factors, thermal comfort has been widely recognized as a critical determinant of passenger satisfaction, particularly in high-occupancy transport modes such as buses. For instance, a field study conducted in China reported that passengers experienced notable thermal discomfort despite the presence of an air-conditioning system, due to elevated internal temperatures during operation.

Table 1
PMV–PPD Thermal Comfort Scale

PMV Value	Thermal Sensation	Percentage of People Dissatisfied (PPD)	Comfort Interpretation
+3	Very Hot	~99%	Severe discomfort; unacceptable
+2	Hot	~75%	Uncomfortable
+1	Slightly Warm	~25%	Borderline comfort; may feel warm
0	**Neutral (Comfortable)**	**~5%**	**Optimal comfort zone**
-1	Slightly Cool	~25%	Borderline comfort; may feel cool
-2	Cold	~75%	Uncomfortable
-3	Very Cold	~99%	Severe discomfort; unacceptable

Note. Comfortable conditions are typically achieved when PMV lies within −0.5 to +0.5 (PPD ≤ 10%).

Patania et al. [4] examined thermal comfort conditions experienced by public transport passengers in Catania through field measurements conducted on both air-conditioned subway carriages and non-air-conditioned buses. The study utilized several bioclimatic and comfort indices, including the Predicted Mean Vote (PMV), Predicted Percentage of Dissatisfied (PPD), Humidex, Summer Simmer Index (SSI), and Relative Warmth Index (RWI), to assess the thermo-hygrometric environment. Although the PMV index was referenced, the study did not explicitly report the PMV values or the corresponding thermal sensation categories, which limits a direct interpretation of the thermal comfort level on the standardized −3 to +3 scale. However, the reported PPD values provide strong evidence of discomfort patterns. In the non-air-conditioned buses, PPD values ranged between 90% and 100%, indicating that nearly all passengers experienced thermal dissatisfaction. This high dissatisfaction was linked to significantly elevated internal temperatures and humidity levels, with Humidex and SSI values indicating conditions associated with strong physiological heat stress and even potential heat stroke risk. Conversely, in the air-conditioned subway carriages, PPD values were substantially lower, between 10% and 30%, suggesting near-comfort conditions, although some passengers reported sensations of slight cool discomfort due to internal temperatures frequently falling below 26°C. These findings demonstrate that the presence and control of mechanical cooling systems strongly influence the thermal comfort outcomes of public transport passengers, and highlight the need for balanced temperature regulation to avoid both overheating and overcooling in enclosed transport environments.

Research on long-distance public transportation emphasizes the importance of maintaining thermal comfort over prolonged travel durations. However, literature on such studies remains more extensive in the building sector than in transportation. While some automotive-related studies exist, they predominantly focus on private cars[32] [30]. As highlighted by previous research [33], the thermal environment in large-capacity public transport vehicles such as urban buses and rail systems differs substantially from that of private cars. The larger cabin volume in buses accommodates more passengers but also introduces greater spatial variability in temperature and airflow patterns. Factors such as vertical temperature gradients, uneven air recirculation, extensive window surface area, and frequent door opening further contribute to fluctuations in the internal thermal environment. These variations can

cause localized discomfort and complicate climate control management.

Due to these challenges, several studies have incorporated both experimental measurements and Computational Fluid Dynamics (CFD) simulations to analyse airflow and temperature distribution within vehicle interiors. CFD-based modelling allows a detailed examination of complex air movement and heat exchange processes, thereby facilitating the evaluation and improvement of thermal comfort conditions for passengers.

2.3.1 Thermal Comfort Factors

Thermal comfort refers to an individual's subjective perception of the thermal environment, reflecting their satisfaction with surrounding conditions [7]. People respond differently to the same environmental conditions; hence, the thermal sensation experienced by each individual may vary. This variability implies that not all occupants require identical environmental conditions to achieve comfort. Thermal comfort is influenced by six key factors, which are divided into two categories: environmental (measured) factors and personal factors. Environmental factors include air temperature, air velocity, mean radiant temperature (MRT), and relative humidity (RH), while personal factors comprise metabolic activity (human activity level) and clothing insulation.

These six factors are precisely those used in the calculation of the Predicted Mean Vote (PMV) and Predicted Percentage of Dissatisfied (PPD) indices, which quantify thermal comfort. The PMV predicts the mean thermal sensation vote of a large group of people on a seven-point scale ranging from cold (-3) to hot (+3), while the PPD estimates the percentage of occupants likely to feel thermally dissatisfied [7]. Accurately assessing these variables in enclosed spaces, such as vehicle cabins, is therefore essential for evaluating occupant comfort using the PMV–PPD model.

2.3.1.1 Air Temperature

Air temperature refers to the average temperature of the air surrounding the human body, considering both spatial and temporal variations [33][7]. In vehicles

equipped with air-conditioning systems, the internal temperature is often non-uniform. For summer conditions, the recommended thermal comfort range is between 23 and 28°C [7]. Typically, the air temperature at the lower cabin region (ankle level) is higher than at head level, with a vertical temperature gradient of approximately 3°C[17][32]. Variations in cabin temperature are also influenced by vehicle size and interior materials; for example, larger vehicles with leather upholstery may experience different warming or cooling dynamics compared to smaller economy-class cars[33][17]. These spatial differences directly affect PMV calculations, as air temperature is a critical input parameter.

2.3.1.2 Air Velocity

Air velocity refers to the speed of air movement surrounding the human body at a given location and time. The body is particularly sensitive to airflow around regions such as the head, neck, and feet, and this sensitivity varies between individuals. When airflow is uneven or excessively high, local thermal discomfort—often referred to as draught discomfort—may occur. Therefore, the ability to regulate both the magnitude and direction of airflow is essential for maintaining acceptable comfort conditions, as outlined in the [9].

In vehicle cabins, conditioned air is supplied through adjustable air vents as part of the air-conditioning and ventilation system. This airflow influences the thermal microenvironment and affects convective heat loss from the body. Because vent placement and air distribution vary throughout the cabin, local air velocities and temperatures are not uniform. Previous studies have reported that typical in-vehicle air velocities generally range from 0.1 to 0.4 m/s, depending on system setting and vent direction [34]. Research has also shown that airflow distribution tends to stratify vertically, where warmer air rises to the upper cabin region and cooler air settles lower, leading to noticeable temperature and velocity gradients around the occupant [33].
For optimal comfort, airflow should:

- Maintain a stable and comfortable local skin temperature,
- Support natural convection around the body,
- Avoid draughts, particularly near the head and eyes,
- Deliver clean and fresh air effectively to the breathing zone.

From the perspective of the PMV–PPD thermal comfort model, air velocity is a key environmental variable because it regulates convective heat exchange between the skin and the surrounding air. In warm environments, increasing air velocity can reduce PMV values by enhancing heat dissipation; however, if airflow becomes excessive in cooler environments, PPD increases due to localized draught discomfort. Therefore, achieving balanced and well-directed airflow is essential in vehicle cabins to attain acceptable thermal comfort for the majority of occupants.

2.3.1.3 Relative Humidity

Relative humidity (RH) is defined in ASHRAE Standard 55 as the ratio of the actual water vapour content in the air to the maximum amount of water vapour that the air can hold at a given temperature and pressure. In an enclosed vehicle environment, the water vapour pressure is generally uniform; therefore, RH can be reliably measured at a single representative location within the cabin. The human body is sensitive to variations in RH because humidity directly influences the rate of evaporative heat loss from the skin, which is essential for maintaining thermal balance.

Research has shown that thermal comfort is generally perceived to be optimal when RH is maintained near approximately 50% [34] The level of humidity within the cabin affects the evaporation of perspiration from the skin, which is the primary mechanism for heat dissipation in warm conditions. According to ASHRAE Standard 55, thermal comfort is typically not adversely affected when RH is maintained within the range of 30% to 70%, as this range supports adequate evaporative cooling without inducing excessive dryness. However, when RH exceeds 70%, the evaporation of sweat is hindered, resulting in sensations of stuffiness and discomfort. Conversely, when RH falls below 30%, the air becomes excessively dry, potentially causing irritation of the skin and mucous membranes, which may also negatively affect perceived thermal comfort [33].

Table 2 summaries the recommended indoor temperature and RH values in relation to prevailing outdoor conditions.

Table 2
Recommended Indoor Temperature and RH Values

Season	Outdoor Temperature (°C)	Indoor Temperature (°C)	Minimum Relative Humidity (%)	Maximum Relative Humidity (%)
Winter	≤ ±20	22	35	70
Summer	+20	22	-	70
	+25	23	-	65
	+30	25	-	60
	+32	26	-	55

Recommended indoor temperature and relative humidity ranges are adopted from ASHRAE Standard 55 and ISO 7730

The Mean Radiant Temperature (MRT) is defined as the uniform temperature of an imaginary enclosure in which the net radiant heat exchange between the human body and the environment is equivalent to that in the actual physical surroundings. This definition is formally established in ISO 7730:2005 and is also presented in the ASHRAE Handbook—Fundamentals. MRT represents the combined radiant influence of surrounding surfaces and is therefore the area-weighted average of the temperatures of all surfaces visible to the body. Because radiant heat transfer can significantly influence the human thermal balance, particularly in enclosed or solar-heated environments, MRT is a key parameter in evaluating thermal comfort.

MRT can be measured using radiative sensors or estimated indirectly based on the temperature and geometric relationships of surrounding surfaces. In practice, the operative temperature is often used to simplify thermal comfort assessment, as it incorporates the combined effects of air temperature and MRT while assuming minimal influence from air velocity. This operative temperature may be measured directly using an unheated ellipsoid-type sensor, providing a practical approximation for vehicle cabin environments [33].

Two key personal characteristics that influence thermal comfort are human activity level, q_o (1 met = 58.2 W/m²), and clothing insulation, I_{cl} (1 clo = 0.155 m²K/W). According to ASHRAE 55 and ISO 7730, 1 met represents the rate of energy produced per unit surface area of an average person at rest (58.2 W/m²), and 1 clo represents the thermal insulation of clothing that maintains comfort at a given environment Occupants inside a vehicle are generally almost completely motionless, resulting in low metabolic rates. Higher activity levels generate more metabolic heat, which, if excessive, can lead to sweating and thermal discomfort. Activity level also influences human thermal sensitivity, comfort perception, and preferred indoor temperatures [7]. Table 5 presents an estimation of metabolic rates for common activities.

Table 3
Estimation of Metabolic Rate for Basic Activities

Basic Activity	**Estimation of Metabolic Rate**
Lying down	0.8 met – 47 W/m²
Sitting quietly	1.0 met – 58 W/m²
Seated office work	1.2 met – 70 W/m²
Light work	1.6 met – 93 W/m²
Medium work	2.0 met – 117 W/m²
Heavy work	3.0 met – 175 W/m²

Sources: Values adopted from ISO 7730.

Clothing insulation (I_{cl}) reflects the thermal resistance provided by clothing and varies according to both the material and the thickness of garments. Higher insulation reduces heat loss from the body and helps maintain thermal balance, either preventing heat loss in cold conditions or contributing to overheating if excessive. Table 6 provides typical clothing insulation values for various clothing ensembles.

Table 4
Clothing Levels and Thermal Insulation

Description	Thermal Insulation Range (Clo)
Winter outdoor clothing	2 – 3
Normal indoor clothing	1.2 – 1.5
Summer indoor clothing	0.8 – 1.2
Indoor lightweight clothing	0.3 – 0.5

Sources: Values adopted from ASHRAE 55 & ISO 7730

Each part of the human body has a distinct skin temperature, and clothing insulation can be used by occupants to adjust their thermal environment. The simplest method for regulating personal comfort in a vehicle is by adding or removing clothing layers.

2.4 Thermal comfort Evaluation by Using Fanger's Predicted Mean Vote (PMV) and Predicted Percentage Dissatisfied (PPD)

In 1970, Fanger developed the Predicted Mean Vote (PMV) and Predicted Percentage of Dissatisfied (PPD) indices, which have since become the foundation of modern thermal comfort assessment. Following extensive experimental validation, these indices were adopted by the majority of experts and incorporated into the international standard ISO 7730, establishing a theoretical framework for evaluating human thermal comfort. The PMV index predicts the average thermal sensation of a large group of occupants based on environmental and personal parameters, including air temperature, mean radiant temperature, air velocity, relative humidity, metabolic rate, and clothing insulation [35]. The resulting PMV value corresponds to the Thermal Sensation Scale, as presented in Table 5.

Table 5
Thermal Sensation Scale of PMV

Thermal Sensation	PMV
Hot	+3
Warm	+2

Slightly Warm	+1
Neutral	0
Slightly Cool	-1
Cool	-2
Cold	-3

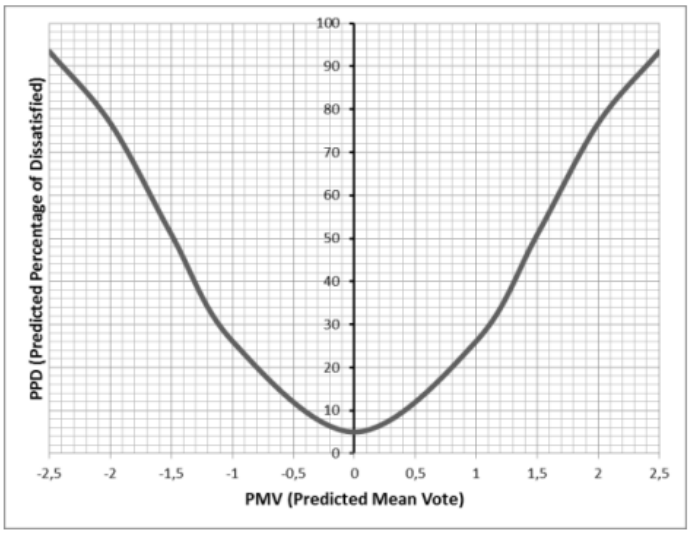

Figure 3: The Relationship between PMV and PPD

Figure 3 illustrates the relationship between PMV and PPD. The curve demonstrates that the PPD reaches its minimum value at PMV = 0, which represents thermal neutrality [35]. At this point, approximately 5% of occupants are still predicted to be dissatisfied, indicating that complete satisfaction cannot be achieved even under ideal thermal conditions. As the PMV value deviates from the neutral point toward warmer (positive) or cooler (negative) sensations, the PPD increases rapidly. When PMV approaches ±2.5, the PPD exceeds 90%, suggesting that most occupants perceive the environment as either uncomfortably hot or cold.

Thermal comfort standards such as ISO 7730 and ASHRAE 55 recommend maintaining PMV values within the range of –0.5 to +0.5, corresponding to a PPD below 10%, to ensure acceptable comfort levels [36]. The PMV–PPD model is widely applied in various computational and simulation tools to evaluate thermal comfort under different environmental conditions. These include the Centre for the Built Environment (CBE) Thermal Comfort Tool, EnergyPlus, and Computational Fluid Dynamics (CFD)

software such as ANSYS Fluent, SolidWorks Flow Simulation, SimScale, and OpenFOAM. For example, in [37] Prabhakaran employed SolidWorks Flow Simulation to evaluate indoor thermal comfort and airflow distribution based on PMV and PPD indices. Similarly, TRNSYS has been utilized to optimize air-conditioning system control and assess thermal comfort performance using PMV–PPD indicators [5]. These software platforms enable detailed analysis and prediction of comfort parameters, bridging experimental data and computational models to improve HVAC system design and occupant well-being. Unlike buildings, thermal comfort in vehicles is influenced by additional factors such as solar radiation, uneven radiant temperatures, and inadequate insulation, all of which complicate the achievement of uniform comfort levels [38].

2.5 Previous Research using Predicted Mean Vote (PMV) and Predicted Percentage Dissatisfied (PPD) Indices to Evaluate Thermal Comfort

Previous studies on airflow and thermal comfort in vehicles have investigated various configurations using methods such as Predicted Mean Vote (PMV), Predicted Percentage of Dissatisfied (PPD), and Dynamic Thermal Sensation (DTS) to evaluate overall thermal comfort [39]. Unlike PMV–PPD, which provides a quantitative assessment of thermal comfort based on steady-state heat balance and predicts the percentage of dissatisfied occupants, DTS accounts for transient or time-varying thermal conditions, capturing occupants' thermal responses to changing environments. DTS is particularly useful in scenarios where temperatures or airflow fluctuate, whereas PMV–PPD assumes steady-state conditions. One study examined two cars with different air distribution systems under fully loaded conditions, with a total of five occupants. The simulation was conducted using the vehicle's CAD geometry and a shell finite element model that incorporated interior components. Results indicated that the vehicle equipped with both front and rear air vents demonstrated superior temperature distribution and enhanced thermal comfort for occupants.

Through the increasing popularity of public transportation, several studies have focused on airflow and passenger thermal comfort in air-conditioned buses using Computational Fluid Dynamics (CFD) simulations along with PMV and PPD indices

[25]. In the study done in [25], thermal comfort in a standard air-conditioned bus was evaluated under different operational scenarios, including ventilation at maximum capacity, ventilation at maximum capacity with an installed air deflector, and vehicle operation at 14 m/s with two rear windows open. The findings revealed that the addition of an air deflector improved passenger comfort due to more uniform air distribution. The study, however, was limited by a lack of real-world validation and did not consider variations in passenger activity or occupancy levels. Similarly, research on a four-seater car cabin applied PMV–PPD indices to assess thermal comfort under controlled conditions. The study emphasized that PMV–PPD calculations require the human body to be in a near-steady-state thermal equilibrium over an extended period, as the PMV equation is based on steady-state heat transfer between the human body and the surrounding environment. Environmental conditions were set to sunny days with an ambient temperature of 33°C and moderate humidity, while the occupants' physical states were assumed to involve no vigorous activity, normal skin temperature, and standard perspiration rates.

Another study [40] employed numerical simulations alongside PMV–PPD indices to evaluate the thermal environment inside a vehicle cabin. Two cases were considered: simulations without a virtual manikin and simulations including a virtual manikin. The left air vent guiding vane angle varied from 0° to 30°, and thermal responses were measured at sixteen points on the manikin, including the head, knees, and feet. Results indicated that PMV and PPD values largely remained within acceptable ranges close to thermal neutrality, with the optimal air vent vane angle determined to be 0°. Increasing the angle of the vent caused a decrease in PMV values, suggesting an increased cooling sensation.

In the present research, CFD simulations will be conducted using SolidWorks software to evaluate airflow and thermal comfort in an Automated Rapid Transit (ART) system. PMV and PPD indices will be employed as references to assess passenger thermal comfort and to guide the analysis of environmental conditions within the transit vehicle.

2.6 Simulation of Air Flow and Thermal Comfort Employing Computer Fluid Dynamic (CFD)

Table 6
Researches on Air Flow and Thermal Comfort with The Application of CFD Simulation

No	Applications	Year	Authors	References	Notes
1	Ventilation & Thermal Comfort	2018	M. V. Wilson	[41]	CFD simulations used a pressure-based solver with k-ε turbulence model. Geometry was simplified, and no experimental validation was reported.
2	Air flow & Thermal Comfort	2019	I. L. Scurtu and A. N. Jurco	[25]	PMV–PPD indices applied for thermal comfort. Bus geometry simplified, turbulence model not specified, no field validation reported.
3	Air Flow & Distribution study	2015	N. E. Ahmad Shafie et al	[3]	Standard k-ε turbulence model applied; steady-state incompressible flow assumed. Experimental boundary conditions measured, but thermal comfort evaluation not performed.
4	Thermal Comfort Study (inside of car cabin)	2017	B. Zhang et al.	[40]	Realizable k-ε turbulence model applied; CFD results validated against

					experimental data (<5% deviation), reliable for interior thermal comfort prediction.
5	Air Flow & Thermal Comfort study (inside of car cabin)	2018	P. Danca et al.	[42]	Virtual manikin used; steady-state simulation, PMV–PPD indices applied. No physical validation reported.
6	Air flow simulation using CFD	2015	S. Lin et al.	[43]	k-ε turbulence model; indoor airflow patterns analyzed, but thermal comfort not evaluated. No experimental validation included.
7	Air flow & Thermal Comfort using CFD	2019	A. Raczkowski et al.	[44]	k-ε turbulence model; PMV–PPD indices applied for naturally ventilated indoor space; validation limited to CFD predictions.

Computational Fluid Dynamics (CFD) has been widely applied to analyse airflow and thermal comfort in transport environments, allowing researchers to simulate the distribution of air velocity, temperature, and other thermal parameters within vehicle cabins. CFD enables the prediction of airflow behaviour under different ventilation setups and boundary conditions, providing a cost-effective and detailed approach to study occupant comfort without extensive physical experimentation. In transport studies, CFD is commonly coupled with thermal comfort indices such as Predicted Mean Vote (PMV) and Predicted Percentage Dissatisfied (PPD) to assess passenger comfort quantitatively [45].

For example, Wilson [41] employed CFD to evaluate the airflow pattern and ventilation effectiveness in an air-conditioned bus cabin. The bus geometry was

modelled in SolidWorks and simulations conducted in ANSYS Fluent using a pressure-based solver with the k-ε turbulence model. The study found that air velocity was higher in the middle of the bus than at the front, and that inlet airflow speed was critical to ensuring passenger comfort. However, the study focused only on airflow distribution without applying a thermal comfort model, and validation against experimental data was not reported.

In another study [25], CFD simulations were performed for three bus ventilation scenarios: (i) maximum ventilation, (ii) maximum ventilation with air deflectors, and (iii) bus traveling at 14 m/s with two rear windows open. Air velocity and temperature distributions were analyzed, and PMV–PPD indices were used to assess comfort. The study concluded that the configuration with mounted air deflectors provided the most uniform air distribution and improved thermal comfort (PMV range 0–1.28). Limitations included geometric simplifications to reduce computational cost and the absence of a turbulence model specification.

Similarly, a study on a university shuttle bus compared mixing and displacement ventilation systems [3]. CFD simulations employed a standard k-ε turbulence model with steady-state assumptions, incompressible airflow, and boundary conditions derived from field measurements (23°C, 2.9 m/s air velocity). The displacement ventilation system produced a more uniform airflow and temperature distribution; however, thermal comfort was not evaluated, and results were limited to steady-state conditions.

CFD has also been applied in car cabin studies. Zhang et al. [40] used CFD with STAR-CCM+ to simulate airflow, temperature, and PMV–PPD indices in a four-seater car, incorporating the effects of solar and wall heat radiation. The Realizable k-ε turbulence model was applied, and the simulation was validated against experimental data with less than 5% deviation. Results showed that airflow uniformity and air inlet placement significantly influenced thermal comfort, with PMV values concentrated around 0.8–0.9 and PPD between 20% and 25%.

Another vehicle study [42] examined the impact of a driver's body on airflow and thermal comfort using CFD simulations with and without a virtual manikin. The

left air vent angle was varied from 0° to 30°, and PMV–PPD indices were calculated assuming a metabolic rate of 1 met and clothing insulation of 0.7 clo. The results indicated that the most advantageous vane angle was 0°, maintaining PMV and PPD values near thermal neutrality, while larger angles increased cooling sensation.

In addition, studies on indoor environments have supported CFD application for thermal comfort research. For instance, simulations in lecture rooms [43] and naturally ventilated spaces [44] demonstrated airflow patterns and PMV–PPD-based comfort evaluation, reinforcing the reliability of CFD for analysing complex thermal environments in both buildings and vehicles.

While CFD has proven effective in simulating airflow and assessing thermal comfort in buses, cars, and indoor spaces, several gaps remain. Few studies have focused on Automated Rapid Transit (ART) systems, especially under hot–humid climates typical of Malaysia. Moreover, limited research has simultaneously combined detailed airflow analysis with PMV–PPD evaluation in high-capacity passenger vehicles. This highlights the need for CFD-based investigations specifically targeting ART cabins, incorporating realistic operational conditions and validated thermal comfort assessments.

CHAPTER 3
RESEARCH METHODOLOGY

3.1 Introduction

This chapter outlines the methods employed in this thesis to achieve the stated goals and objectives. It details the research techniques, design, and analysis, and provides the rationale behind the selected approaches.

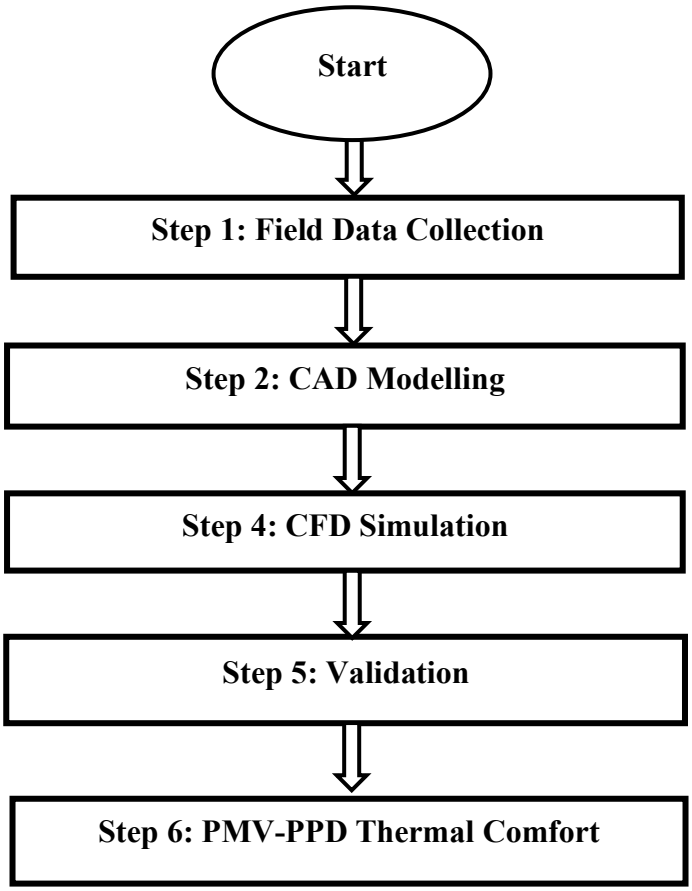

In this research, a systematic approach was followed in the project methodology. The process began with a comprehensive study of the Automated Rapid Transit (ART) system and a review of existing airflow and thermal comfort studies conducted on conventional buses. A CAD model of the ART was created using SolidWorks, informed by data collected from the real ART system. This was followed by a Computational Fluid Dynamics (CFD) analysis to simulate airflow patterns. Finally, the Predicted

Mean Vote (PMV) and Predicted Percentage of Dissatisfied (PPD) indices were applied to evaluate thermal comfort based on the simulation results.

3.2 Selected Space and Characteristics

The Automated Rapid Transit (ART) vehicle examined in this study is the ART L3 model, a three-carriage urban transit system with an overall length of approximately 30 meters. The ART is a bi-directional vehicle equipped with driver's cabs at both ends, enabling full-speed operation in either direction. Its design includes a central accordion joint that connects the carriages and allows the vehicle to articulate during turning manoeuvres.

For the purpose of this study, the middle carriage was specifically selected as the simulation domain, as it represents the most thermally stable and operationally consistent section of the vehicle. Unlike the front and rear carriages, the middle module is less affected by door openings, driver cabin equipment, and external heat infiltration, making it the most appropriate location for assessing internal airflow behaviour and passenger thermal comfort with minimal external disturbance.

Figure 4 presents the schematic geometry of the ART L3. This schematic is essential for illustrating the spatial configuration, airflow pathways, and internal features considered in the Computational Fluid Dynamics (CFD) model, thereby ensuring clarity and reproducibility of the modelling approach.

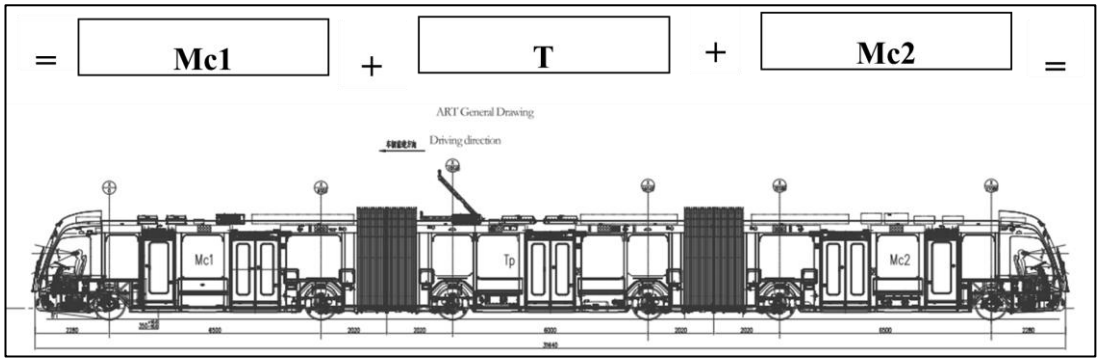

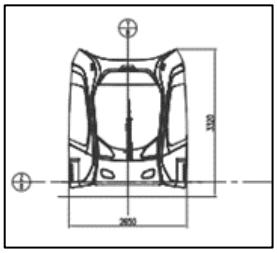

Figure 4: General Drawing of ART

Which Includes: -

- = : ART Vehicle coupler
- + : Articulation & Inter-car Equipment
- Mc : Motor car (with Driving Cab)
- T : Trailer car

Additionally, focusing on a single carriage ensured that the Computational Fluid Dynamics (CFD) model remained computationally feasible within the constraints of available time and software capability. The high geometric complexity and detailed specifications of the full three-carriage ART configuration would substantially increase meshing requirements, computational load, and simulation duration. Therefore, restricting the simulation domain to Carriage T allowed for a balance between model accuracy, computational efficiency, and timely completion of the analysis.

Table 7
Transport Capacity

Condition	Definition	Passenger Capacity			
		Mc1	T	Mc2	Total
Seated Capacity（AW1）	The number of seats	7	**16**	10	33
Normal Capacity（AW2）	Seated capacity + 6 passengers/m^2	80	**74**	85	239
Ultra-capacity（AW3）	All Passenger Capacity + 8 passengers/m^2	107	**90**	110	307

Table 7 summarizes the three passenger-load conditions used in this study: AW1 (Seated Capacity), AW2 (Normal Capacity), and AW3 (Ultra-capacity). These

conditions were derived from the passenger capacity specifications of the ART L3 vehicle and represent progressively increasing occupancy levels. The seated capacity (AW1) includes only passengers occupying available seats. The normal capacity (AW2) adds standing passengers at a density of 6 passengers/m², reflecting typical peak-hour loading. The ultra-capacity condition (AW3) incorporates a maximum loading scenario, defined as the total seated and standing capacity plus an additional 8 passengers/m², simulating extreme crowding situations.

These three loading conditions were specifically applied as boundary conditions in the CFD simulation and thermal comfort analysis. In the CFD model, the number and distribution of passengers were incorporated as heat sources (metabolic heat), physical obstructions to airflow, and contributors to the internal flow resistance. Each AW condition therefore modifies the airflow patterns, temperature distribution, and turbulence levels within the carriage. For the PMV–PPD thermal comfort evaluation, the corresponding passenger load was used to determine metabolic heat generation, internal heat accumulation, and variations in mean radiant temperature and air velocity. This ensured that each scenario (AW1, AW2, AW3) realistically represented actual passenger density and its influence on thermal comfort.

3.3 Field Measurements

Field measurements were conducted to obtain baseline data on the air temperature and air velocity inside the ART carriage. These measurements served as fundamental inputs for defining the boundary conditions and for validating the Computational Fluid Dynamics (CFD) model. A UNI-T Mini LCD Anemometer (UT363) was employed due to its demonstrated measurement reliability, portability, and cost efficiency.

All measurements were taken under the AW0 condition, in which no passengers were present in the carriage. This condition reflects the baseline operational state recorded during the ART pilot testing phase. Air velocity and temperature readings were collected at the air inlet, as well as at several surrounding points within the carriage, to capture spatial variations in airflow and thermal conditions. The recorded data are presented in Appendix 2.

In the CFD simulations, human models representing different passenger categories were included as dummies to replicate the presence of occupants within the carriage. These models were assigned a constant metabolic heat generation rate corresponding to their activity level, allowing them to act as heat sources within the simulation. This approach ensured that both the physical obstruction effect on airflow and the thermal contribution of passengers were accurately represented in the analysis, providing realistic boundary conditions for subsequent PMV–PPD thermal comfort evaluation.

Model validation was performed using the AW0 dataset prior to progressing with the full numerical modelling. The validation process involved comparing simulated air velocity and air temperature values against the field-measured data collected at corresponding locations within the carriage. Agreement between the experimental measurements and CFD predictions ensured that the model accurately represented the physical behaviour of the airflow system. Only after achieving acceptable alignment between measured and simulated conditions was the model considered suitable for subsequent analyses under passenger-loaded scenarios (AW1, AW2, and AW3).

3.4 Numerical Modelling Physical Modelling

3.4.1 Measurement of ART

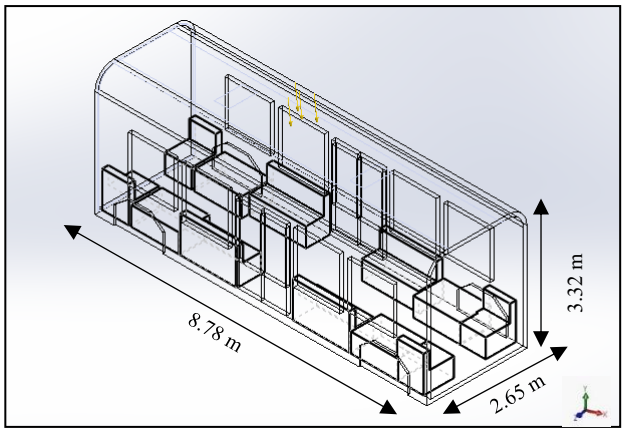

Figure 5: Measurement of ART Middle Carriage

Computer-Aided Design (CAD) was utilised in this study to develop and analyse the geometric model of the Automated Rapid Transit (ART) system. A three-dimensional CAD model was constructed in SolidWorks based on the ART's general engineering drawings, ensuring that the principal dimensions accurately reflected those of the actual vehicle. To improve computational efficiency and ensure a manageable meshing process, the model was simplified while retaining all geometric features that substantially influence airflow behaviour. This approach is consistent with established CFD practices, where simplified interior geometries have been demonstrated to provide reliable airflow and thermal comfort predictions [25][41]. Although such simplifications may introduce minor deviations in highly localised airflow regions, the overall velocity distribution, temperature fields, and PMV–PPD outcomes remain dependable when major boundary conditions and key obstructions are preserved.

For this reason, only the middle carriage—measuring approximately 8.78 m (L) × 2.65 m (W) × 3.32 m (H)—was selected as the computational domain, as it represents the typical interior layout of the ART. The simplified model includes essential structural and ventilation components such as eight windows and one exit door on each side, air inlets positioned along the right and left sections of the ceiling, and two central return grilles. Interior features, including passenger seats and block-shaped human models, were incorporated to represent occupant presence and maintain the physical fidelity required for accurate airflow and thermal comfort analysis.

3.1.1 Geometry Development and Passenger Modelling

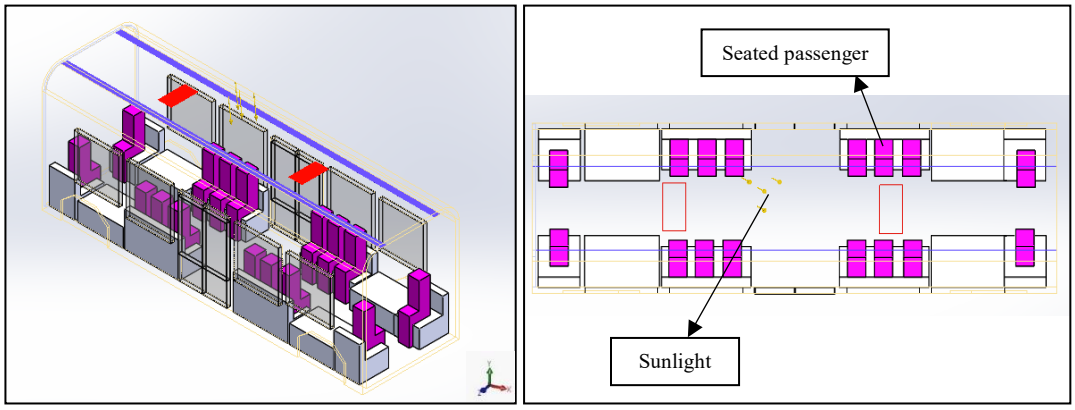

Figure 6: (i) ART Model Isometric View (AW1) and (ii) Top View (AW1)

A three-dimensional geometric model of the ART middle carriage was developed using SolidWorks, as illustrated in Figures 6, 7, and 8. Each figure corresponds to one of the passengers' loading conditions modelled in this study: AW1 (16 passengers), AW2 (74 passengers), and AW3 (90 passengers). In these representations, purple blocks denote seated passengers, while brown and grey blocks denote standing passengers. Although simplified into block geometries for computational feasibility, the human models were assigned thermal properties consistent with standard metabolic heat production and clothing insulation levels. These values were implemented as surface heat fluxes in accordance with ASHRAE Standard 55 and ISO 7730, ensuring that simulated occupants contributed realistically to the internal thermal load.

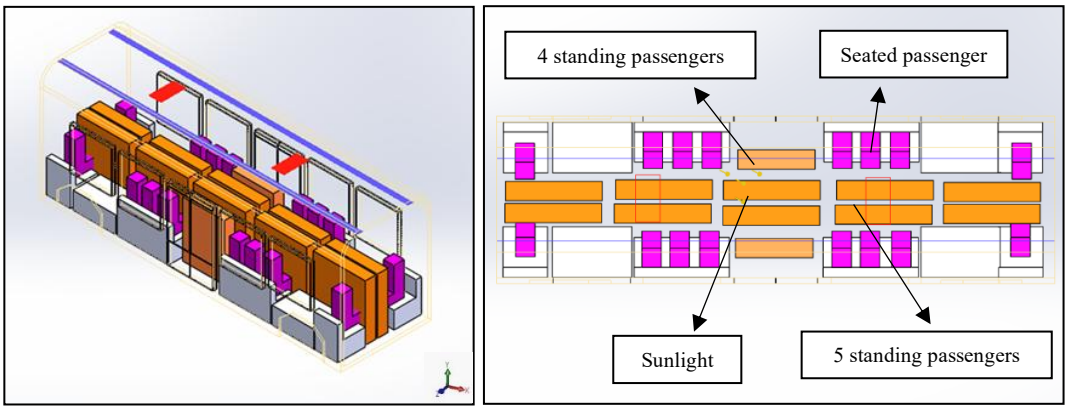

Figure 7: (i) ART Model Isometric View (AW2) and (ii) Top View (AW2)

Figure 7 indicates a total of 74 passengers which falls under AW2 category and includes 16 seated passengers and 58 standing passengers. Standing passengers were represented by a brown block (5 passengers) and light brown block (4 passengers).

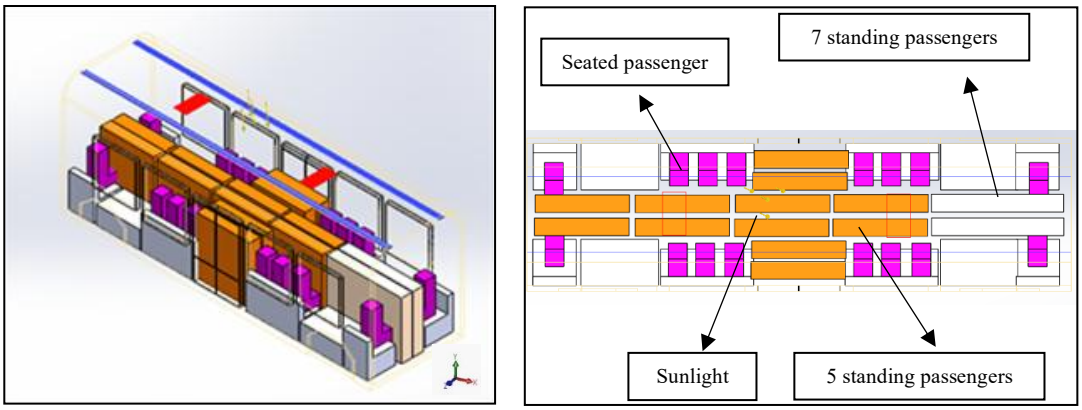

Figure 8: (i) ART Model Isometric View (AW3) and (ii) Top View (AW3)

A total of 90 passengers were represented in Figure 8 with category AW3 that includes 16 seated passengers and 74 standing passengers. Standing passengers were represented by a brown coloured blocks (each block indicates 5 passengers) and white coloured blocks (each blocks indicate 7 passengers).

Solar radiation was incorporated as an external heat source, with a uniform solar load of 600 W/m² applied to represent the effect of sunlight on the carriage surfaces [46][47]. The interior geometric domain includes essential elements such as seating, passenger block models, and primary enclosure surfaces to preserve the airflow characteristics relevant to ventilation performance and thermal comfort analysis.

3.1.2 Modelling Assumptions

The development of the ART middle carriage model was based on the following assumptions:

1. All interior components influencing airflow, including seats and human models were included within the simulation domain.
2. Passengers were assumed to be stationary and fixed in position throughout the simulation period. Each human model acted as a heat source, with thermal output defined using standard metabolic rates (in met) and clothing insulation values (in clo) derived from ASHRAE and ISO guidelines. These thermal loads were applied using appropriate heat flux boundary conditions.

3.1.3 Boundary Conditions for CFD Simulation

The CFD boundary conditions were defined to ensure realistic representation of the airflow and thermal environment within the ART carriage:

- Air Inlets: Fresh air was introduced through the ceiling inlets at velocities corresponding to the three airflow scenarios in this study.
- Turbulence Model: k–ε turbulence model was selected to capture the airflow behaviour and mixing characteristics within the enclosed space.
- Wall Surfaces: All walls were treated as no-slip.
- Air Return Grilles: Two ceiling-mounted return grilles served as outlets for air extraction, completing the ventilation cycle.
- Thermal Loads: Solar radiation, passenger metabolic heat and clothing insulations were included and kept constant.

These boundary conditions collectively ensure that the CFD model accurately captures the interaction between mechanical ventilation, solar loading, and human-generated heat within the ART environment.

3.4.2 Modelling Consideration of Human

A human body model was incorporated into the CFD simulation to accurately represent passenger presence, which is a critical factor in thermal comfort evaluation.

In this study, passengers were represented using simplified block geometries. Such simplifications are commonly used in CFD analyses of occupied spaces and have been shown to adequately capture the effects of human presence on airflow and thermal distribution without significantly affecting the simulation outcomes [48].

To represent standing passengers in the CFD domain, simplified geometric block models were used instead of detailed anthropomorphic manikins. This approach is widely employed in indoor airflow and transport-ventilation studies, as it provides realistic flow obstruction effects while maintaining computational efficiency. In accordance with standard adult anthropometric data, each standing passenger was modelled with a height of 1.60–1.70 m, a shoulder-width of approximately 0.45 m, and a body depth of 0.25–0.30 m. The use of simplified geometries is supported by recent CFD literature, where detailed scanned or digital human models are typically reserved for high-fidelity thermal or aerosol studies [17]. Additionally, pedestrian-level wind and indoor environmental analyses commonly evaluate airflow at heights corresponding to human stature (1.5–1.75 m), further validating the chosen dimensional range for representing standing passengers[49]. Together, these considerations ensure that the adopted passenger representation provides a realistic yet computationally tractable approximation of human presence within the ART cabin. Table 8 presents the dimensions and corresponding projected areas of the human block models used in this study.

Table 8
Measurement of Seated and Standing Passengers

Passengers	**Dimensions**			**Area (m^2)**
	Length	**Width**	**Height**	
Seated Passengers	0.573	0.310	1.083	0.175
Standing Passengers (4 persons)	1.219	0.310	1.625	0.372
Standing Passengers (5 persons)	1.524	0.310	1.625	0.465
Standing Passengers (7 persons)	2.133	0.310	1.625	0.651

Note. Block dimensions approximate typical adult sizes and follow common practices in CFD passenger modelling [50][51].

Previous studies have indicated that using highly detailed manikins, which closely resemble the human body, substantially increases both simulation time and

computational cost [52]. To enhance efficiency, the present study adopts a simplified block-shaped representation for passengers, as well as simplified geometries for interior furnishings. This approach allows for reduced modelling complexity without compromising the overall fidelity of the simulation. Furthermore, prior research has demonstrated that employing simplified manikin shapes is acceptable when necessary and does not significantly affect the accuracy of the results [48].

3.4.3 Airflow System

In this simulation analysis, constant boundary conditions were applied using three distinct supply air velocities—1.6, 2.9, and 3.2 m/s—and two inlet temperatures of 14.7°C and 8.7°C. These values were selected based on the actual operating conditions measured during field observations of the ART system, ensuring that the simulation reflects realistic ventilation performance. The velocity range also aligns with typical air distribution parameters reported in previous studies on public transport ventilation, while the temperature values represent the minimum and average supply air temperatures recorded during operation.

Given the complexity of the airflow behaviour within the ART middle carriage, the internal fluid flow was assumed to be fully turbulent. To achieve accurate predictions of turbulent behaviour, the standard k–ε turbulence model was employed in the CFD simulations [40]. The k–ε model is widely regarded as a robust and broadly applicable turbulence model for predicting indoor airflow patterns and has been extensively validated for HVAC and transportation ventilation studies[53].

Several idealized assumptions were incorporated to establish a controlled simulation environment and avoid unnecessary computational complexity:

a. The ART middle-carriage air-conditioning system is assumed to operate under normal and fully functional cooling conditions, consistent with previous bus cooling performance studies [28].
b. The middle carriage is considered fully enclosed, except for operational openings such as doors, windows, and exhaust vents, following common CFD modelling practices for vehicle interiors [27].

c. The external surface temperature of the ART is assumed constant, reflecting typical simplifications used for atmospheric and structural boundary conditions in CFD simulations [54].
d. Internal heat gains from electronic devices and lighting are neglected due to their relatively minor thermal impact compared to passenger metabolic loads [9] [38].
e. Geometric elements inside the carriage, including seats and human models, were included to represent realistic obstruction effects and thermal interactions, consistent with previous CFD studies using human surrogates or manikins [42][48].

The Standard k–ε turbulence model developed by Launder and Spalding (1974) was employed in this study due to its robustness, numerical stability, and computational efficiency in modelling fully turbulent indoor airflow. The Standard k–ε formulation remains one of the most widely used turbulence models for HVAC and ventilation studies, particularly in enclosed environments where the flow is steady and moderately complex. Its proven reliability and low computational cost make it suitable for simulating airflow distribution within the ART carriage [55].

Turbulent Kinetic Energy (k) Equation:

$$\frac{\partial k}{\partial t} + U_j \frac{\partial k}{\partial x_j} = \frac{\partial k}{\partial x_j}\left[\left(v + \frac{v_t}{\sigma_k}\right)\frac{\partial k}{\partial x_j}\right] + P_k - \epsilon \quad (1)$$

Dissipation Rate (ϵ) Equation:

$$\frac{\partial \epsilon}{\partial t} + U_j \frac{\partial \epsilon}{\partial x_j} = \frac{\partial}{\partial x_j}\left[\left(v + \frac{v_t}{\sigma_k}\right)\frac{\partial \epsilon}{\partial x_j}\right] + C_{1\epsilon}\frac{\epsilon}{k}P_k - C_{2\epsilon}\frac{\epsilon^2}{k} \quad (2)$$

Model Coefficients:

v_t: Turbulent viscosity

v_t: $C_\mu \frac{k^2}{\epsilon}$

Production of Turbulent Kinetic Energy (P_k)

$$P_k = v_t \left(\frac{\partial U_i}{\partial x_j} + \frac{\partial U_j}{\partial x_i} \right) \frac{\partial U_i}{\partial x_j} \tag{3}$$

Standard Coefficients:

$$C_\mu = 0.09$$
$$\sigma_k = 1.00$$
$$\sigma_\epsilon = 1.30$$
$$C_{1\epsilon} = 1.44$$
$$C_{2\epsilon} = 1.92$$

These coefficients follow the original formulation by Launder and Spalding (1974) [55].

In fluid dynamics, flow regimes are generally classified into laminar, transitional, and turbulent, each exhibiting distinct characteristics. Laminar flow is smooth and orderly; transitional flow represents an intermediate state in which small disturbances grow; and turbulent flow is dominated by chaotic fluctuations in velocity and pressure. Despite these behavioural differences, all regimes are governed by the same fundamental conservation equations.

In the context of this study, the airflow inside an Automated Rapid Transit (ART) cabin is most realistically modelled as turbulent. Forced mechanical ventilation in transit cabins often produces relatively high flow velocities, leading to large Reynolds numbers. CFD studies of train aerodynamics have reported Reynolds numbers on the order of 10^6 to 10^7, based on characteristic dimensions such as train height or width [56][50] These high Reynolds numbers indicate that inertial forces dominate over viscous forces, promoting turbulence. Although turbulent flow complicates numerical simulation due to its inherently unsteady and three-dimensional nature, accounting for turbulence is essential to accurately capture airflow patterns and thermal comfort conditions in ART cabins.

The airflow within the ART cabin is governed by the Continuity Equation (mass

conservation) and the Navier–Stokes Equations (momentum conservation). The continuity equation ensures mass is conserved within the flow domain:

Continuity Equation (Mass Conservation)

$$\frac{\partial \rho}{\partial t} + \frac{\partial (\rho u)}{\partial x} + \frac{\partial (\rho v)}{\partial y} + \frac{\partial (\rho w)}{\partial z} = 0 \tag{4}$$

The momentum equations describe the rate of change of momentum in the *x*, *y*, and *z* directions, accounting for pressure gradients, viscous effects, and body forces:

Conservation of Momentum

$$x - direction:$$

$$\rho \left[\frac{\partial u}{\partial t} + u\frac{\partial u}{\partial x} + v\frac{\partial u}{\partial y} + w\frac{\partial u}{\partial z}\right] \tag{5}$$
$$= -\frac{\partial p}{\partial x} + \mu\left(\frac{\partial^2 u}{\partial x^2} + \frac{\partial^2 u}{\partial y^2} + \frac{\partial^2 u}{\partial z^2}\right)$$
$$+ \frac{1}{3}\mu\left(\frac{\partial^2 u}{\partial x^2} + \frac{\partial^2 u}{\partial y^2} + \frac{\partial^2 u}{\partial z^2}\right) + \rho g_x$$

$$y - direction:$$

$$\rho\left[\frac{\partial v}{\partial t} + u\frac{\partial v}{\partial x} + v\frac{\partial u}{\partial y} + w\frac{\partial v}{\partial z}\right] = -\frac{\partial p}{\partial y} + \mu\left(\frac{\partial^2 v}{\partial x^2} + \frac{\partial^2 v}{\partial y^2} + \frac{\partial^2 v}{\partial z^2}\right) + \frac{1}{3}\mu\left(\frac{\partial^2 v}{\partial x^2} + \frac{\partial^2 v}{\partial y^2} + \frac{\partial^2 v}{\partial z^2}\right) + \rho g_y \quad (6)$$

$$z - direction:$$

$$\rho\left[\frac{\partial w}{\partial t} + u\frac{\partial w}{\partial x} + v\frac{\partial w}{\partial y} + w\frac{\partial w}{\partial z}\right] = -\frac{\partial p}{\partial z} + \mu\left(\frac{\partial^2 w}{\partial x^2} + \frac{\partial^2 w}{\partial y^2} + \frac{\partial^2 w}{\partial z^2}\right) + \frac{1}{3}\mu\left(\frac{\partial^2 w}{\partial x^2} + \frac{\partial^2 w}{\partial y^2} + \frac{\partial^2 w}{\partial z^2}\right) + \rho g_z \quad (7)$$

Where:

$p =$ static pressure
$\mu =$ dynamic viscosity
$\rho g_x, \rho g_y, \rho g_z =$ Body forces in the x, y and z direction

These governing equations are solved numerically using SolidWorks Flow Simulation, which discretizes the cabin geometry into small computational cells and applies the finite volume method to iteratively compute airflow parameters. Implementing these equations in the CFD solver ensures both mass and momentum are conserved within the ART cabin, allowing the simulation to accurately predict air velocity distributions, temperature fields, and turbulent effects generated by forced ventilation and passenger presence. Consequently, this approach provides a reliable basis for assessing thermal comfort conditions for passengers under realistic operational conditions.

3.5 Inlet and Outlet Mechanism

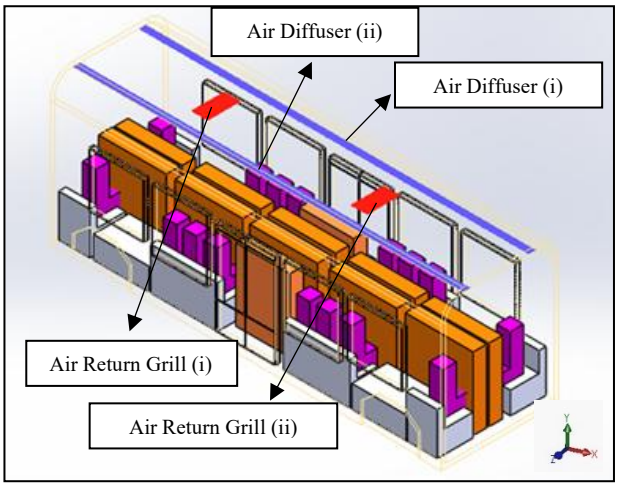

Figure 9: Location of Air Diffuser and Air Return Grill

The ART carriage is equipped with a series of modular roof-mounted ventilation and air conditioning units, designed in accordance with the technical requirements of the system. Each air conditioner comprises two air ducts and two plenum chambers, with air diffusers positioned above both sides of the passenger compartment. The air ducts are elongated in shape to provide uniform air supply along the entire length of the compartment. Additionally, two air return grills, each measuring 0.38 m × 0.75 m, were measured during field inspection and are installed between the diffusers in the central region of the cabin to facilitate air exhaust.

In the CFD simulations, air was supplied from the diffusers vertically downward at a uniform velocity of 1.6 m/s, corresponding to the low-velocity scenario, and scaled proportionally for the higher-velocity conditions of 2.9 m/s and 3.2 m/s. This setup establishes a well-defined inlet boundary condition, ensuring accurate representation of the airflow patterns within the passenger compartment and enabling realistic prediction of velocity distributions, air mixing, and thermal comfort throughout the cabin.

3.6 Thermal Parameters

Boundary conditions are critical for obtaining reliable simulation results, as highlighted by J. P. O'Sullivan [54] To ensure accurate representation of the ART cabin environment, on-site inspections were conducted to collect relevant boundary data necessary for calculating passenger comfort conditions. The numerical values used in this study were obtained from previous studies that incorporated field measurements and were subsequently applied in the simulations to solve the governing equations.

For the purposes of this study, it is assumed that the ART cabin surfaces maintain a constant exterior temperature. Heat contributions from lighting and electronic devices, such as digital gadgets, are considered negligible due to their relatively low power ratings and minimal impact on the overall cabin thermal load. For example, standard LED cabin lighting and personal electronic devices typically generate less than 5 W/m², which is small compared to the heat load from passengers and HVAC supply air [9].

The boundary conditions were applied consistently across the three passenger scenarios (AW1, AW2, AW3) and maintained constant, except for the operating temperature and air velocity. Passenger heat gains were modelled using a metabolic rate of 1.0 met and a clothing insulation level of 1.0 clo, representing a typical lightly active seated passenger wearing standard indoor clothing. The simulations were assumed to be in steady-state conditions [1][40]. A single set of values was used for all passengers to maintain uniformity in the thermal load and to avoid unnecessary variability, as the ART operates in a controlled indoor environment where differences in clothing and activity are minimal and have limited influence on steady-state conditions. The floor, ceiling, walls, and passenger seats were treated as adiabatic surfaces, as heat transfer through these components was found to be negligible compared to internal convective and radiative effects. Solar radiation was applied at 600 W/m² to represent external thermal input on the cabin structure. Air was supplied vertically downward through roof-mounted diffusers at uniform velocities of 1.6, 2.9, and 3.2 m/s, reflecting low, medium, and high operational airflow rates measured on-site. The inlet temperatures of 14.7 °C (stationary) and 8.7 °C (moving) were also obtained from field measurements. Return air was extracted through pressure outlet grills, allowing the outlet temperature

to adjust freely to conserve mass and reflect realistic exhaust behaviour. Together, these boundary conditions provide a robust and physically representative framework for accurately predicting airflow behaviour and thermal comfort within the ART cabin. Table 9 provides a summary of the numerical and thermal boundary conditions employed in this study.

Table 9
Boundary Conditions

No.	Variables	Boundary Conditions
1.	Passenger	• Metabolic Rate = 1.0 met • clothing insulation = 1.0 clo
2.	Floor	• Adiabatic
3.	Ceiling	
4.	Walls	
5.	Passenger's seats	
6.	Solar Radiation	• 600 W/m^2
7.	Air inlet (Diffuser)	• Vertical downward flow • Velocity = 1.6, 2.9, 3.2 m/s • Temperature = 14.7 °C (stationary), 8.7 °C (moving)
8.	Air outlet (Return Grill)	• Pressure outlet • Velocity determined by flow conservation • Temperature unconstrained

3.7 Meshing and CFD Framework

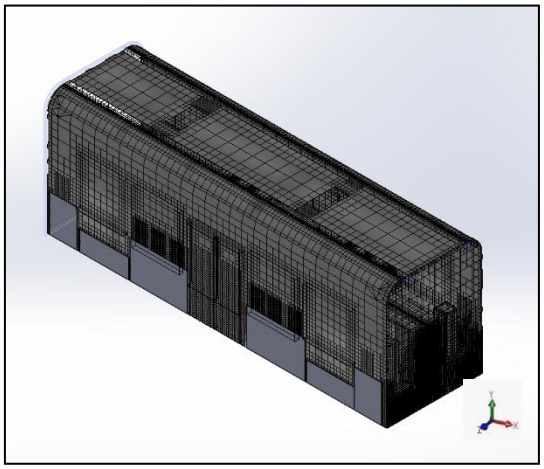

Figure 10: ART Meshed Model

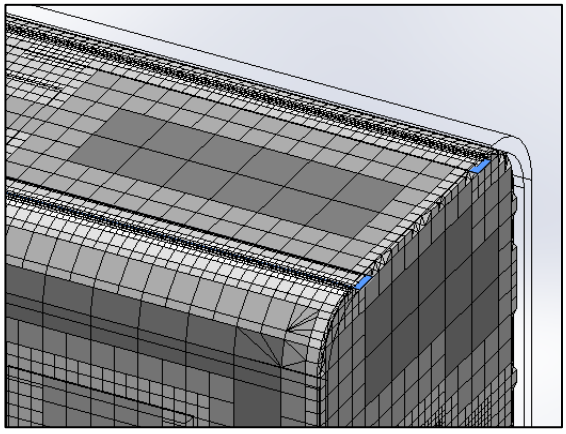

Figure 11: Zoomed-in Mesh near Diffusers

Figure 10 illustrates the computational mesh developed for the ART cabin model. The complex three-dimensional geometry was discretized into a finite number of control volumes using the Cartesian mesh approach implemented in SolidWorks Flow Simulation, which is based on the finite volume method. This meshing strategy was selected due to its robustness, low cell skewness, and reduced numerical diffusion compared with tetrahedral or hybrid unstructured meshes, particularly for enclosed airflow simulations [57]. The final computational domain consisted of 960,626 cells, providing sufficient geometric fidelity to capture the internal airflow characteristics. Figure 11 represent a mesh near diffuser area.

Table 10
Mesh Independence Test

Mesh	Averaged operative temperature (°C)	% change vs previous
Coarse	23.18	—
Medium	23.29	+0.47%
Fine	23.24	−0.21%

To assess the numerical sensitivity of the CFD model, a mesh-independence study was performed using the AW0 (empty cabin) configuration [58]. The averaged operative temperature was selected as the monitoring parameter due to its direct relevance to thermal comfort assessment. A mesh-independence criterion of 0.5% variation between successive mesh levels was adopted. As shown in Figure 11, the Coarse mesh produced an averaged operative temperature of 23.18 °C, while the Medium and Fine meshes yielded values of 23.29 °C and 23.24 °C, respectively. The variations between mesh levels were within the prescribed threshold and decreased with increasing refinement, confirming mesh-independent behavior. Consequently, the selected mesh resolution was considered numerically adequate and applied to all subsequent simulations. SolidWorks Flow Simulation was then used to compute the airflow patterns, temperature fields, and velocity distributions within the ART cabin.

3.8 Model Validation

Numerical modelling and the verification of CFD simulation parameters are essential to ensure the accuracy and reliability of the predicted airflow and thermal conditions. In this study, the CFD model was developed using the actual geometric dimensions of the ART middle carriage (8.78 m in length, 2.65 m in width, and 3.32 m in height). The ventilation components were also modelled according to on-site measurements, including the linear diffuser (8.78 m × 0.17 m) and the return outlet vent (0.38 m × 0.75 m). A Cartesian coordinate system (x, y, z) was defined at the bottom corner of the carriage model to specify airflow direction, where supply air entered through diffusers located on both sides of the ceiling and exited through the centrally positioned return vent. To replicate real cabin conditions as closely as possible, the indoor environment was modelled under turbulent flow, and thermal manikins with human-equivalent geometric and thermal properties were incorporated to represent passengers. The model also included eight passenger seats, four tyre compartments,

eight windows, and two sets of doors with glazing.

For validation, a baseline simulation (AW0) with zero passengers was conducted to correspond directly with the conditions during the physical measurements of the ART. Model validation was performed by comparing the simulated air temperature with the average experimental data obtained on-site. The validation was quantified using percentage error for absolute temperature difference. The results demonstrated strong agreement between the simulation and measurements, with temperature differences within ±2 °C. These values fall within acceptable limits for indoor airflow modelling, confirming that the developed CFD model is sufficiently accurate for analysing the thermal comfort and airflow distribution in subsequent passenger-loading scenarios.

3.9 Evaluation of PMV and PPD

3.9.1 Theory

For the assessment of thermal comfort, this study adopts Fanger's model, proposed by Fanger (1970) and later standardized in ISO 7730 and ASHRAE Standard 55. It is widely recognized for its strong empirical foundation and ability to provide realistic and reliable predictions of perceived thermal conditions [59]. The model computes indoor thermal comfort indices using the Predicted Mean Vote (PMV) and Predicted Percentage of Dissatisfied (PPD) metrics. According to the PMV–PPD framework, an individual's thermal sensation is governed by the balance between the body's heat production and heat loss to the surrounding environment, together with the corresponding physiological responses that regulate this balance [60]. This makes Fanger's approach particularly suitable for evaluating thermal comfort in enclosed and mechanically ventilated environments such as the ART cabin. The Predicted Mean Vote (PMV) index was computed using the classical thermal comfort equation originally The PMV formulation is expressed as:

$$PMV = (0.303e - 2.100 \times M + 0.028) \times [(M - W) - H - E_c - C_{res} - E_{res}] \quad (8)$$

PMV can be calculated by the equation shown above in (1)
Where,

M = human energy metabolic rate
W = external work (W/m^2)
H = convection and radiation heat loss
E_c = cooling and heat dissipation of perspiration on the skin (W/m^2)
C_{res} = respiratory sensible heat loss (W/m^2)
E_{res} = respiratory latent heat loss (W/m^2

This formulation explicitly models the human body's thermal balance by accounting for metabolic activity, heat losses through convection and radiation, and both sensible and latent heat losses through respiration and perspiration.
In this study, several CFD outputs serve as direct inputs to the PMV calculation. Specifically, the local air temperature, air velocity, and mean radiant temperature

(MRT) obtained from the simulation are used to determine the convective heat loss term H and to compute the environmental parameters required in the PMV model. Additionally, relative humidity and clothing insulation values are specified based on measurement data and standardized assumptions. These combined environmental and personal parameters allow the PMV–PPD indices to be accurately evaluated for all locations within the ART cabin.

Convection and radiation heat loss. The convective human body radiation heat loss is calculated using the following equation

$$H = 3.96 \times 10^{-8} \times f_{c1} \times [(t_{c1} + 273)^4 - (t_r + 273)^4] - f_{c1} \times h_c \times (t_{c1} - t_a) \quad (9)$$

Where,

f_{cl} = actual ratio of the naked surface and the dressed body surface

t_{cl} = clothing surface temperature

t_r = mean radiant temperature (°C)

h_c = coefficient of convective heat transfer (W/m^{2}K)

t_a = air temperature around human body (°C)

$$When\ I_{cl} < 0.078, f_{cl} = 1.00 + 1.290 I_{cl} \quad (10)$$

$$When\ I_{cl} > 0.078, f_{cl} = 1.05 + 0.645 I_{cl} \quad (11)$$

Where,

I_{cl} = clothing thermal resistance (Clo)

t_{cl} = Clothes' surface temperature (°C)

The clothing surface temperature, t_{cl} was calculated using the following equation (5), which accounts for heat transfer through clothing via convection and radiation:

$$t_{cl} = 35.7 - 0.028(M - W) - I_{cl}\{3.96 \times 10^{-8} \times f_{cl}[(t_{cl} + 273)^4 - (t_r + 273)^4] + f_{cl} \times h_c \times (t_{cl} - t_a)\} \quad (12)$$

Equation (5) assumes a steady-state condition, with a fixed metabolic rate M and no external work (W=0). These assumptions are necessary to ensure that the

equation represents the thermal balance of the human body under controlled indoor conditions, such as those simulated in the ART cabin.
In this formulation, I_{cl} represents the clothing insulation, f_{cl} is the clothing surface area factor, h_c is the convective heat transfer coefficient, t_r is the mean radiant temperature, and t_a is the ambient air temperature.

The convective heat transfer coefficient h_c was calculated using using equations (6) and (7) that account for both natural and forced convection around the human body. Specifically, h_c is determined according to the following criteria:

$$When\ 2.38 \times (t_{cl} - t_a)^{0.25} > 12.1 \times \sqrt{V_{ar}}, h_c = 2.38 \times (t_{cl} - t_a)^{0.25} \quad (13)$$

$$When\ 2.38 \times (t_{cl} - t_a)^{0.25} < 12.1 \times \sqrt{V_{ar}}, h_c = 12.1 \times \sqrt{V_{ar}} \quad (14)$$

where t_{cl} is the clothing surface temperature, t_a is the ambient air temperature, and V_{ar} is the local air velocity (m/s). These equations ensure that the convective heat transfer accounts for the dominant mode of heat exchange: natural convection when the temperature difference is large relative to air velocity, and forced convection when air movement dominates. In the context of this study, V_{ar} values were obtained directly from the CFD simulation results, allowing accurate computation of h_c throughout the ART cabin for the thermal comfort analysis.

The heat dissipation E_c of sweat and on the skin is calculated using equation (15).

$$E_c = 3.05 \times 10^{-3} \times [5733 - 6.99\,(M - W) - P_a] + 0.42 \times [(M - W) - 58.15] \quad (15)$$

where P_a is the air water vapor pressure surrounding the body, and the unit is P_a.

Respiratory sensible heat loss which is, the sensible heat loss of breath brought on by temperature changes as a result of inhaling air, is an expression for formula (16)

$$C_{res} = 0.0014 \times M \times (34 - t_a) \quad (16)$$

Respiratory latent heat loss, known as the process of breathing air temperature, does not result in heat loss, and the calculation for respiratory latent heat loss written as

$$E_{res} = 1.72 \times 10^{-5} \times M \times (5867 - P_a) \quad (17)$$

The PMV equation involves nine parameters that collectively determine the thermal sensation of an individual. Although the PMV model formally includes nine parameters, in practice six are dominant in determining thermal comfort: air temperature, mean radiant temperature, air velocity, relative humidity, clothing insulation, and metabolic rate. These six variables are the primary indicators affecting a person's thermal comfort in the ART cabin. According to the thermal comfort formulation, when clothing, work intensity, and air water vapor pressure are prescribed or fixed, the key variables influencing occupant thermal sensation are air velocity, mean radiant temperature, and air temperature, which underscores the importance of accurately capturing these environmental conditions in the CFD simulations.

The Predicted Percentage of Dissatisfied (PPD) index, which quantifies the proportion of occupants likely to feel thermally uncomfortable, was calculated using the following standardized equation:

$$PPD = 100 - 95 \times e^{-(0.03353 \times PMV^4 + 0.2179 \times PMV^2)} \quad (18)$$

This formula is standardized in ISO 7730 and is derived directly from the PMV value. The PPD provides a complementary measure to PMV, allowing the evaluation of both the mean thermal sensation and the expected percentage of dissatisfied occupants under the given indoor environmental conditions.

Historically, the calculation of thermal comfort indices such as PMV and PPD was performed manually, which proved to be complex and often non-user-friendly, making it challenging for practitioners to apply these methods effectively [52]. The PMV index, widely adopted as a measure of thermal comfort, has been standardized in ISO 7730 [8] and quantifies the mean thermal sensation of a large group of occupants on a seven-point scale. Six parameters are required for PMV calculation: air velocity, air temperature, relative humidity, mean radiant temperature, metabolic rate, and clothing insulation. The PPD index, derived from the PMV, predicts the percentage of

occupants likely to feel thermally dissatisfied, providing a practical measure of comfort and discomfort in a given environment [61].

Due to the complexity of the equations, computational tools were employed in this study. SolidWorks Flow Simulation, specifically its HVAC Applications module, was used to calculate PMV and PPD values efficiently [25] In this study, the coupling between CFD results and thermal comfort calculation was performed automatically within the solver, where local airflow, temperature, and humidity fields obtained from the simulation were directly used to evaluate PMV and PPD at each computational cell. This automated coupling ensures that spatial variations in airflow and thermal conditions are accurately reflected in the thermal comfort assessment. Critical parameters—including air temperature, mean radiant temperature, air velocity, humidity, clothing insulation, and metabolic rate—were specified based on field measurements and simulations results.

The PMV calculations are based on the steady-state heat transfer between the human body and its surrounding environment, assuming a constant metabolic rate [40]. Accordingly, it is assumed that the human body is in a relatively stable thermal equilibrium over a prolonged period. After computation, PMV and PPD values were visualized on fixed-value contours. For reference, the recommended thermal comfort ranges, $-0.5 < PMV < 0.5$ and $PPD < 10\%$, are based on ISO 7730 and ASHRAE Standard 55, indicating acceptable levels of thermal satisfaction for the majority of occupants.

CHAPTER 4
RESULTS AND DISCUSSION

4.1 Introduction

To validate the CFD model, a baseline simulation of the ART with zero passengers (AW0) was conducted to replicate the real operating conditions during the field measurements collected at the middle carriage. The simulated operative temperature was compared against the measured surrounding temperatures obtained from six measurement points, as presented in Table 11.

Table 11
Measured Surrounding Temperature Inside ART

Time	Sunlight Condition	Surrounding Air Temperature (°C)
10:15 am	Shaded	25.1
10:15 am	Direct sun	25.1
10:45 am	Shaded	26.2
10:45 am	Direct sun	26.2
11:45 am	—	21.8
1:00 pm	—	25.3

Note: The symbol "—" indicates that shading conditions were not specifically recorded, as the cabin was fully exposed to direct sunlight during these periods.

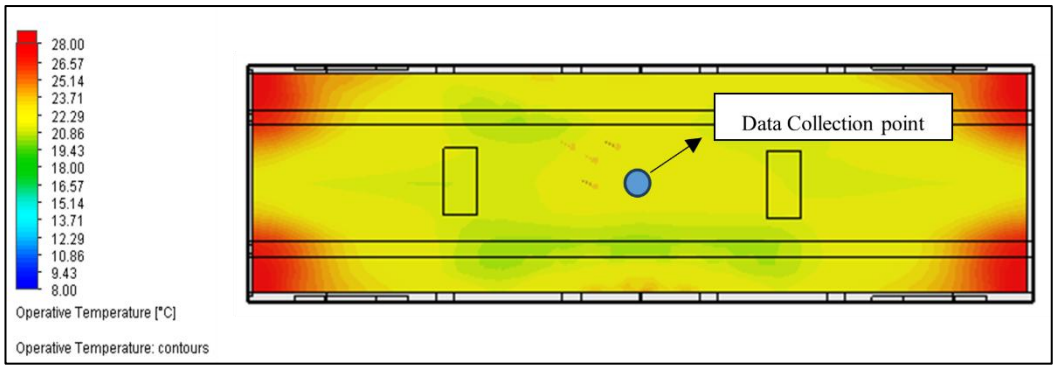

Figure 12: Simulated ART Under AW0 Condition

Average Measured Temperature, $\Delta T_{measured,avg}$ = 24.95 °C
Simulated Temperature = 23.20 °C

The measured temperatures ranged from 21.8°C to 26.2°C, with an average value of 24.95°C. The percentage difference between the simulated and measured temperatures was calculated using the standard formula:

$$Percentage\ Difference\ = \frac{|T_{simulated}\ -\ T_{measured,avg}|}{T_{measured,avg}} \times 100\% \qquad (19)$$

Where,

$T_{simulated}$ = Simulated Operative Temperature

$T_{measured,avg}$ = Average Measured Surrounding Temperature

$$Percentage\ Difference\ = \frac{|23.20℃ -\ 24.95℃|}{24.95℃} \times 100\%$$

$$Percentage\ Difference\ =\ 7.01\%$$

By using the average measured temperature (24.95 °C), the resulting percentage error was 7.01%. This falls within the acceptable range for indoor temperature validation[62][63], as ASHRAE acknowledges that indoor air temperature measurements commonly vary by ±1–2 °C due to instrument accuracy and spatial non-uniformity. Hence, the CFD model is suitably validated for subsequent thermal comfort analysis.

There shall be several important parts in this result sections consisting passenger category AW1, AW2 and AW3 which are; Air Velocity Distributions, Temperature Distributions, Predicted Mean Value (PMV), Predicted Percentage Dissatisfied (PPD), PMV and PPD Value according to CBE Thermal Comfort Tools for category AW2 and AW3.

4.2 Air Velocity Distribution

The table below presents the results of the velocity distribution analysis for the three simulated passenger-loading categories. These categories (AW1, AW2, and AW3) were modelled using varying air velocities and inlet indoor temperatures. It is important to clarify that all results shown in this section are CFD simulation outputs only**.** Validation of the CFD model was conducted earlier under AW0 (no-passenger) conditions, as described in Section 3.8. The present simulations for AW1–AW3 therefore rely on the same CFD model that has already been validated.

Table 12 presents the velocity distribution contours for category AW1, which includes 16 seated passengers. The contours are plotted on the x-plane with a cutoff at 1.32 m. Tables 13 and 14 show the corresponding contours for categories AW2, consisting of 16 seated and 58 standing passengers, and AW3, consisting of 16 seated and 74 standing passengers, respectively, using the same x-plane cutoff.

Across all passenger-loading conditions, three inlet air velocities—1.6, 2.9, and 3.2 m/s—were simulated, with each velocity paired with two distinct inlet air temperatures of 14.7 °C (stationary) and 8.7 °C (moving). These airflow settings were derived from field measurements obtained earlier using a handheld anemometer. The resulting velocity distributions provide a comparative view of how airflow patterns vary with increasing passenger density and inlet conditions within the ART carriage.

Table 12
Air Velocity Distributions for Category AW1

	AW1		
	1.6 m/s	**2.9 m/s**	**3.2 m/s**
14.7°C	Front View 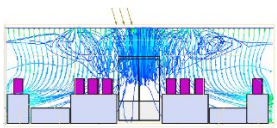	Front View 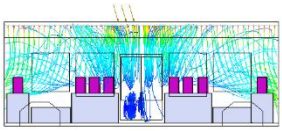	Front View 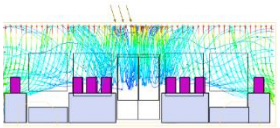
	Cross Section View 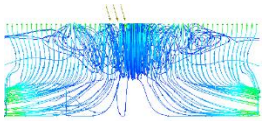	Cross Section View 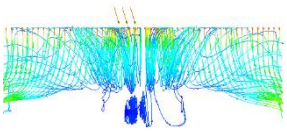	Cross Section View 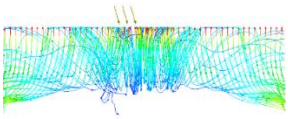
8.7°C	Front View 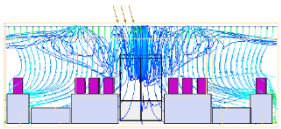	Front View 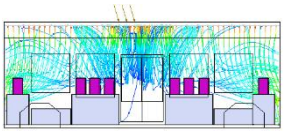	Front View 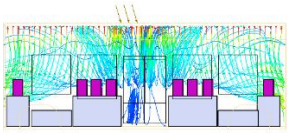
	Cross Section View 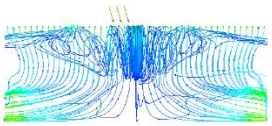	Cross Section View 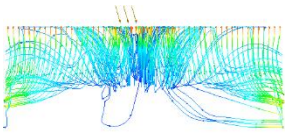	Cross Section View 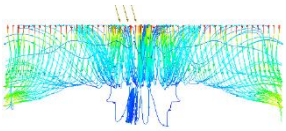

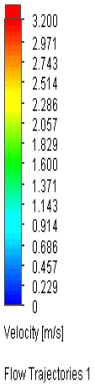

Table 12 presents the velocity distribution contours for the AW1 category, which includes 16 seated passengers. Each combination of inlet velocity and temperature is illustrated using both front and cross-sectional views to capture the spatial variations of airflow within the carriage. At an inlet temperature of 14.7°C and an air velocity of 1.6 m/s, the airflow exhibits moderate recirculation zones near the center of the carriage and higher velocity regions along the sidewalls. The blue contours in the middle region indicate areas of relatively low air velocity. Based on the CFD results at approximately 1.1 m height, the local velocity near the breathing zone is approximately 0.23 m/s, which is within the ASHRAE 55 and ISO 7730 recommended comfort limit of 0.2–0.3 m/s for sedentary occupants. At the lower temperature of 8.7°C, the overall airflow trajectory shifts slightly, although the general distribution pattern remains similar.

As the inlet velocity increases to 2.9 m/s at 14.7°C, the airflow becomes more energetic, producing stronger curvature of streamlines around passenger bodies and seats. Turbulence intensity increases, and the cross-sectional contours show more distinct gradients. The CFD output at 1.1 m height shows breathing-zone velocities of approximately 0.46 m/s, which begin to exceed the upper comfort threshold, indicating a potential for draft discomfort. At the corresponding 8.7°C case, sharper velocity gradients and vertical layering effects are observed, suggesting enhanced stratification due to the combined effects of higher momentum and cooler air.

At the highest simulated inlet velocity of 3.2 m/s, the velocity contours reveal strongly turbulent and non-uniform airflow, particularly near obstructions such as seat backs and passenger geometries. This condition generates the most irregular distribution patterns, with cross-sectional contours showing pronounced velocity fluctuations. At 8.7°C, the high-velocity, low-temperature combination results in significant turbulence and stratification, where cold air settles unevenly and produces substantial variation in local velocity magnitudes. Breathing-zone CFD velocities reach approximately 0.6 m/s, which are well above the acceptable comfort range defined in ASHRAE 55 and ISO 7730.

Overall, the findings indicate that increases in inlet velocity led to greater turbulence and reduced uniformity of airflow within the passenger cabin. Furthermore, lower inlet temperatures exacerbate vertical stratification, particularly at higher velocities. When examined in relation to the thermal comfort criteria, the CFD results suggest that only the lower inlet velocity condition (1.6 m/s) maintains airflow within the recommended comfort limits at passenger height, whereas the 2.9 m/s and 3.2 m/s conditions exceed these limits and may contribute to thermal discomfort due to excessive draft.

Table 13
Air Velocity Distributions for Category AW2

	AW2		
	1.6 m/s	**2.9 m/s**	**3.2 m/s**
14.7°C	Front View: 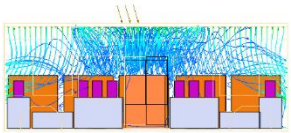	Front View: 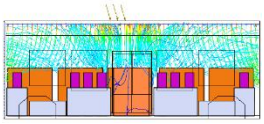	Front View: 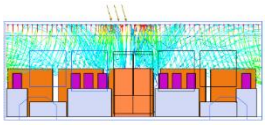
	Cross Section View 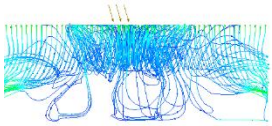	Cross Section View 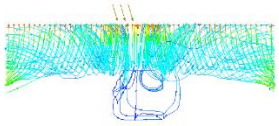	Cross Section View 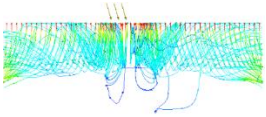
8.7°C	Front View: 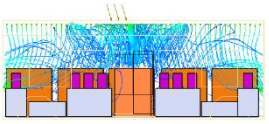	Front View: 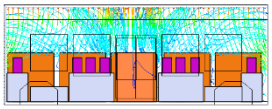	Front View: 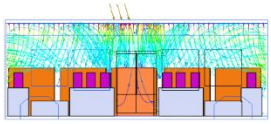
	Cross Section View 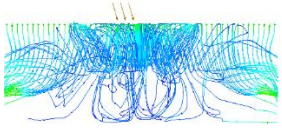	Cross Section View 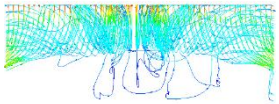	Cross Section View 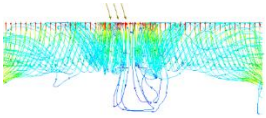

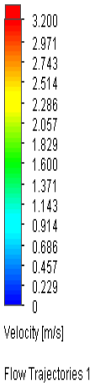

Table 13 presents the velocity trajectories for category AW2, which includes 16 seated passengers and 58 standing passengers. Airflow behaviour was examined under three inlet velocities (1.6 m/s, 2.9 m/s, and 3.2 m/s) and two inlet temperatures (14.7°C and 8.7°C). To strengthen the interpretation of the results, airflow magnitudes at typical breathing heights—approximately 1.1 m for seated passengers and 1.7 m for standing passengers—are reported and compared against the ASHRAE 55 comfort threshold of 0.2–0.3 m/s.

At the inlet temperature of 14.7°C and velocity of 1.6 m/s, airflow trajectories remain relatively uniform with limited disruption around passenger bodies. The velocity field predominantly falls within the range of 0.05–0.39 m/s, indicating stable airflow with minimal variations across the cabin. The average velocity at 1.1 m height is approximately 0.13 m/s for in the middle-seated passengers and around 0.39 m/s for seated passengers at the corner area, while at 1.7 m height it is between 0.13-0.32 m/s. Both values fall within or only slightly exceed the ASHRAE 55 comfort limits,

suggesting that draft discomfort is unlikely under this condition

At 2.9 m/s, the airflow becomes more variable due to intensified interaction with both seated and standing passengers. The trajectories show curvature around the passenger geometries, and the velocity field spans a wider range of 0.23–0.85 m/s. This increased variability corresponds to stronger velocity gradients and more distinct recirculation regions. Breathing-zone velocities rise to around 0.35 m/s for seated passengers in the middle while around 0.6 m/s for seated passengers at the corner area. The breathing-zone velocities for standing passengers increased to 0.63 m/s (1.7 m height), exceeding the comfort limit of 0.3 m/s and indicating a heightened likelihood of draft discomfort.

At the highest inlet velocity of 3.2 m/s, airflow patterns become highly non-uniform. Trajectories show pronounced deviations and more frequent recirculation zones, especially around the upper bodies of standing passengers. The velocity field spans an even broader range of 0.20–0.91 m/s, reflecting significant spatial variation. Velocities at 1.1 m height reach 0.46 m/s, while those at 1.7 m height rise to 0.69 m/s, both substantially above the ASHRAE 55 comfort threshold and indicative of considerable draft discomfort at passenger level.

Overall, increasing inlet air velocity leads to larger velocity ranges throughout the cabin, more pronounced airflow disturbances near standing passengers, and higher breathing-zone velocities that exceed recommended comfort levels at moderate and high inlet velocities. For AW2, the higher density of standing passengers significantly influences the airflow, contributing to greater non-uniformity and stronger velocity fluctuations across the seating and standing zones.

.

Table 14
Air Velocity Distributions for Category AW3

	AW3		
	1.6 m/s	**2.9 m/s**	**3.2 m/s**
14.7°C	Front View 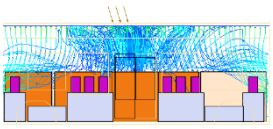	Front View 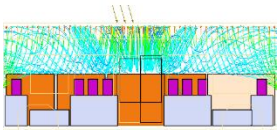	Front View 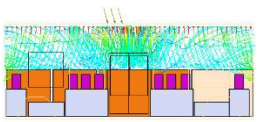
	Cross Section View 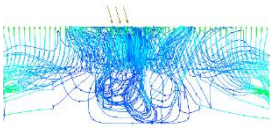	Cross Section View 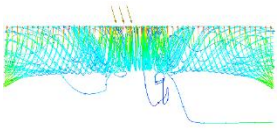	Cross Section View 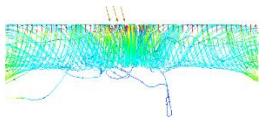
8.7°C	Front View 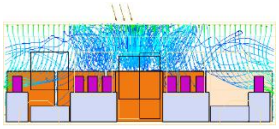	Front View 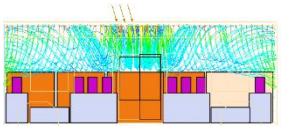	Front View 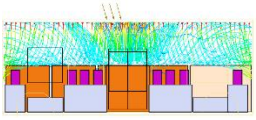
	Cross Section View 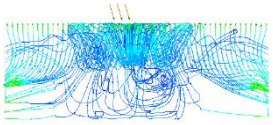	Cross Section View 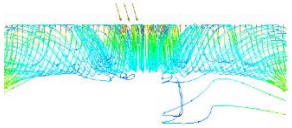	Cross Section View 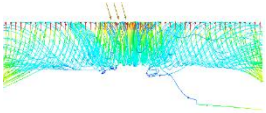

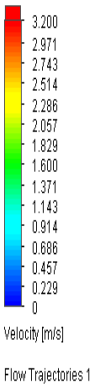

Table 14 presents the velocity distribution contours for the AW3 condition, which comprises 16 seated and 74 standing passengers, extracted at the x-plane (1.32 m). Each figure illustrates the airflow behavior under three inlet air velocities (1.6 m/s, 2.9 m/s, and 3.2 m/s) combined with two inlet temperatures (14.7°C and 8.7°C).

At an inlet velocity of 1.6 m/s, the flow trajectories remain relatively uniform, with streamlines following a stable path around the passenger geometries. Disturbances are minimal, and the velocity field mainly spans the lower range of the contour scale 0.05–0.3 m/s, indicating limited variation across the cabin. As the inlet velocity increases to 2.9 m/s, the airflow becomes more complex; trajectories begin to deviate, and small recirculation zones emerge near obstacles and boundary layers. The velocity field broadens 0.5–0.70 m/s, reflecting the increased momentum and interaction with passenger bodies. At the highest inlet velocity of 3.2 m/s, the flow exhibits highly irregular behaviour, with pronounced velocity variations 0.70–0.90 m/s) and more extensive recirculation regions. Streamlines show significant fluctuations rather than

the vague description of “fully turbulent flow,” indicating substantial spatial velocity variation driven by high inlet momentum and dense passenger occupancy.

Air supply in the ART middle carriage is delivered through two diffusers located along both sides of the ceiling, with return air extracted via two central ceiling-mounted return grilles. The overall simulated velocity field spans a range of 0 to 3.2 m/s**,** consistent with the imposed inlet boundary conditions. As demonstrated in the contour plots, higher inlet velocities produce greater spatial variability in airflow patterns and contribute to higher local velocities at passenger level.

Based on the simulation results, the maximum air velocity inside the occupied cabin region (i.e., excluding the diffuser discharge zone) is approximately 2.286 m/s. This value is important when compared to indoor comfort criteria. Contrary to the earlier statement, an airflow velocity of 2.286 m/s does *not* comply with the ASHRAE 55-2004 limit of 0.8 m/s, which is the recommended upper threshold to avoid draft discomfort in typical indoor environments for lightly clothed or sedentary occupants. Therefore, the results clearly indicate that the velocities experienced inside the AW3 cabin exceed ASHRAE 55 acceptable limits.

However, previous studies have shown that acceptable indoor air speeds vary widely depending on climate conditions. Various authors have reported ranges between 0.5 and 2.5 m/s for acceptable indoor airflow, particularly in warm, humid climates. In tropical regions such as Malaysia, where outdoor temperatures and humidity levels are consistently high, occupants often prefer higher air speeds for enhanced cooling sensation[64]. Thus, while the AW3 velocities exceed ASHRAE 55 comfort thresholds, they may still be perceived as beneficial or tolerable by passengers in a hot–humid climatic context.

Overall, the AW3 airflow behavior is strongly influenced by the high passenger density, resulting in broader velocity ranges and greater non-uniformity. While such air velocities provide increased convective cooling, they exceed international thermal comfort limits and may produce draft sensations unless offset by local climatic adaptation or passenger preference.

4.3 Temperature Distribution

The temperature field within the Automated Rapid Transit (ART) middle carriage was analyzed using the same input conditions applied for the velocity-distribution study. The temperature distribution contours for conditions AW1, AW2 and AW3 are presented in Tables 16, 17 and 18, respectively. All contour maps are taken on the y-plane at a height of 1.13 m above the floor. For each passenger-loading condition the model was run for three inlet air velocities (1.6, 2.9 and 3.2 m/s) and for two operative inlet temperatures; the inlet conditions were selected to match field measurements obtained with a handheld anemometer during on-site tests.

The CFD results show that inlet air velocity is a primary driver of the spatial temperature distribution within the middle carriage: higher inlet velocities increase convective mixing and reduce local temperature gradients in some regions, while in other regions strong flows produce localized cooling near discharge zones and shear layers. Nevertheless, the temperature field is also influenced by occupant-related and environmental factors. In particular, human physiological characteristics and clothing insulation modify the local thermal environment: typical skin temperatures on the trunk (chest and abdomen) are reported in the literature to fall approximately between 33.5°C and 36.9°C, and skin temperature varies by body region and environmental exposure [65].

Because occupants in the present simulations are assumed to be sedentary (seated or standing with minimal movement), a constant metabolic rate was applied for all human models; clothing insulation was treated as a parameter in the boundary conditions, and its influence on convective and evaporative heat transfer was accounted for in the simulation setup. The combined effects of inlet velocity, metabolic heat production, and clothing insulation lead to the observed variations in local operative temperature and near-body microclimates.

Table 15
Air Temperature Distributions for Category AW1

	AW1		
	1.6 m/s	**2.9 m/s**	**3.2 m/s**
14.7°C	Top View 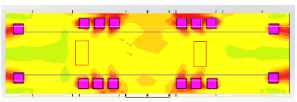	Top View 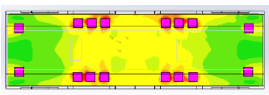	Top View 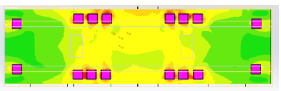
	Front View 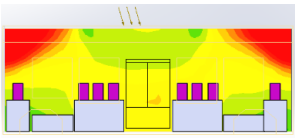	Front View 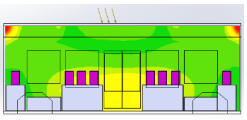	Front View 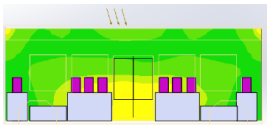
8.7°C	Top View 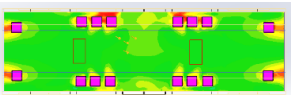	Top View 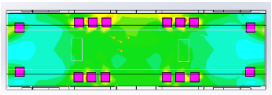	Top View 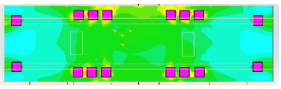
	Front View 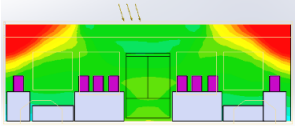	Front View 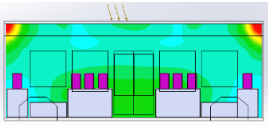	Front View 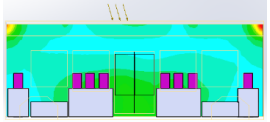

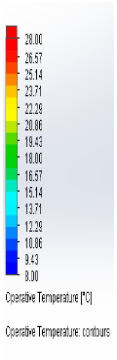

Table 15 presents the temperature distribution contours for the AW1 condition, consisting of 16 seated passengers in the middle carriage of the ART. Simulations were conducted using inlet air velocities of 1.6, 2.9, and 3.2 m/s, each paired with inlet temperatures of 14.7°C and 8.7°C. These boundary conditions are consistent across all passenger-loading categories to facilitate comparison.

For the inlet temperature of 14.7°C and an air velocity of 1.6 m/s, the top-view contours indicate that the temperature in the vicinity of the seated passengers is approximately 28°C. This region has been explicitly highlighted in the contour figure using arrows/labels to guide the reader, addressing the difficulty of visually identifying numerical values in unannotated contour plots. At higher velocities of 2.9 m/s and 3.2 m/s, the temperature distribution exhibits only minor variations, with most occupied-zone temperatures remaining within the range of 25°C to 28°C. This limited change is

attributed to the relatively small difference in momentum between the two higher inlet velocities.

When the inlet temperature was reduced to 8.7°C, a further decrease in the temperature surrounding the seated passengers was observed, particularly at air velocities of 2.9 m/s and 3.2 m/s. These cooler regions have also been labelled in the contour maps to provide clear visual confirmation of the temperature gradients near the passenger area. Overall, the results show that temperature distribution within the AW1 carriage is strongly dependent on the inlet temperature, with air velocity exerting a secondary but still noticeable influence.

Table 16
Air Temperature Distributions for Category AW2

	AW2		
	1.6 m/s	**2.9 m/s**	**3.2 m/s**
14.7°C	Top View 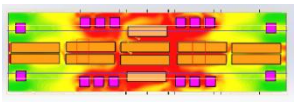	Top View 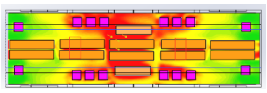	Top View 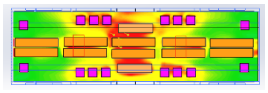
	Front View 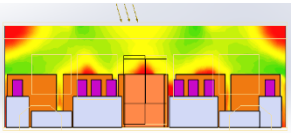	Front View 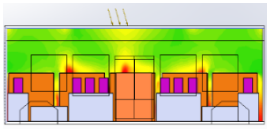	Front View 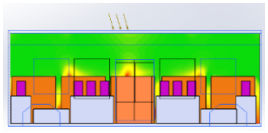
8.7°C	Top View 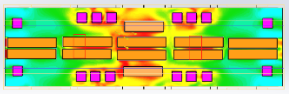	Top View 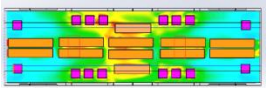	Top View 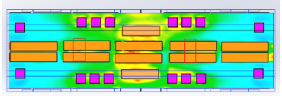
	Front View 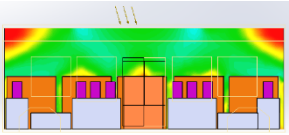	Front View 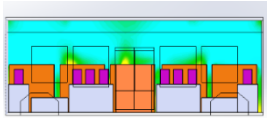	Front View 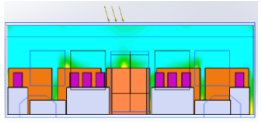

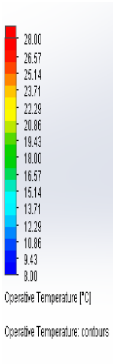

Table 16 presents the air temperature distribution for the AW2 category, which includes a total of 74 passengers—16 seated and 58 standing—inside the middle carriage of the ART. Standing passengers were represented by block-shaped manikins in the CFD model: two blocks positioned near the ART doors represent four standing passengers each, while ten blocks in the central area represent five passengers per block.

From the top-view temperature contours, it is observed that at an inlet temperature of 14.7°C and an air velocity of 1.6 m/s, the temperature in the central section of the carriage is higher than in the side regions. This increase is attributed to the higher passenger density in the central area, which contributes additional metabolic heat. Quantitatively, the CFD results indicate that the temperature in the central region is approximately 5.71°C higher than at the sides. This numerical difference confirms that passenger density is a key factor influencing local temperature variations in the

ART.

Table 17
Air Temperature Distributions for Category AW3

	AW3		
	1.6 m/s	**2.9 m/s**	**3.2 m/s**
14.7°C	Top View 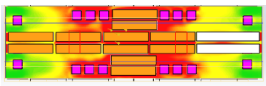	Top View 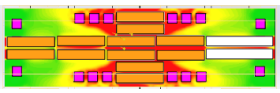	Top View 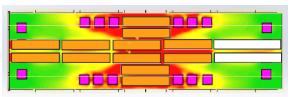
	Front View 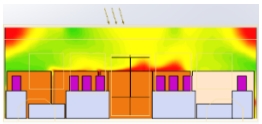	Front View 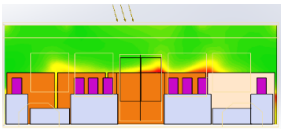	Front View 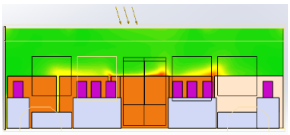
8.7°C	Top View 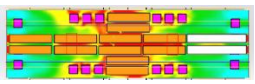	Top View 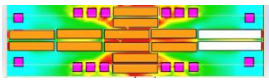	Top View 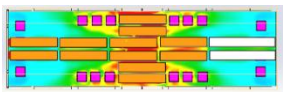
	Front View 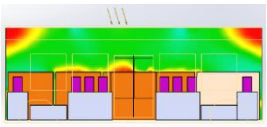	Front View 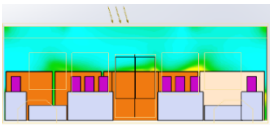	Front View 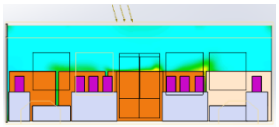

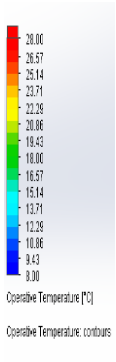

Table 17 presents the temperature distribution for the AW3 category, which includes 16 seated passengers and 74 standing passengers. The standing passengers are represented in the CFD model by twelve brown-coloured human blocks, each representing five standing passengers, and two white-coloured human blocks, each representing seven standing passengers.

From the top-view temperature contours, it is observed that at an inlet temperature of 14.7°C, increasing the air velocity from 1.6 m/s to 3.2 m/s reduces the temperature in the densely populated central region of the carriage. A similar trend is observed at an inlet temperature of 8.7°C, indicating that air velocity plays a significant role in shaping the local temperature distribution. To support this observation, the central section of the carriage has been annotated in the contour figures, and the extracted CFD results show that the average temperature in the central region is approximately 23.4°C, compared with 17.1°C in the side regions, resulting in a difference of 6.3°C. This quantitative comparison confirms that passenger density and

airflow dynamics jointly influence local thermal conditions.

In addition to airflow effects, thermal comfort is influenced by the overall number of occupants and their distribution. Higher air velocities produce larger temperature gradients, which can enhance convective cooling but may also create local discomfort if passenger density is high. Therefore, adjusting air velocity according to passenger load is critical for maintaining a comfortable environment within the ART.

Another important factor affecting temperature distribution is solar radiation entering through the carriage windows. In this study, solar radiation was incorporated into the CFD simulation as a fixed boundary condition of 600 W/m², as specified in Table 9. This value was applied uniformly to the window surfaces to represent peak daytime exposure. However, only the thermal load from solar radiation was simulated; the detailed optical behaviour of the windows (e.g., transmission, absorption, shading coefficient) was not modelled explicitly. Instead, the influence of window placement was considered conceptually to explain localized temperature increases near the window surfaces. This approach highlights the importance of window design and shading strategies in ensuring optimal thermal comfort under varying operating and environmental conditions.

4.4 Predicted Mean Vote (PMV) and Predicted Percentage Dissatisfied (PPD) Data

4.4.1 Predicted Mean Vote (PMV)

Tables 18, 19, and 20 present the predicted surrounding PMV values inside the middle carriage of the ART, obtained using the SolidWorks Flow Simulation HVAC Module. These results were evaluated to assess the thermal comfort experienced by passengers under the three airflow conditions. The PMV index scale, established by [8], was used as the reference for interpreting comfort levels, as summarised in Table 5. According to [9], acceptable thermal comfort is achieved when the PMV value lies within the range of −0.5 to +0.5.

Table 18
PMV Value for Category AW1

	AW1		
	1.6 m/s	**2.9 m/s**	**3.2 m/s**
14.7°C	Top View 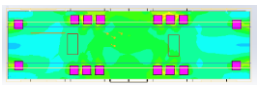	Top View 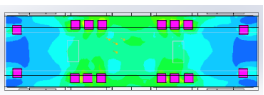	Top View 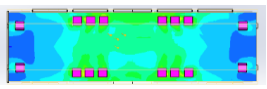
	Front View 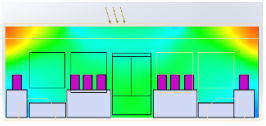	Front View 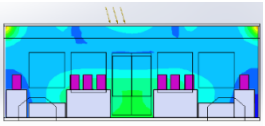	Front View 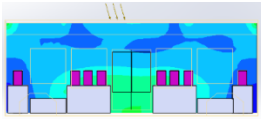
8.7°C	Top View 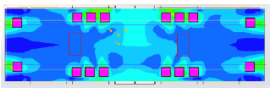	Top View 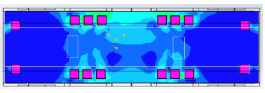	Top View 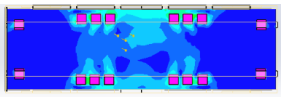
	Front View 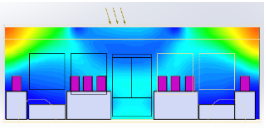	Front View 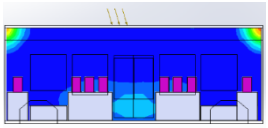	Front View 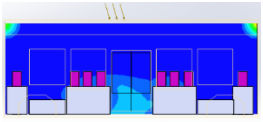

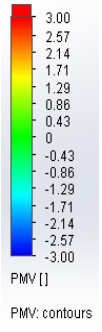

Across the three passenger loading conditions—AW1, AW2, and AW3—evaluated under two inlet temperatures and three air velocities, the AW1 scenario exhibited the most distinct spatial variation in thermal sensation among seated passengers. Under this condition, passengers seated at the far ends of the carriage recorded lower PMV values –3.00 (cold) to –1.30 (cool) compared to those seated in the middle, who experienced moderately higher PMV values –1.30 (cool) to 0.43 (approximately neutral). This pattern reflects the lower temperature distribution observed near the corner regions, which produced a cooler microenvironment and consequently reduced thermal comfort. At an inlet temperature of 14.7 °C, corner-seated passengers experienced PMV values ranging from -0.43 to –1.71, indicating noticeably cooler conditions relative to the central seating zones. When the inlet temperature was reduced further to 8.7 °C, PMV values across all air velocities shifted toward –1.30 to –3.00, signifying a consistently colder thermal sensation throughout the carriage under this lower-temperature condition.

Table 19
PMV Value for Category AW2

	AW2		
	1.6 m/s	**2.9 m/s**	**3.2 m/s**
14.7°C	Top View 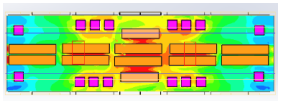	Top View 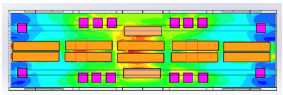	Top View 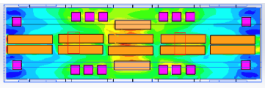
	Front View 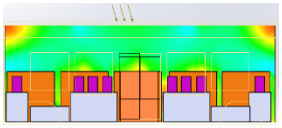	Front View 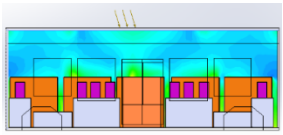	Front View 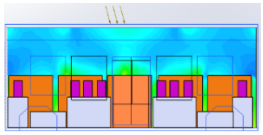
8.7°C	Top View 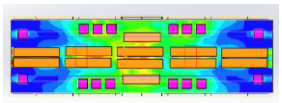	Top View 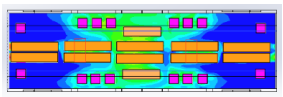	Top View 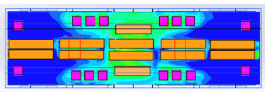
	Front View 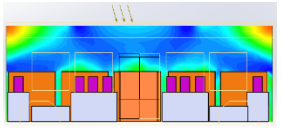	Front View 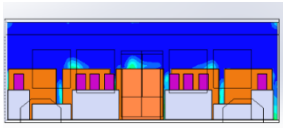	Front View 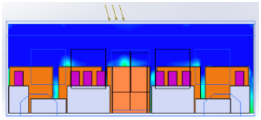

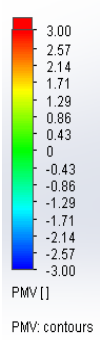

Table 19 presents the thermal comfort distribution for the AW2 passenger loading condition, with PMV values extracted at the y-plane located 1.32 m above the carriage floor. At an inlet temperature of 14.7 °C with velocity of 1.6 m/s, in the central region of the carriage exhibited noticeably higher PMV values, with the middle section reaching approximately +3.00 (hot) for standing passengers while, +1.71 (slightly warm) for seated passenger indicating a sensation that exceeds the ASHRAE Standard 55 acceptable comfort range of −0.5 to +0.5. This increase in perceived warmth is attributed to the closer proximity between passengers in the central area, which amplifies localized thermal accumulation. Conversely, at an inlet temperature of 8.7 °C, increasing air velocity led to lower PMV values in the middle of the cabin, reflecting colder thermal sensations under higher airflow conditions.

Table 20
PMV Value for Category AW3

AW3			
	1.6 m/s	**2.9 m/s**	**3.2 m/s**
14.7°C	Top View 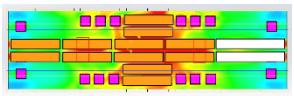	Top View 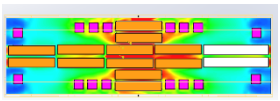	Top View 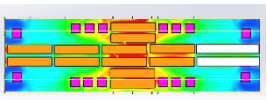
	Front View 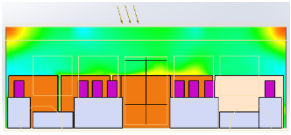	Front View 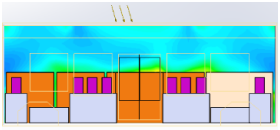	Front View 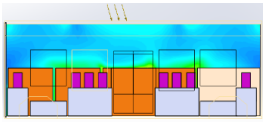
8.7°C	Top View 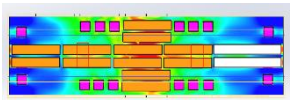	Top View 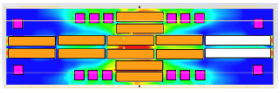	Top View 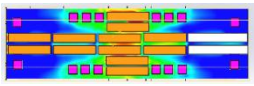
	Front View 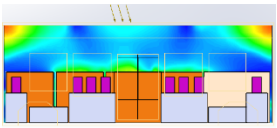	Front View 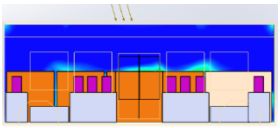	Front View 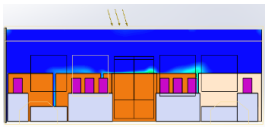

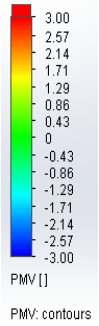

Based on the PMV values presented for the AW3 category in Table 20, the thermal comfort distribution within the carriage is strongly influenced by passenger density, metabolic rate, and clothing insulation. Thus, standing passengers in high-density areas, particularly in the middle of the carriage, exceeded the ASHRAE Standard 55 comfort range (−0.5 to +0.5), experiencing slightly warm to hot conditions with PMV values reaching approximately +3, whereas seated passengers at the corners felt uncomfortably cold, with PMV values approaching −3. At an inlet temperature of 14.7 °C, middle-standing passengers experienced the warmest sensations, while side-standing passengers reported neutral to cool conditions. Seated passengers in the middle experienced slightly warm to neutral conditions.

At an inlet temperature of 8.7 °C, increasing air velocity produced varied thermal sensations in the middle of the carriage, ranging from neutral to slightly cool as the velocity increased from 1.6 m/s to 3.2 m/s, while corner passengers continued to experience colder conditions. These variations reflect the combined effects of local

temperature distribution, airflow patterns, and spatial passenger density on perceived thermal comfort, with all passengers assumed to have identical metabolic rates and clothing insulation values.

4.4.2 Percentage Dissatisfied (PPD)

The values obtained from the PMV (Predicted Mean Vote) and PPD (Predicted Percentage of Dissatisfied) methods exhibit a strong correlation. When the PMV value falls within the neutral range, the corresponding PPD typically indicates less than 10% of individuals are dissatisfied with the thermal environment. Both indices serve to predict the proportion of occupants experiencing discomfort due to ambient temperature conditions. Based on the PPD results presented in Tables 21, 22, and 23, which compare two inlet temperature settings across three air velocities, it was observed that single seated passengers located at the corners of the carriage experienced the highest levels of thermal dissatisfaction. However, even when the PMV value is zero, representing a neutral thermal sensation, some individuals may still report discomfort, highlighting the inherent variability in human thermal perception.

Table 21
PPD for Category AW1

	AW1		
	1.6 m/s	**2.9 m/s**	**3.2 m/s**
14.7°C	Top View 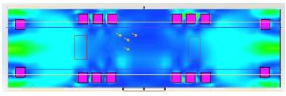	Top View 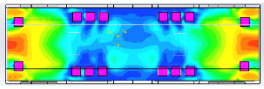	Top View 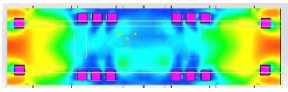
	Front View 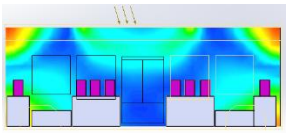	Front View 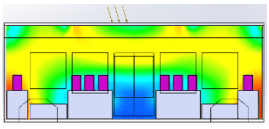	Front View 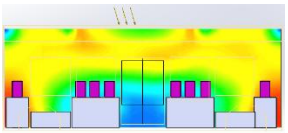
8.7°C	Top View 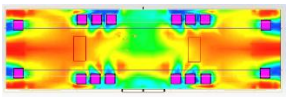	Top View 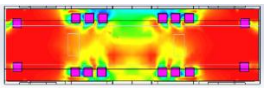	Top View 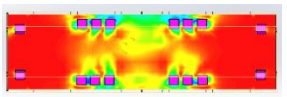
	Front View 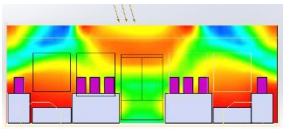	Front View 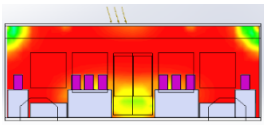	Front View 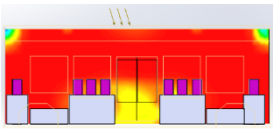

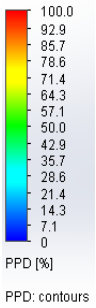

Based on the PPD results presented in Table 21, which compare two inlet temperatures across three air velocities, single seated passengers located at the corners of the ART carriage experienced the highest levels of thermal dissatisfaction, with PPD values 100%. According to ISO 7730 [8], even when the PMV is zero, approximately 5–10% of occupants are predicted to feel dissatisfied, which explains why some passengers at the corners may experience discomfort despite a neutral thermal sensation. Under moving conditions with an inlet temperature of 8.7 °C, the dissatisfaction among corner-seated passengers increased with higher air velocities, with PPD values rising from 29% to 100%. This heightened discomfort corresponds to the slightly cool to cold sensations experienced in these areas, as reflected in the corresponding PMV values. Overall, the PPD values were consistently highest for single seated passengers at the corners, particularly at lower temperatures and increased air velocities, confirming that colder local conditions significantly contribute to passenger thermal dissatisfaction.

Table 22
PPD for Category AW2

	AW2		
	1.6 m/s	**2.9 m/s**	**3.2 m/s**
14.7°C	Top View 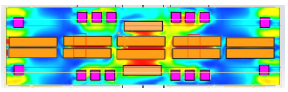	Top View 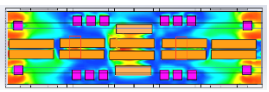	Top View 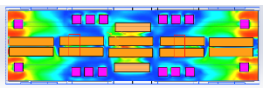
	Front View 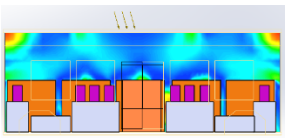	Front View 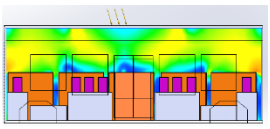	Front View 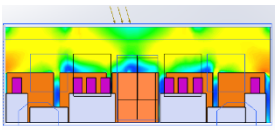
8.7°C	Top View 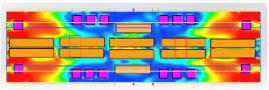	Top View 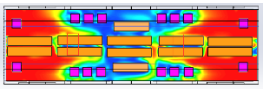	Top View 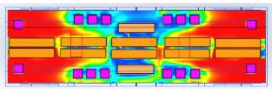
	Front View 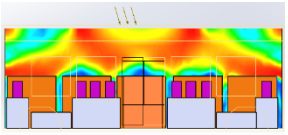	Front View 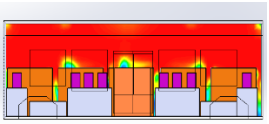	Front View 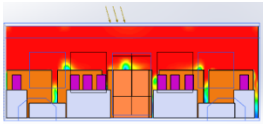

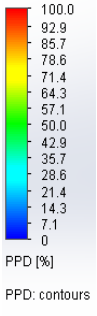

According to the PPD results presented in Table 22, under an inlet temperature of 14.7°C, single seated passengers at the corners of the ART experienced increasing PPD values, reaching approximately 50% as air velocity rose, indicating higher thermal dissatisfaction. In contrast, standing and seated passengers located in the central region of the carriage exhibited a decrease in PPD values, ranging from 100% to 7% with increasing velocities. These values correspond to PMV readings ranging from slightly cool to neutral and slightly warm, reflecting improved thermal comfort. At an inlet temperature of 8.7 °C, corner-seated passengers continued to show higher PPD values, approximately 100% at 3.2 m/s, compared to other occupants, due to the colder local sensations in these areas. Similar to the AW1 condition, the elevated PPD values at the corners highlight that colder microclimates significantly affect passenger comfort, while the central regions benefit from airflow-induced improvements as velocities increase.

Table 23
PPD for Category AW3

	AW3		
	1.6 m/s	**2.9 m/s**	**3.2 m/s**
14.7°C	Top View 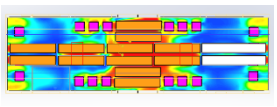	Top View 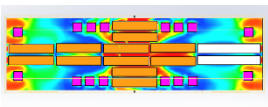	Top View 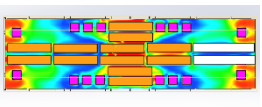
	Front View 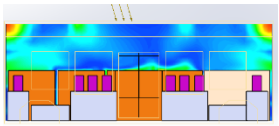	Front View 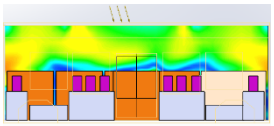	Front View 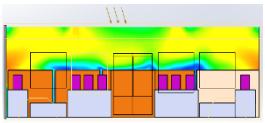
8.7°C	Top View 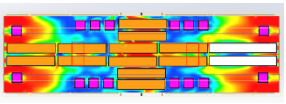	Top View 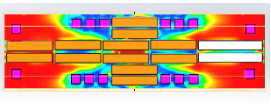	Top View 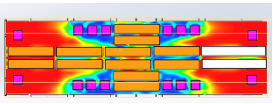
	Front View 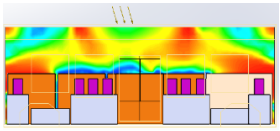	Front View 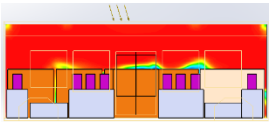	Front View 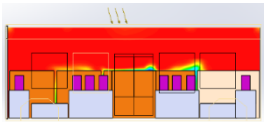

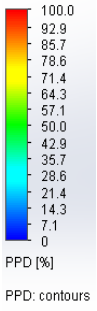

Table 23 presents the PPD results for the AW3 passenger category. At an inlet temperature of 14.7 °C, the PPD values for single seated passengers at the corners of the ART increased with rising air velocities, reaching approximately 60% at 3.2 m/s, indicating higher thermal dissatisfaction. In contrast, standing and seated passengers in the central region of the carriage exhibited lower PPD values, decreasing to approximately 29% to 7% corresponding to PMV values ranging from slightly cool to neutral and slightly warm, which reflect improved thermal comfort. At an inlet temperature of 8.7 °C, corner-seated passengers continued to show higher PPD values, approximately 100% due to the colder local sensations in these regions, while central passengers maintained lower PPD values, around 7.1% at highest velocity 3.2 m/s.

Overall, the PPD results indicate that passenger comfort in the ART cabin is strongly influenced by seating location, inlet temperature, and airflow velocity. Corner-seated passengers consistently experienced higher thermal dissatisfaction, particularly at elevated air velocities, whereas central passengers benefited from increased airflow, as evidenced by their lower PPD values. Based on ISO 7730 comfort limits, middle

seating generally remains within the acceptable PPD threshold (<10%), while corner seating frequently exceeds this limit, with values reaching ~30% at higher velocities, indicating non-uniform comfort across the cabin. These findings highlight the importance of considering both passenger density and airflow patterns when assessing thermal comfort in confined transit environments.

4.4.3 PMV and PPD Value based on CBE Thermal Comfort Tool (AW2)

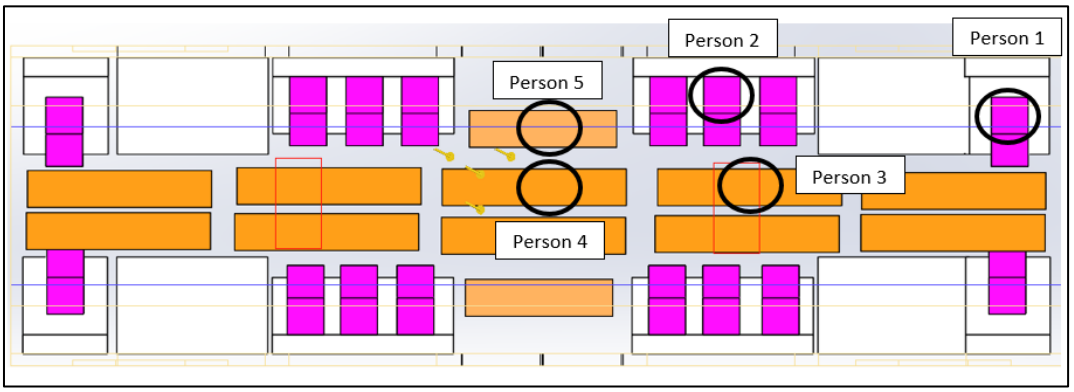

Figure 13: Selected Passengers for CBE Thermal Comfort Tool Analysis (AW2)

Figures 14 and 15 present the PMV and PPD values computed using the CBE Thermal Comfort Tool to evaluate the comfort levels of selected passengers in the ART under the AW2 condition (Figure 13) at temperature of 14.7°C. In Figure 13, Persons 1–5 were selected because they represent critical airflow regions within the carriage, including corner, middle, and near-diffuser zones. These locations were chosen to capture variations in thermal comfort across non-uniform airflow patterns.

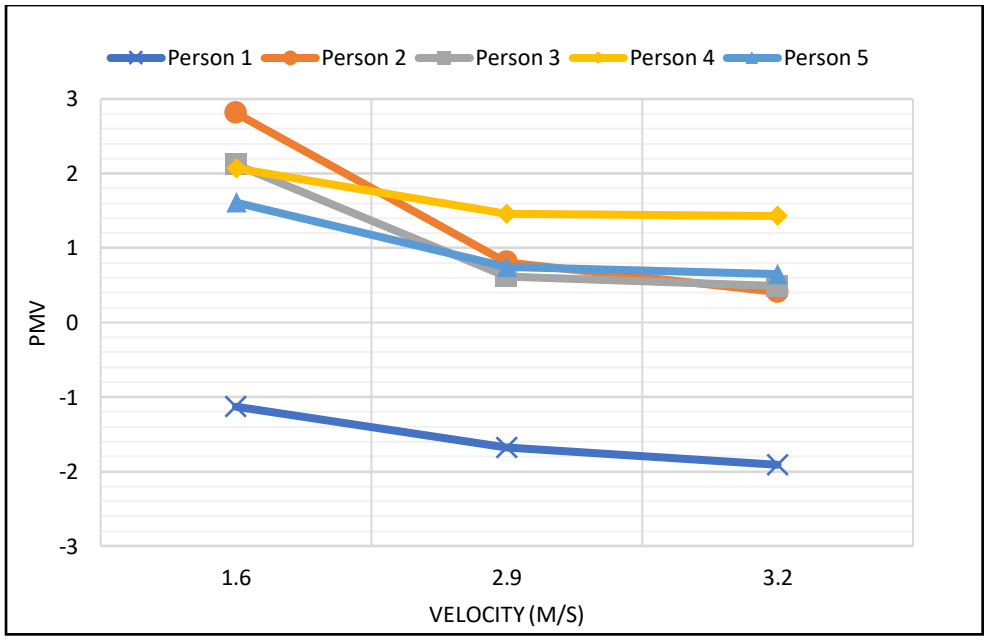

Figure 14: PMV Value of Selected Passengers at 14.7°C

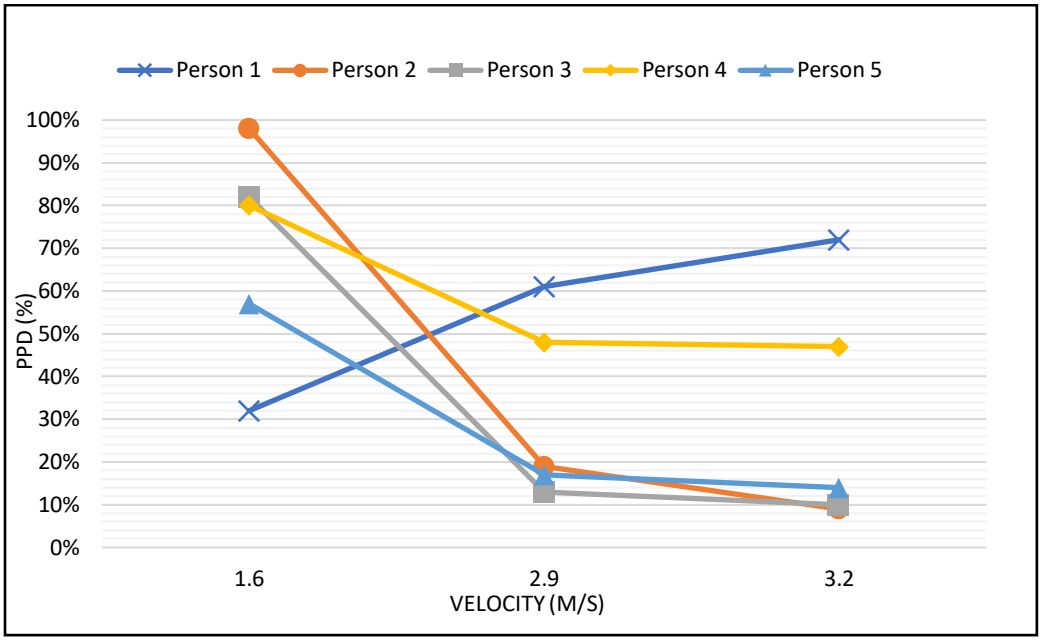

Figure 15: PPD Value of Selected Passengers at 14.7°C

Table 24
Summary Table for AW2 Category at 14.7 °C

Velocity (m/s)	Person	PMV (Value)	PPD (%)	Summary
1.6	1	-1.12	32	Feels cool, moderate discomfort.
	2	2.81	98	Feels warm, high discomfort.
	3	2.12	82	Feels warm, high discomfort.
	4	2.06	80	Feels warm, high discomfort.
	5	1.61	57	Feels slightly warm, moderate discomfort.
2.9	1	-1.68	61	Feels cool, moderate discomfort.
	2	0.81	19	Feels warm, low discomfort.
	3	0.62	13	Feels neutral, low discomfort.
	4	1.46	48	Feels warm, moderate discomfort.
	5	0.75	17	Feels neutral, low discomfort.
3.2	1	-1.91	72	Feels cooler, higher discomfort.
	2	0.41	9	Feels neutral, low discomfort.
	3	0.49	10	Feels neutral, low discomfort.
	4	1.43	47	Feels warm, moderate discomfort.
	5	0.65	14	Feels neutral, low discomfort.

The thermal comfort analysis for AW2 at 14.7°C demonstrates notable spatial variability across the five evaluated passenger positions under different air velocities. At 1.6 m/s, the PMV results range from –1.12 (cool) to +2.81 (very warm), indicating a wide spread of thermal sensations. Persons 2–4 exhibit strongly warm sensations (PMV = 2.06–2.81), while Person 1 experiences a cool sensation (PMV = –1.12). These deviations from neutrality highlight pronounced non-uniformity in the cabin environment. When the velocity increases to 2.9 m/s, PMV values for most passengers converge toward neutrality (PMV = 0.62–0.81), suggesting improved comfort for Persons 2, 3, and 5. However, Person 1 remains cool (PMV = –1.68), and Person 4 continues to feel warm (PMV = 1.46), reflecting persistent localized thermal imbalance.

At the highest velocity of 3.2 m/s, PMV values for Persons 2, 3, and 5 fall within near-neutral ranges (PMV = 0.41–0.65), whereas Person 1 becomes even cooler (PMV = –1.91) and Person 4 remains warm (PMV = 1.43). A general decreasing trend in PMV with increasing air velocity is observed for most passengers at 14.7°C; however, this trend is not consistent for Person 1. Therefore, the trend is described as approximate rather than strictly linear. Overall, the PMV analysis shows that although higher velocities generally improve thermal neutrality for most occupants, extreme positions still experience persistent thermal deviations. The standard PMV index scale specified in ISO 7730 [8] and summarized in Table 25 is used to evaluate the thermal comfort of passengers inside the ART carriage. According to ASHRAE 55 [9], a PMV range between –0.5 and +0.5 corresponds to acceptable comfort conditions in which fewer than 10% of occupants are expected to be dissatisfied [66].

Table 25
PMV Thermal Comfort Scale

Thermal Sensation	PMV
Hot	+3
Warm	+2
Slightly Warm	+1
Neutral	0
Slightly Cool	-1
Cool	-2
Cold	-3

The PPD results reinforce these findings. At 1.6 m/s, dissatisfaction levels are substantially high for Persons 2–4 (PPD = 80–98%), while Person 1 and Person 5 experience moderate discomfort (PPD = 32–57%). At 2.9 m/s, thermal acceptability improves significantly for Persons 2, 3, and 5, whose PPD decreases to 13–19%, indicating low dissatisfaction. Person 1, however, still records moderate discomfort (61%), and Person 4 remains moderately dissatisfied (48%). At 3.2 m/s, PPD values for Persons 2, 3, and 5 remain low (9–14%), confirming that most passengers benefit from higher airflow. Nevertheless, Person 1 continues to experience high dissatisfaction (72%), and Person 4 remains moderately dissatisfied (47%), demonstrating that airflow increases do not equally benefit all locations.

Collectively, the PMV and PPD analyses indicate that increasing air velocity enhances thermal comfort for most passengers in AW2, particularly Persons 2, 3, and 5, who consistently approach acceptable comfort ranges at higher velocities. However, localized thermal extremes persist, especially for Person 1—who consistently experiences cool discomfort—and Person 4, who remains in the warm discomfort zone. These patterns confirm the presence of non-uniform thermal zones within the cabin.

These results directly address Objective 2, which focuses on evaluating passenger thermal comfort under different passenger densities. For the AW2 condition (16 seated and 58 standing passengers), the findings show that higher passenger loads do not inherently degrade overall thermal comfort, as most occupants maintain acceptable comfort levels at moderate and high airflow velocities. However, the identification of critical positions, particularly those experiencing persistent cool or warm discomfort demonstrates how occupant density interacts with airflow patterns to create localized comfort challenges. This outcome satisfies Objective 2 by revealing that while the majority of passengers benefit from increased airflow, certain seating or standing positions remain vulnerable to thermal discomfort, thus underscoring the importance of optimizing airflow distribution to ensure uniform comfort across the cabin.

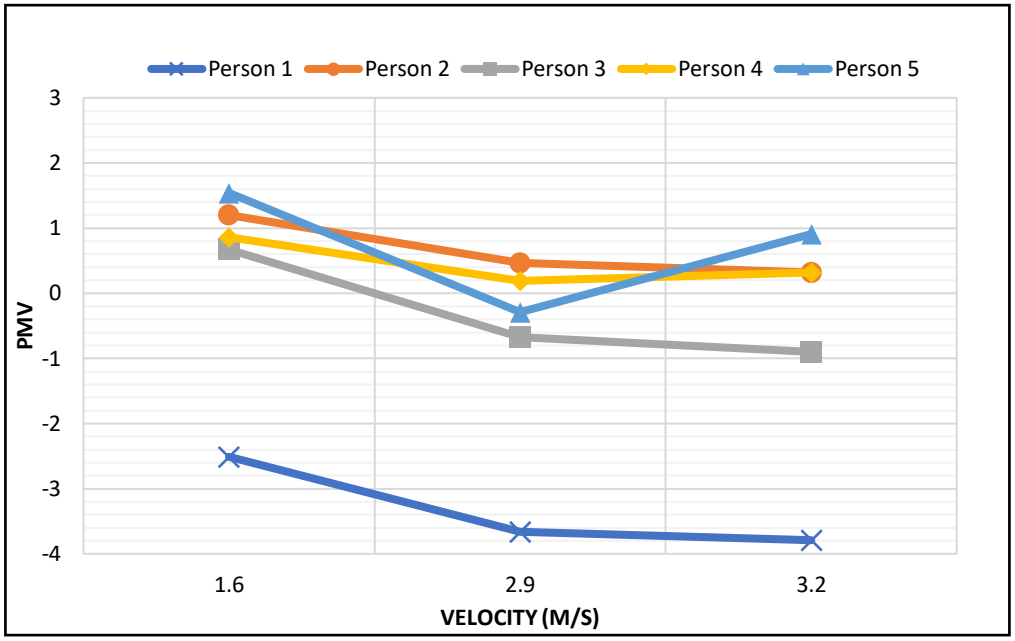

Figure 16: PMV Value of Selected Passengers at 8.7°C

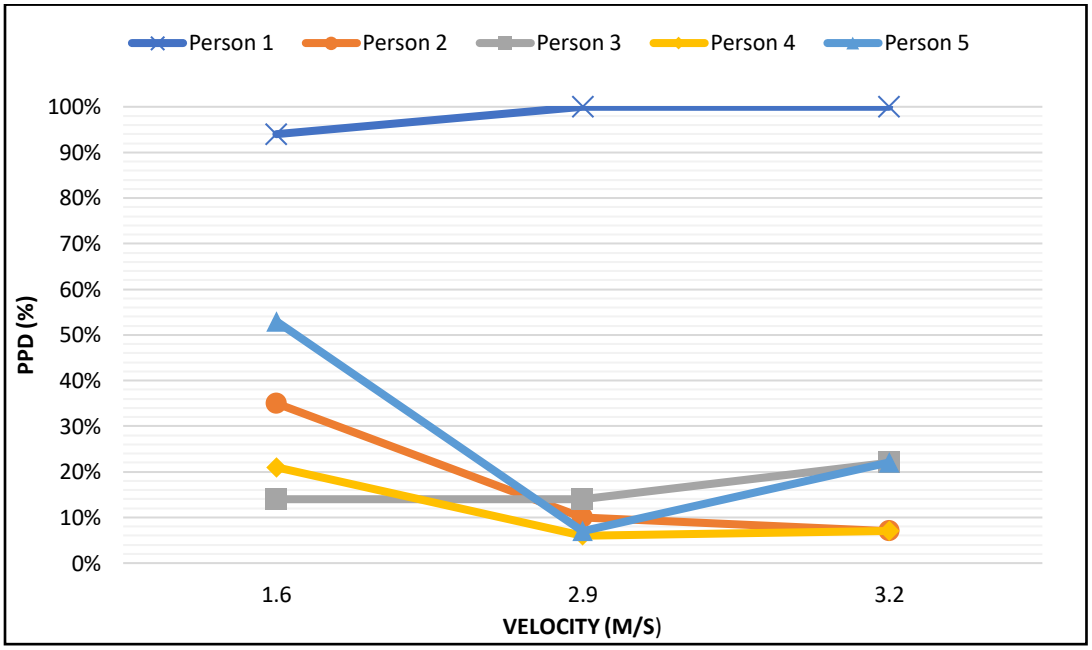

Figure 17: PPD Value of Selected Passengers at 8.7°C

Table 26
Summary Table for AW2 Category at 8.7 °C

Velocity (m/s)	Person	PMV (Value)	PPD (%)	Summary
1.6	1	-2.5	94	Feels very cool, high discomfort.
	2	1.2	35	Feels warm, moderate discomfort.
	3	0.67	14	Feels neutral, low discomfort.
	4	0.86	21	Feels neutral, low discomfort.
	5	1.54	53	Feels warm, moderate discomfort.
2.9	1	-3.66	100	Feels very cool, maximum discomfort.
	2	0.47	10	Feels warm, very low discomfort.
	3	-0.67	14	Feels neutral, low discomfort.
	4	0.19	6	Feels neutral, very low discomfort.
	5	-0.28	7	Feels neutral, very low discomfort.
3.2	1	-3.79	100	Feels very cool, maximum discomfort.
	2	0.32	7	Feels warm, very low discomfort.
	3	-0.9	22	Feels neutral, moderate discomfort.
	4	0.32	7	Feels neutral, very low discomfort.
	5	0.91	22	Feels warm, moderate discomfort.

According to Figure 16 and 17, the PMV and PPD results for AW2 at 8.7°C demonstrate clear spatial variability in thermal conditions across the five evaluated passenger locations. At 1.6 m/s, the PMV values range from –2.50 (very cool) to +1.54 (warm), indicating substantial differences in thermal sensation within the cabin. Person 1 consistently experiences strong cold sensations (PMV = –2.50), whereas the remaining individuals fall within slightly warm to near-neutral conditions (PMV = 0.67 to 1.54). These PMV trends reflect notable thermal non-uniformity, with only Persons 3 and 4 approaching thermal neutrality.

Table 26 depict that, when the velocity increases to 2.9 m/s, the PMV values for

most individuals shift closer to neutrality, with Persons 2–5 recording PMV values between –0.67 and +0.47, indicating improved thermal acceptability. However, Person 1 becomes even colder (PMV = –3.66), suggesting that airflow redistribution intensifies cold stress at their position. A similar pattern is observed at 3.2 m/s, where Persons 2–5 maintain PMV values within a near-neutral to slightly warm range (PMV = –0.90 to +0.91), but Person 1 remains in severe cold discomfort (PMV = –3.79). Overall, the PMV analysis reveals that increasing velocity benefits the majority of occupants, yet extreme cold persists for passengers located at specific positions.

The PPD results further reinforce these trends. At 1.6 m/s, dissatisfaction levels are high for both Person 1 (94%) and Person 5 (53%), while Persons 3 and 4 achieve low PPD values (14–21%), indicating acceptable comfort. At 2.9 m/s, thermal acceptability improves considerably, with Persons 2–5 reporting very low PPD values (6–14%), demonstrating that higher airflow rates generally enhance comfort for most passengers. However, Person 1 reaches maximum predicted dissatisfaction (PPD = 100%), meaning that colder airflow disproportionately affects their location. At 3.2 m/s, Persons 2, 4, and 5 maintain low dissatisfaction levels (7–22%), while Persons 1 and 3 record moderate-to-high PPD values (22–100%). These results confirm that airflow adjustments do not uniformly improve satisfaction across all seating positions.

In summary, the PMV and PPD analyses reveal that for AW2 at temperature of 8.7°C, thermal conditions remain acceptable for most passengers (Persons 2–5) across the different velocity settings, but Person 1 continues to experience marked cold discomfort at all velocities. This persistent deviation reflects localized thermal non-uniformities within the ART cabin.

4.4.4 PMV and PPD Value based on CBE Thermal Comfort Tool (AW3)

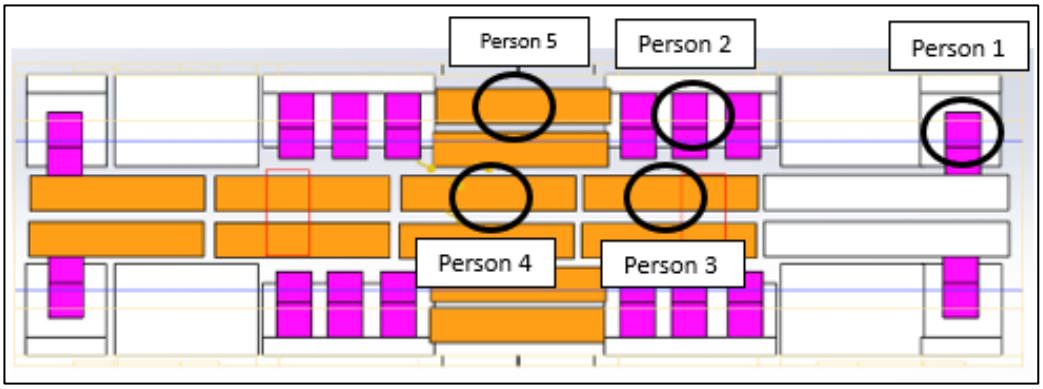

Figure 18: Selected Passengers for CBE Thermal Comfort Tool Analysis (AW3)

Figures 19 and 20 present the PMV and PPD values calculated using the CBE Thermal Comfort Tool to evaluate the thermal comfort of selected passengers in the ART under the AW3 condition at 8.7 °C. Figure 18 shows the seating and standing positions of Persons 1–5, selected to represent critical airflow regions within the carriage, including locations near diffusers, middle areas, and corner zones. The analysis was conducted for two inlet temperatures, 14.7 °C and 8.7 °C, across three air velocities.

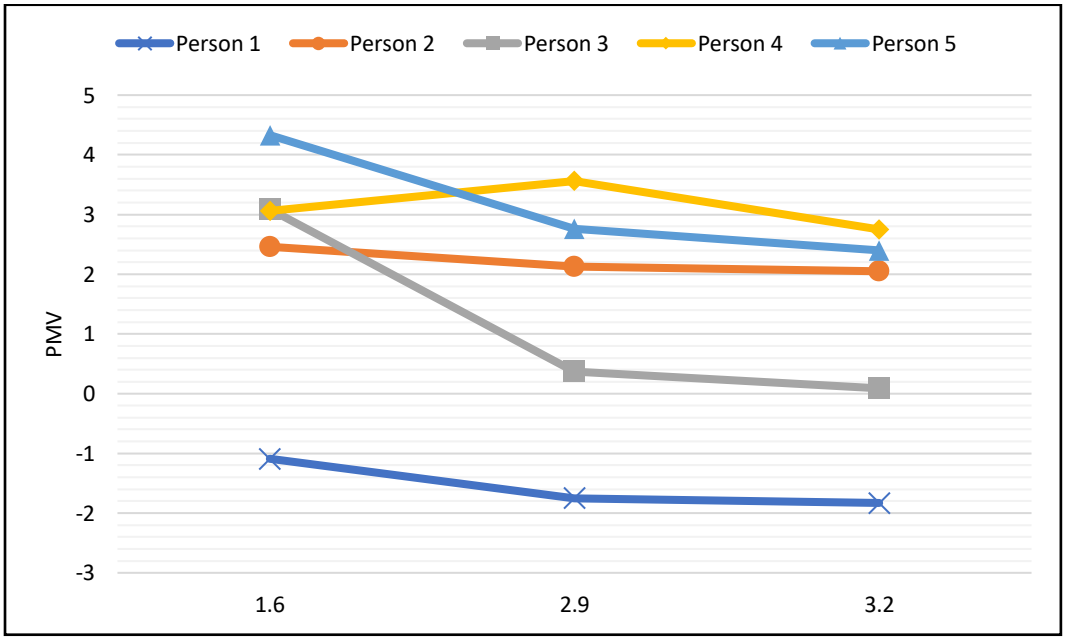

Figure 19: PMV Value of Selected Passengers at 14.7° C

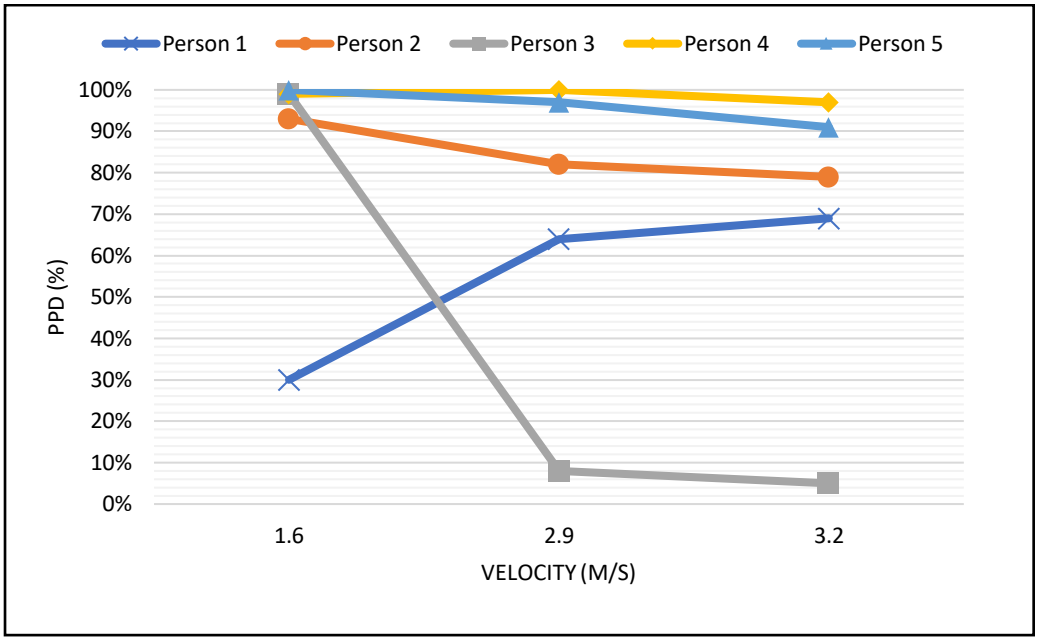

Figure 20: PPD Value of Selected Passengers at 14.7 °C

Table 27
Summary Table for AW3 Category at 14. 7 °C

Velocity (m/s)	Person	PMV (Value)	PPD (%)	Summary
1.6	1	-1.09	30	Feels cool, low discomfort.
	2	2.46	93	Feels warm, high discomfort.
	3	3.09	99	Feels very warm, maximum discomfort.
	4	3.06	99	Feels very warm, maximum discomfort.
	5	4.33	100	Feels extremely warm, maximum discomfort.
2.9	1	-1.75	64	Feels cooler, moderate discomfort.
	2	2.13	82	Feels warm, high discomfort.
	3	0.37	8	Feels neutral, very low discomfort.
	4	3.56	100	Feels very warm, maximum discomfort.
	5	2.76	97	Feels very warm, high discomfort.
3.2	1	-1.83	69	Feels cooler, higher discomfort.
	2	2.04	79	Feels warm, high discomfort.
	3	0.09	5	Feels neutral, very low discomfort.
	4	2.75	97	Feels very warm, maximum discomfort.
	5	2.4	91	Feels very warm, high discomfort.

The thermal comfort analysis for AW3 at temperature of 14.7 °C, represent the highest passenger density scenario, reveals pronounced non-uniformity in thermal sensation and dissatisfaction across the evaluated passenger positions. At 1.6 m/s, the PMV values range from –1.09 (cool) to +4.33 (extremely warm), indicating substantial thermal imbalance within the cabin. Person 1 experiences mild cool discomfort (PPV = 30%), whereas Persons 2–5 report strongly warm to extremely warm sensations (PMV = 2.46–4.33), with correspondingly high PPD values of 93–100%. These conditions demonstrate that, at lower airflow, thermal discomfort is widespread under high passenger loading.

As the velocity increases to 2.9 m/s, thermal conditions improve only for Person 3, whose PMV shifts toward neutrality (PMV = 0.37; PPD = 8%). However, the remaining occupants continue to experience warm discomfort, with PMV values ranging from 2.13 to 3.56 and PPD values between 82% and 100%. Person 1 becomes cooler (PMV = –1.75), accompanied by moderate dissatisfaction (PPD = 64%), indicating that higher airflow redistributes, but does not resolve, thermal imbalance. The extremely warm zone surrounding Person 4 remains prominent (PMV = 3.56; PPD = 100%), suggesting localized heat accumulation exacerbated by dense passenger loading.

At 3.2 m/s, similar patterns persist. Person 3 maintains near-neutral comfort (PMV = 0.09; PPD = 5%), while Persons 2, 4, and 5 continue to experience elevated warm discomfort (PMV = 2.04–2.75; PPD = 79–97%). Person 1 becomes slightly cooler (PMV = –1.83) with moderately high dissatisfaction (PPD = 69%), reinforcing the presence of a cold airflow zone that disproportionately affects their location. These results highlight that even at the highest velocity, thermal comfort remains highly uneven, with only one occupant position achieving acceptable levels.

Overall, the PMV and PPD analyses for AW3 at temperature of 14.7° C shows that under the highest passenger density, the ART cabin exhibits persistent thermal extremes, with most passengers (Persons 2, 4, and 5) experiencing sustained warm discomfort across all airflow conditions. Only Person 3 consistently approaches neutral comfort at higher velocities, while Person 1 continues to experience cool discomfort. This clearly indicates strong localized thermal gradients driven by passenger load, airflow pathways, and heat accumulation.

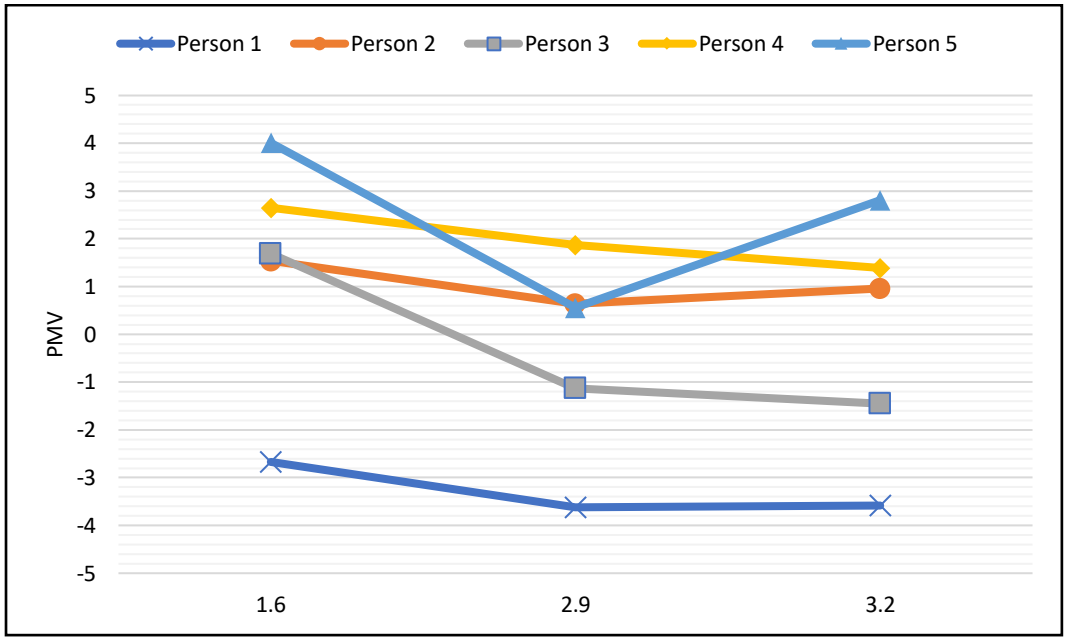

Figure 21: PMV Value of Selected Passengers at 8.7°C

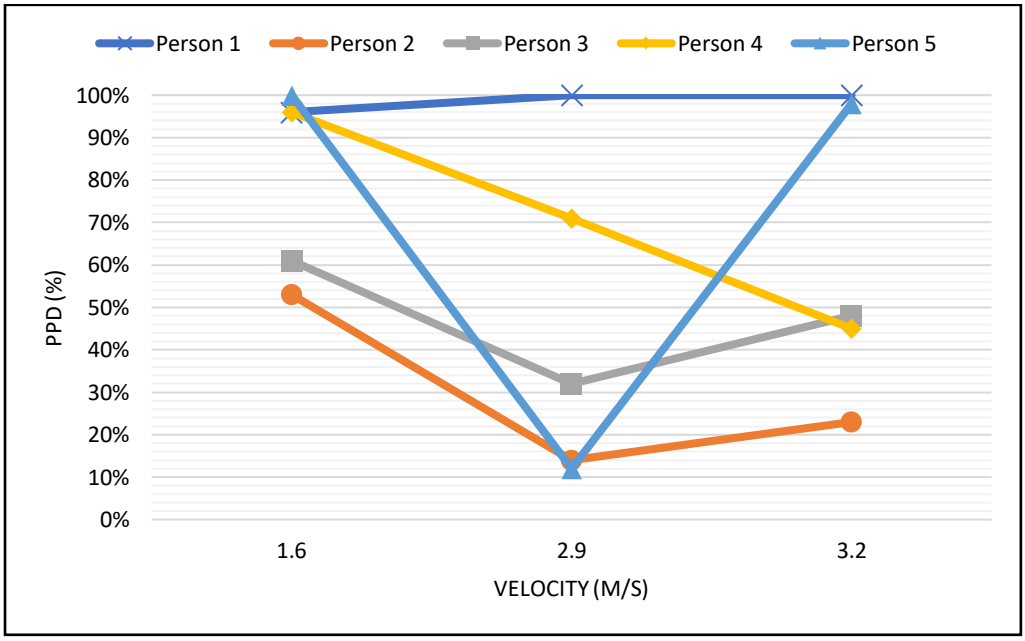

Figure 22: PPD Value of Selected Passengers at 8.7 °C

Table 28
Summary Table for AW3 Category at 8.7°C

Velocity (m/s)	Person	PMV (Value)	PPD (%)	Summary
1.6	1	-2.67	96	Feels very cool, maximum discomfort.
	2	1.54	53	Feels warm, moderate discomfort.
	3	1.69	61	Feels warm, moderate discomfort.
	4	2.65	96	Feels very warm, maximum discomfort.
	5	4.01	100	Feels extremely warm, maximum discomfort.
2.9	1	-3.62	100	Feels very cool, maximum discomfort.
	2	0.64	14	Feels neutral, very low discomfort.
	3	-1.12	32	Feels cool, moderate discomfort.
	4	1.87	71	Feels warm, high discomfort.
	5	0.56	12	Feels neutral, very low discomfort.
3.2	1	-3.58	100	Feels very cool, maximum discomfort.
	2	0.96	23	Feels warm, low discomfort.
	3	-1.45	48	Feels cool, moderate discomfort.
	4	1.39	45	Feels warm, moderate discomfort.
	5	2.81	96	Feels very warrm, maximum discomfort.

The thermal comfort results for AW3 at an inlet temperature of 8.7 °C reveal substantial thermal non-uniformity across the evaluated passenger positions under different airflow conditions. At 1.6 m/s, the PMV values range widely from –2.67 (very cool) to +4.01 (extremely warm), reflecting significant thermal imbalance within the cabin. Person 1 experiences severe cold discomfort (PPD = 96%), while Persons 2 and 3 report warm sensations (PMV = 1.54–1.69) associated with moderate dissatisfaction (PPD = 53–61%). Persons 4 and 5 experience very warm to extremely warm conditions (PMV = 2.65–4.01) with maximum dissatisfaction (PPD = 96–100%) which is well

above the acceptable threshold of 20% defined by ISO 7730 and ASHRAE 55. These results demonstrate that at lower velocities, the high passenger density produces extreme warm zones as well as distinct cold spots.

Increasing the velocity to 2.9 m/s produces mixed improvements. Comfort improves markedly for Persons 2 and 5, who achieve near-neutral PMV values (0.56–0.64) and very low dissatisfaction (PPD = 12–14%). However, Person 1 becomes even colder (PMV = –3.62; PPD = 100%), indicating intensified cold airflow exposure. Person 3 shifts toward cooler sensations (PMV = –1.12; PPD = 32%), while Person 4 continues to experience warm discomfort (PMV = 1.87; PPD = 71%). This pattern suggests that airflow redistribution reduces heat accumulation for certain positions but introduces or exacerbates cold discomfort in others.

At 3.2 m/s, thermal variation persists. Persons 2 and 4 experience warm but manageable conditions (PMV = 0.96–1.39; PPD = 23–45%), indicating moderate thermal acceptability. Person 3 continues to experience cool sensations (PMV = –1.45; PPD = 48%), while Person 1 remains in severe cold discomfort (PMV = –3.58; PPD = 100%), confirming a persistent cold airflow zone. Person 5 shifts back to very warm conditions (PMV = 2.81; PPD = 96%), indicating significant heat accumulation at their position even under higher velocities.

In summary, the PMV and PPD outcomes demonstrate that under AW3 conditions, most occupants (Persons 2–5) remain within acceptable comfort thresholds across all tested velocities. In contrast, Person 1 experiences persistent cold discomfort, confirming the existence of localized thermal imbalances within the ART cabin.

These findings directly support Objective 2, which aims to evaluate passenger thermal comfort under varying passenger density conditions. Under AW3 (the highest loading scenario), the results clearly show that increased occupancy intensifies thermal non-uniformity, producing both extreme cold and extreme warm zones within the cabin. While moderate airflow (2.9–3.2 m/s) improves comfort for some positions, the majority of passengers remain outside acceptable comfort ranges. This demonstrates that higher passenger density substantially amplifies localized thermal discomfort, thereby fulfilling the research objective of identifying critical passenger locations with

poor comfort performance in crowded ART conditions.

CHAPTER 5
CONCLUSION

This research focused on analysing the airflow and thermal comfort within the Automated Rapid Transit (ART) system using computational fluid dynamics (CFD) simulations and thermal comfort indices (PMV and PPD). The findings indicate that airflow dynamics significantly impact passenger comfort, especially in confined environments with varying passenger loads and air velocities. Higher air velocities resulted in more turbulent and non-uniform airflow patterns, which, in turn, influenced thermal comfort. In particular, passengers located near the corners of the carriage experienced more discomfort due to colder air distribution, as reflected by higher PPD values, aligning with [3] and [38]. Each research objective was successfully achieved. Higher air velocity increased turbulence, particularly near the air diffusers and around standing passengers, leading to uneven air distribution.

The first objective, which aimed to measure the current air temperature and airflow velocity in the ART carriages throughout the pilot testing period, was accomplished through on-site monitoring and data collection. The measured data provided essential boundary conditions for the CFD simulation setup, ensuring realistic representation of the airflow and thermal environment within the carriages. These empirical measurements served as the baseline to validate the accuracy and reliability of the CFD results

The second objective was to investigate the effects of airflow and temperature distribution within ART carriages under varying passenger loads and air-conditioning speeds. The CFD simulations revealed that airflow behaviour was highly sensitive to velocity changes. Higher air velocities produced more turbulence, particularly near air diffusers and around standing passengers, which led to uneven air distribution. The formation of eddies and recirculation zones created local temperature variations that affected passenger comfort. Passengers seated near the corners consistently experienced the greatest discomfort due to colder air concentration and restricted circulation, where PPD values exceeded 90% at 1.6 m/s. These findings highlight that airflow irregularities in confined areas significantly reduce comfort.

After analysing the airflow and passenger thermal comfort across different operating conditions using the PMV–PPD model, the results indicated that the combination of 2.9 m/s air velocity and an inlet temperature of 8.7 °C provided the most balanced and comfortable environment. At this conditions, PMV values ranged between –0.6 and +0.6, while PPD values remained below 20%, indicating near-neutral comfort. This optimal setting ensured uniform airflow and acceptable comfort across both AW2 (74 passengers) and AW3 (90 passengers) conditions. Moreover, operating at 2.9 m/s instead of 3.2 m/s reduced energy consumption without compromising comfort, emphasizing the importance of balancing thermal performance with sustainability.

In conclusion, this research demonstrated that optimizing airflow and temperature distribution is critical for improving passenger comfort and energy efficiency in the ART system [17][30]. The integration of CFD analysis with PMV–PPD assessment provided valuable insights into airflow–comfort relationships, confirming the potential of CFD as a practical and reliable tool for HVAC optimization in public transport [38][63]. Overall, this study contributes to the growing body of knowledge on thermal comfort optimization in transit systems and underscores the need for integrating efficient HVAC designs, adaptive control strategies, and ergonomic interior layouts to enhance passenger satisfaction, service quality, and environmental sustainability.

5.1 Recommendations

To enhance passenger comfort in the Automated Rapid Transit (ART) system, several measures are recommen5.ded. First, it is essential to implement dynamic airflow control systems that adjust air velocity in real-time based on passenger load and temperature conditions, ensuring consistent comfort throughout the cabin. Studies in [3] and [41] demonstrated that adaptive airflow control significantly improved passenger comfort in high-occupancy settings by responding to fluctuating load and environmental conditions. Additionally, the introduction of thermal zoning within the ART carriages could provide localized climate control, particularly for passengers seated near the corners, who tend to experience colder airflows. Passenger education on how to use available climate control features, such as adjustable air vents, could further improve individual comfort. It is also advised to conduct further studies to evaluate

thermal comfort under different environmental conditions and passenger behaviours, such as movement inside the cabin or varying levels of clothing insulation [40]. Finally, the use of adaptive HVAC systems that respond to real-time data from passenger loads and environmental conditions could significantly improve overall comfort and energy efficiency, ensuring the ART system remains an attractive and sustainable public transport option.

REFERENCES

[1] Z. Yang, “Rapid Transit : A Case Study of Tianjin BRT and the Problem Solving Towards Hamilton LRT.”

[2] T. Munnelly *et al.*, “03 May Mobilus Brings In th Rapid Transit (ART) System to Urban Transportation in,” pp. 1–7, 2021.

[3] N. E. Ahmad Shafie, H. Mohamed Kamar, and N. Kamsah, “Effects of ventilation setups on air flow velocity and temperature fields in bus passenger compartment,” *J. Teknol.*, vol. 77, no. 30, pp. 49–53, 2015, doi: 10.11113/jt.v77.6867.

[4] F. Patania, A. Gagliano, F. Nocera, and A. Galesi, “Thermal comfort analysis of public transport passengers in Catania,” *WIT Trans. Ecol. Environ.*, vol. 157, no. March 2016, pp. 327–338, 2012, doi: 10.2495/AIR120291.

[5] M. D. N. Almeida, A. A. de P. Xavier, and A. O. Michaloski, “A review of thermal comfort applied in bus cabin environments,” *Appl. Sci.*, vol. 10, no. 23, pp. 1–21, 2020, doi: 10.3390/app10238648.

[6] B. Y. A. Chen, “Why do we keep the air conditioning on in buses and trains when it ’ s chilly out ?,” pp. 1–7, 2020.

[7] M. Simion, L. Socaciu, and P. Unguresan, “Factors which Influence the Thermal Comfort Inside of Vehicles,” *Energy Procedia*, vol. 85, no. November 2015, pp. 472–480, 2016, doi: 10.1016/j.egypro.2015.12.229.

[8] ISO, *Ergonomics of the thermal environment — Analytical determination and interpretation of thermal comfort using calculation of the PMV and PPD indices and local thermal comfort criteria*. International Organization for Standardization, Geneva, Switzerland, 2005.

[9] ASHRAE, *ANSI/ASHRAE Standard 55-2020: Thermal Environmental Conditions for Human Occupancy*. 2020.

[10] C. Iclodean, N. Cordos, and B. O. Varga, “Autonomous shuttle bus for public transportation: A review,” *Energies*, vol. 13, no. 11, 2020, doi: 10.3390/en13112917.

[11] K. Lumpur *et al.*, “Mobilus welcomes arrival of rst automated rapid transit system into Iskandar Malaysia,” 2021.

[12] A. Rail and R. Transit, “China ’ s self-driving trackless ’ rail bus ’ starts first overseas run,” pp. 5–7, 2022.

[13] Y. Jia, X. Song, and G. Li, “Service Quality Evaluation and Analysis of Autonomous-Rail Rapid Transit in Yibin City of China,” pp. 1–34, 2025.

[14] “First automated rapid transit system arrives in Malaysia | Investvine,” pp. 1–3, 2021.

[15] C. Pricelist, “Automated rapid transit arrives in Johor for testing , to be test line for Iskandar Malaysia BRT system project,” no. January, pp. 1–7, 2021.

[16] A. R. Transit, “Putrajaya offers free rides on trackless tram for FT Day,” 2024.

[17] Y. Tao, M. Yang, B. Qian, F. Wu, and T. Wang, “Numerical and Experimental Study on Ventilation Panel Models in a Subway Passenger Compartment,” *Engineering*, vol. 5, no. 2, pp. 329–336, 2019, doi: 10.1016/j.eng.2018.12.007.

[18] Y. A. Çengel and Cimbala John M, *Fluid Mechanics: Fundamentals and Applications*. McGraw-Hill Education, New York, NY, USA, 2014.

[19] A. Palmowska and I. Sarna, “CFD MODELLING OF THERMAL COMFORT IN THE PASSENGER COACH,” 2022, doi: 10.2478/ACEE-2022-0044.

[20] W. Zhou, M. Liu, and L. Duan, “Analysis of Airflow Organization in Buses Air-Conditioned by Direct Evaporative Coolers,” pp. 1–16, 2025.

[21] Y. Wu, W. Zhou, X. Liang, D. Chen, X. Su, and X. Li, “Numerical and experiment study on ventilation performance of the equipment compartment of Alpine high-speed train Numerical and experiment study on ventilation performance of the equipment compartment of Alpine high-speed train,” vol. 17, 2023, doi: 10.1080/19942060.2023.2252514.

[22] H. Yang, Y. Wang, and T. He, “The Analysis on the Effect of Passenger car Air Conditioning and Distribution with Different Inlet Parameters,” no. Icismme, pp. 229–233, 2015, doi: 10.2991/icismme-15.2015.45.

[23] M. Hossam, M. Fouad, and A. Abou-Zaid, “Numerical Investigation of Airflow Patterns and Thermal Comfort in a Bus Cabin,” *SAE Int. J. Passeng. Cars - Mech. Syst.*, vol. 13, no. 2, pp. 145–156, 2020, doi: 10.4271/06-13-02-0012.

[24] S. R. Kale, S. V. Veeravalli, H. D. Punekar, and M. M. Yelmule, “Air flow through a non-airconditioned bus with open windows,” *Sadhana - Acad. Proc. Eng. Sci.*, vol. 32, no. 4, pp. 347–363, 2007, doi: 10.1007/s12046-007-0029-3.

[25] I. L. Scurtu and A. N. Jurco, “Airflow and thermal comfort of the bus passengers,” vol. 14, no. 1, pp. 171–174, 2019.

[26] Guillermo Giraldo, “How To Use CFD To Simulate Airflow in an Operating Room,” *SIMSCALE Blog*, pp. 1–13, 2019.

[27] N. Rorres and E. Engineer, “Airflow Through Buses,” no. June, 2020.

[28] S. Üna, “An experimental study on a bus air conditioner to determine its conformity to design and comfort conditions,” *J. Therm. Eng.*, vol. 3, no. 1, pp. 1089–1101, 2017, doi: 10.18186/thermal.277288.

[29] A. M. Abdel-Ghany, I. M. Al-Helal, and M. R. Shady, “Human thermal comfort and heat stress in an outdoor urban arid environment: A case study,” *Adv. Meteorol.*, vol. 2013, no. i, 2013, doi: 10.1155/2013/693541.

[30] R. Musat and E. Helerea, “Parameters and Models of the Vehicle Thermal Comfort,” *Acta Univ. Sapientiae Electr. Mech. Eng.*, vol. 1, no. January 2009, pp. 215–226, 2009.

[31] T. P. Lin, R. L. Hwang, K. T. Huang, C. Y. Sun, and Y. C. Huang, “Passenger thermal perceptions, thermal comfort requirements, and adaptations in short- and long-haul vehicles,” *Int. J. Biometeorol.*, vol. 54, no. 3, pp. 221–230, 2010, doi: 10.1007/s00484-009-0273-9.

[32] Ü. PALA, “Investigation of Thermal Comfort for Bus Passengers during a Cooling Test Inside a Climatic Chamber,” *J. Polytech.*, no. February, 2020, doi: 10.2339/politeknik.608597.

[33] Q. Zhou, “Thermal Comfort in Vehicles,” *Univ. Gavle Fac. Eng. Sustain. Dev.*, no. August, pp. 1–31, 2013.

[34] R. Musat and E. Helerea, “Parameters and Models of the Vehicle Thermal Comfort,” *Acta Univ. Sapientiae Electr. Mech. Eng.*, vol. 1, no. January, pp. 215–226, 2009.

[35] C. Ekici, “A review of thermal comfort and method of using Fanger’s PMV equation,” *5th Int. Symp. Meas. Anal. Model. Hum. Funct. ISHF 2013*, no. January 2013, pp. 61–64, 2013.

[36] S. Guenther, “What Is PMV? What Is PPD? The Basics of Thermal Comfort | SimScale,” pp. 1–8, 2020.

[37] R. Thirumalai, D. Prabhakaran, S. F. Curling, M. Spear, and G. A. Ormondroyd, “Simulation Model to Evaluate Human Comfort Factors for an Office in a Building †,” pp. 2–5, 2018, doi: 10.3390/proceedings2151126.

[38] P. Danca, A. Vartires, and A. Dogeanu, “An Overview of Current Methods for Thermal Comfort Assessment in Vehicle Cabin,” *Energy Procedia*, vol. 85, no. November 2015, pp. 162–169, 2016, doi: 10.1016/j.egypro.2015.12.322.

[39] C. Neacsu, I. Tabacu, M. Ivanescu, and I. Vieru, “The evaluation of the overall

thermal comfort inside a vehicle," *IOP Conf. Ser. Mater. Sci. Eng.*, vol. 252, no. 1, 2017, doi: 10.1088/1757-899X/252/1/012031.

[40] B. Zhang, T. Xue, and N. Hu, "Analysis and improvement of the comfort performance of a car's indoor environment based on the predicted mean vote-predicted percentage of dissatisfied and air age," *Adv. Mech. Eng.*, vol. 9, no. 4, pp. 1–10, 2017, doi: 10.1177/1687814017695693.

[41] M. V. Wilson, "Analysis of Ventilation System and Comfortness of a Passenger in a Bus using CFD," *Int. J. Res. Appl. Sci. Eng. Technol.*, vol. 6, no. 6, pp. 934–961, 2018, doi: 10.22214/ijraset.2018.6141.

[42] P. Danca, F. Bode, I. Nastase, and A. Meslem, "CFD simulation of a cabin thermal environment with and without human body - Thermal comfort evaluation," *E3S Web Conf.*, vol. 32, pp. 1–8, 2018, doi: 10.1051/e3sconf/20183201018.

[43] S. Lin, B. T. Tee, and C. F. Tan, "Indoor airflow simulation inside lecture room: A CFD approach," *IOP Conf. Ser. Mater. Sci. Eng.*, vol. 88, no. 1, 2015, doi: 10.1088/1757-899X/88/1/012008.

[44] A. Raczkowski, Z. Suchorab, and P. Brzyski, "Computational fluid dynamics simulation of thermal comfort in naturally ventilated room," *MATEC Web Conf.*, vol. 252, p. 04007, 2019, doi: 10.1051/matecconf/201925204007.

[45] F. Usman and A. R. A. Bakar, "Thermal Comfort Study Using CFD Analysis in Residential House with Mechanical Ventilation System," *Lect. Notes Civ. Eng.*, vol. 53, no. June, pp. 1613–1628, 2020, doi: 10.1007/978-3-030-32816-0_124.

[46] S. B. Abul, E. H. Muhammad, M. Tabassum, and ..., "Feasibility study of solar power system in residential area," *Int. J. Innov. Comput. Sci. Eng.*, vol. 1, no. 1, pp. 10–17, 2020, [Online]. Available: https://webportal.hct.edu.om/ijicse/pages/upload/library/2020/1/2ndPaperPDFForm.pdf.

[47] K.-Y. Lai and B.-H. Lim, "Optimal inverter sizing ratio for photovoltaic power plants in Malaysia," *Proc. 11th Int. Conf. Appl. Energy, Part 4, Sweden*, vol. 5, pp. 1–5, 2019.

[48] E. D. Stepasheva, M. A. Zasimova, and N. G. Ivanov, "THERMAL MANIKIN SHAPE INFLUENCE ON AIRFLOW AND HEAT TRANSFER IN THE MODEL ROOM WITH DISPLACEMENT VENTILATION," vol. 14, no. 3, pp. 90–106, 2021, doi: 10.18721/JPM.14307.

[49] T. Hågbo, K. Erik, and T. Giljarhus, “Sensitivity of urban morphology and the number of CFD simulated wind directions on pedestrian wind comfort and safety assessments,” *Build. Environ.*, vol. 253, no. February, p. 111310, 2024, doi: 10.1016/j.buildenv.2024.111310.

[50] J. Zhang, K. He, X. Xiong, J. Wang, and G. Gao, “Numerical Simulation with a DES Approach for a High- Speed Train Subjected to the Crosswind,” vol. 10, no. 5, pp. 1329–1342, 2017, doi: 10.18869/acadpub.jafm.73.242.27566.

[51] P. Armand and J. Tâche, “3D modelling and simulation of thermal effects and dispersion of particles carrying infectious respiratory agents in a railway transport coach,” pp. 1–36, 2025.

[52] M. Z. M. Samidi, H. Husain, and M. S. Meon, “CFD Analysis of Thermal Comfort in Hospital Operation Room with Different Air Distribution Design and Operative Temperature.”

[53] P. Mishra and K. R. Aharwal, “A review on selection of turbulence model for CFD analysis of air flow within a cold storage,” *IOP Conf. Ser. Mater. Sci. Eng.*, vol. 402, no. 1, 2018, doi: 10.1088/1757-899X/402/1/012145.

[54] J. P. O. Sullivan, R. A. Archer, and R. G. J. Flay, “Journal of Wind Engineering Consistent boundary conditions for flows within the atmospheric boundary layer,” *Jnl. Wind Eng. Ind. Aerodyn.*, vol. 99, no. 1, pp. 65–77, 2011, doi: 10.1016/j.jweia.2010.10.009.

[55] B. E. Launder and D. B. Spalding, “THE NUMERICAL COMPUTATION OF TURBULENT FLOWS,” vol. 3, pp. 269–289, 1974.

[56] A. Hajipour, A. M. Lavasani, M. E. Yazdi, and A. Mosavi, “Simulation of Turbulent Flow around a Generic High-Speed Train using Hybrid Models of RANS Numerical Method with Machine Learning.”

[57] F. Simulation, “ADVANCED BOUNDARY CARTESIAN MESHING TECHNOLOGY IN.”

[58] A. Žnidarˇ, “A 3D CFD-Based Workflow for Analyses of a Wide Range Electric Machines,” 2022.

[59] N. Netam, S. Sanyal, and S. Bhowmick, “A PMV-PPD model based study of thermal comfort in Low-Income Group house in Chhattisgarh,” *MATEC Web Conf.*, vol. 172, pp. 2–6, 2018, doi: 10.1051/matecconf/201817206006.

[60] M. Kumar, S. Mahapatra, and S. K. Atreya, “Adaptive thermal comfort model for different climatic zones of North-East India,” *Appl. Energy*, vol. 88, no. 7,

pp. 2420–2428, 2011, doi: 10.1016/j.apenergy.2011.01.019.

[61] D. Markov, “Practical evaluation of the thermal comfort parameters,” *Annu. Int. Course Vent. Indoor Clim. Avangard, Sofia*, no. October 2002, pp. 158–170, 2002.

[62] P. Methodology *et al.*, “A Review of Comprehensive Guidelines for Computational Fluid Dynamics (CFD) Validation in Solar Chimney Power,” pp. 1–66, 2024.

[63] K. Sinha, M. S. Yadav, U. Verma, J. S. Murallidharan, and V. Kumar, “Effect of recirculation zones on the ventilation of a public washroom,” *Phys. Fluids*, vol. 33, no. 11, pp. 1–11, 2021, doi: 10.1063/5.0064337.

[64] C. M. Candido, “Indoor air movement acceptability and thermal comfort in hot-humid climates,” *Build. Environ.*, vol. 45, pp. 222–229, 2010.

[65] C. M. Lee, “Regional Variation of Human Skin Surface Temperature,” vol. 31, no. 3, 2019.

[66] U. Journal and O. F. Mechanical, “ANALYSIS OF THERMAL COMFORT MODELS OF USERS OF PUBLIC URBAN AND INTERCITY TRANSPORT,” vol. 8, no. 2, pp. 67–74, 2022.

[67] Arena 3050, “Predicting Thermal Comfort,” *AREN 3050 Environ. Syst. Build. I*, vol. 42, no. 1971, pp. 3–6, 2005.

APPENDICES

APPENDIX 1

Technical Drawing of Automated Rapid Transit (ART)

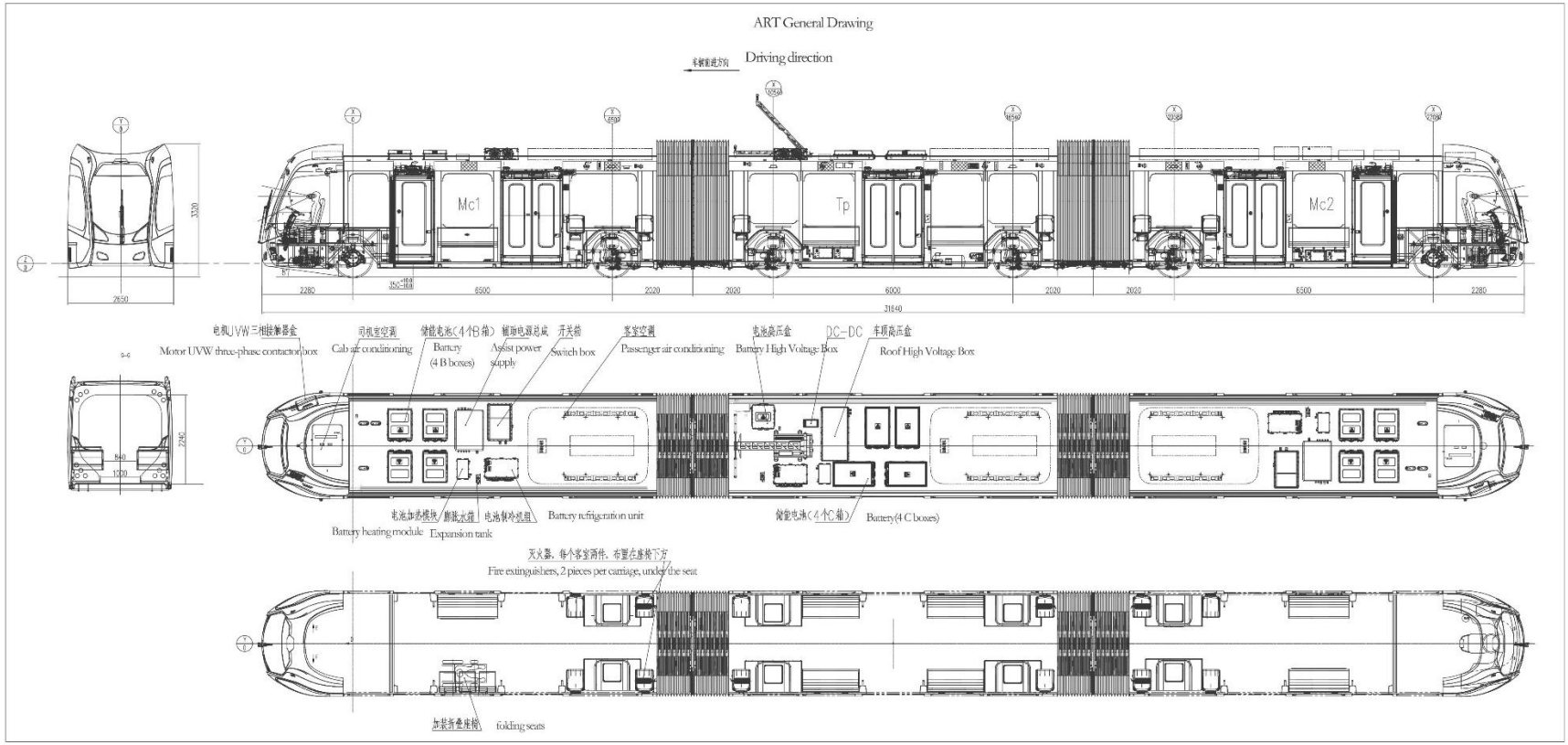

APPENDIX 2

Data Collected on ART using UNI-T Mini LCD Anemometer UT363

Date: 27 August 2021

Location: Terminal Bas Kota Iskandar (Depoh) and ART POC Test Route

Weather: Sunny

Ambient temperature: 32°C

Blower speed: No 2 (1.6 m/s)

Time	Side	Supply air velocity (m/s)	Return air velocity (m/s)	Supply air temp at Supply Diffuser (°C)	Return air temp at Return Grill (°C)	Surface temp (seat) (°C)	Surface temp (floor) (°C)	Surface temp (window) (°C)	Surrounding temp inside ART (°C)
10:15 am (Static, ART not moving)	Shaded	1.6	1.1	14.7°C	20.8	26.4	26.1	31.0	25.1
	Direct sun	1.6	1.1	14.7	20.8	32.2	33.0	36.1	25.1

10:45 am (ART moving)	Shaded	1.6 m/s	1.1	8.7	21.0	23.3	25.4	30.9	26.2
	Direct sun	1.6	1.1	8.7	21.0	32.0	36.0	37.0	26.2
11:45 am (ART moving)		1.6	1.1	7.5	14.5	19.0	22.7	29.9	21.8
1:00 pm (ART moving)		1.6	1.1	8.5	15.0	24.1	25.7	31.8	25.3

Blower Speed: 8 blower speed

No	Speed (m/s)
1	0.4

2	1.6
3	2.6
4	2.9
5	3.0
6	3.2
7	3.4
8	3.6

ART air conditioning system setpoint temperature: 16 - 30°C

Setpoint temperature during operation: daytime 20-21°C, night time 23-24°C

Number of return grill per car – 2 nos

Size of return grill – 38 cm X 75 cm

APPENDIX 3

Model Verification at Condition of Zero Passenger (AW0)

Temperature Distribution

- Metabolic Rate: 1.0 Met (58 W/m2)
- Clothing Insulation: 1.0 Clo (0.155 Km2/W)
- Inlet: 1.6 m/s, 2.9 m/s, 3.2 m/s
- Outlet: 1.1 m/s
- Environment Pressure: 101325 Pa

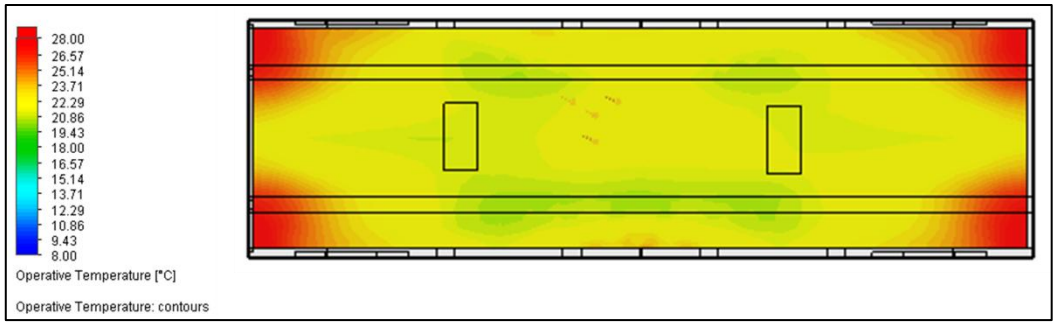

Percentage Difference Between Simulated Value and Real Value of Surrounding Temperature

$$Percentage\ Difference\ = \frac{|Simulated\ Value\ - Real\ Value|}{Real\ Value} \times 100\%$$

$$Percentage\ Difference\ = \frac{|23.2\ ℃\ - 25.1\ ℃|}{25.1\ ℃} \times 100\%$$

$$Percentage\ Difference\ = 7.57\%$$

AUTHOR'S PROFILE

Aina Balqis Azrin earned her Bachelor's degree in Bachelor of Mechanical Engineering (Hons) in 2020 from Universiti Teknologi MARA, Shah Alam. She is currently pursuing her Master's degree in Master of Science in Mechanical Engineering at the same university Her research focuses on evaluating airflow and thermal comfort in an Automated Rapid Transit (ART) system using Predicted Mean Vote (PMV) and Predicted Percentage Dissatisfied (PPD) models. She has experience in computational fluid dynamics (CFD) simulations and statistical analysis for optimizing thermal conditions in public transportation.

LIST OF PUBLICATION:

1. Wan Mazlina Wan Mohamed, Siti Ayu Jalil, and Aina Balqis Azrin. En Route to Green Campus UiTM Shah Alam: Is Public Transport the Key Mode to Cut Carbon Emission?, 2020 IEEE MITRANS International Logistics & Transport Conference (IEEE MILTC) on 2020.

2. Aina Balqis Azrin, Shafiq Suhaimi, Hazran Husain, and Wan Mazlina Wan Mohamed. Effects of Passenger Capacity and Climate Control Settings on the Thermal Comfort Levels of Automated Rapid Transit (ART) System, CFD Letters, Volume 18, Issue 3 on 2026.